Improved Convex Optimal Decision-making Processes in Distribution Systems: Enable Grid Integration of Photovoltaic Resources and Distributed Energy Storage

by

Qifeng Li

A Dissertation Presented in Partial Fulfillment
of the Requirements for the Degree
Doctor of Philosophy

Approved July 2016 by the
Graduate Supervisory Committee:

Vijay Vittal, Chair
Gerald T. Heydt
Hans D. Mittelmann
Raja Ayyanar

ARIZONA STATE UNIVERSITY

August 2016

ABSTRACT

This research mainly focuses on improving the utilization of photovoltaic (PV) resources in distribution systems by reducing their variability and uncertainty through the integration of distributed energy storage (DES) devices, like batteries, and smart PV inverters. The adopted theoretical tools include statistical analysis and convex optimization. Operational issues have been widely reported in distribution systems as the penetration of PV resources has increased. Decision-making processes for determining the optimal allocation and scheduling of DES, and the optimal placement of smart PV inverters are considered. The alternating current (AC) power flow constraints are used in these optimization models. The first two optimization problems are formulated as quadratically-constrained quadratic programming (QCQP) problems while the third problem is formulated as a mixed-integer QCQP (MIQCQP) problem. In order to obtain a globally optimum solution to these non-convex optimization problems, convex relaxation techniques are introduced. Considering that the costs of the DES are still very high, a procedure for DES sizing based on OpenDSS is proposed in this research to avoid over-sizing.

Some existing convex relaxations, e.g. the second order cone programming (SOCP) relaxation and semidefinite programming (SDP) relaxation, which have been well studied for the optimal power flow (OPF) problem work unsatisfactorily for the DES and smart inverter optimization problems. Several convex constraints that can approximate the rank-1 constraint $\boldsymbol{X} = \boldsymbol{x}\boldsymbol{x}^{\mathrm{T}}$ are introduced to construct a tighter SDP relaxation which is referred to as the enhanced SDP (ESDP) relaxation using a non-iterative computing framework. Obtaining the convex hull of the AC power flow equations is beneficial for mitigating the non-convexity of the decision-making processes in power systems, since the AC power

flow constraints exist in many of these problems. The quasi-convex hull of the quadratic equalities in the AC power bus injection model (BIM) and the exact convex hull of the quadratic equality in the AC power branch flow model (BFM) are proposed respectively in this thesis. Based on the convex hull of BFM, a novel convex relaxation of the DES optimizations is proposed. The proposed approaches are tested on a real world feeder in Arizona and several benchmark IEEE radial feeders.

ACKNOWLEDGMENTS

First of all, I would like to express my grateful thanks to Dr. Vijay Vittal, my advisor, who gave me the chance of pursuing my Ph.D. degree at Arizona State University. Dr. Vittal provided valuable guidance and continuous support to me, which significantly reduced my fear of failure in the Ph.D. research. I do appreciate the time working with Dr. Vittal and I believe this experience is just like a beacon in my life, leading me to the way of scientific research and preparing me well for my future career.

Secondly, I am grateful to Dr. Raja Ayyanar, Dr. Hans Mittelmann and Dr. Gerald Heydt for serving as members of my committee. They spent a lot of time talking with me and dispelling my confusion. Without their suggestions, I could not continue to improve my research work. Additionally, I would also like to convey my gratitude to all the members of the Flagstaff PV project team who selflessly offered their help and suggestions to my research.

Last but not least, I want to thank my parents and my friends. Love and support coming from them is the real power to help me focus on the research.

TABLE OF CONTENTS

Page

CHAPTER Page

CHAPTER Page

LIST OF TABLES

Table Page

LIST OF FIGURES

Figure Page

NOMENCLATURE

$\boldsymbol{A}_{ij,t}$	$n \times n$-dimensional matrix (n is the size of the vector $\boldsymbol{x}_t$ defined in Section 4.2) and the only non-zero entries of $\boldsymbol{A}_{ij,t}$ are the two diagonal entries corresponding to $P_{ij,t}$ and $Q_{ij,t}$
$\boldsymbol{A}_i$	4×4-dimensional coefficient matrix of the ith quadratic equality of the branch flow model
$\boldsymbol{a}$	A lower triangular matrix with nonnegative diagonal entries
AC	Alternating current
AMI	Automated Meter Infrastructure
ANN	Artificial neural network
$Arg\{\cdot\}$	Argument function
BFM	Branch flow model
BIM	Branch injection model
B&B	Branch and bound
$\boldsymbol{B}$	(n+1)-dimensional vector
$\boldsymbol{C}$	4×4-dimensional coefficient matrix of the quadratic equality in BFM
c_t	Cost of grid energy at time t
CC	Cost curve
CDF	Cumulative distribution function
CH	Convex hull
$CONV(\cdot)$	Convex hull of a set
d	*A scalar value*

$\boldsymbol{d}$	The opposite direction to the descent direction of an objective function
D	A variable denoting the D^{th} day of a year
DES	Distributed energy storage
DESOA	Distributed energy storage optimal allocation
DESOS	Distributed energy storage optimal scheduling
e	A constant given by the operators in (2.6)
e_i	Real part of the voltage at bus i respectively
e_r	Real part of the voltage at the reference bus respectively
ESDP	Enhanced semidefinite programming
ESS	Energy storage system
E^{ME}	The statistical sample set of maximum error PV energy
E_D^{ME}	The maximum error PV energy of day D
E_i^{DES}	Energy capacity of DES at bus i
E_i^{spl}	Energy surplus of the DES at bus i at the beginning of a day
FACTS	Flexible alternating current transmission systems
$f(\cdot)$	CDF of some statistical sample set
F_i	The i^{th} objective function
f_i	Imaginary part of the voltage at bus i respectively
f_r	Imaginary part of the voltage at the reference bus respectively
$\boldsymbol{I}_2$	2×2 identity matrix

k_i	Loss coefficient with respect to square of voltage magnitude. In distribution systems, this quantity is usually the coefficient of core losses in transformers.
K	A threshold value for triggering the DES controller
LMP	Locational marginal price
LMP_t	Locational marginal price of the substation bus at t
LP	Linear program
M	Number of branches
$\boldsymbol{M}$	4×4-dimensional constructed positive definite matrix
$\boldsymbol{m}$	A lower triangular matrix with nonnegative diagonal entries
MIQCQP	Mixed-integer quadratically constrained quadratic programming
ME	Maximum error
$\max\{\cdot\}$	Calculation of the maximum value of a array
N	Number of buses
N_i	Set of downstream buses which are directly connected to bus i
N_{T}	High voltage bus set of transformers
Ns	DES bus set
N_G	Generator set
N_R	Reactive power regulator set (including the generators which have reactive capabilities)
OOV	Optimal objective value
OPF	Optimal power flow

p	A constant given by the operators in (2.5)
$P_{ij,t}$	Active power flow in p.u. in branch ij at hour t
$\boldsymbol{P}_t$	A vector that contains all $P_{ij,t}$
$p_{i,t}^{CH}$	Charging rate of DES in p.u. at bus i at time t
$\boldsymbol{p}_t^{\mathrm{CH}}$	A vector that contains all $p_{i,t}^{CH}$
$p_{i,t}^{DCH}$	Discharging rate of DES in p.u. at bus i at time t
$\boldsymbol{p}_t^{\mathrm{DCH}}$	A vector that contains all $p_{i,t}^{DCH}$
P_i^{DES}	Power rating of DES in p.u. at bus i
P^{DES}	Total Power rating of DES in p.u. for the feeder
$\boldsymbol{p}^{DES}$	Output of the DES units in the proof of Proposition 4.1 and the illustrative example in Subsection 4.1.3
$p_{i,t}^{DESloss}$	Power losses of DES in p.u. at bus i at hour t
$\boldsymbol{p}_t^{\mathrm{DESloss}}$	A vector that contains all $p_{i,t}^{DESloss}$
P_i^G	Active power generation in p.u. at bus i.
$p_{(i=1),t}^{Grid}$	Active grid power in p.u. at hour t
$p_{i,t}^{L}$	Active load in p.u. at bus i at hour t
P^{ME}	The statistical sample set of maximum error PV power
P_D^{ME}	The maximum error PV power of day D
$P_{D,t}^{PV,lmt}$	The PV generation at t^{th} hour of the D^{th} day at the penetration level that makes system constraint violation first occur

$P_{D,t}^{PV,desired}$	The PV generation at t^{th} hour of the D^{th} day at the desired penetration level
$P_{t_{mc}}^{PV,lmt}$	The PV generation at t_{mc} of the penetration level that makes system constraint violation first occur
$P_{t_{mc}}^{PV,desired}$	The PV generation at t_{mc} of the desired penetration level
$P_{D,t}^{PV}$	The measured PV power at the t^{th} minute of the D^{th} day
$P_{D,t}^{F}$	The forecast PV power at the t^{th} minute of the D^{th} day
PV	Photovoltaic
$Q_{ij,t}$	reactive power flow in p.u. in branch ij at hour t
$\boldsymbol{Q}_t$	A vector that contains all $Q_{ij,t}$
$q_{i,t}^{DCH}$	Reactive discharging rate of DES in p.u. at bus i at time t
$q_{i,t}^{CH}$	Reactive charging rate of DES in p.u. at bus i at time t
$\boldsymbol{q}^{DES}$	Reactive output of the DES units in the proof of Proposition 4.1 and the illustrative example in Subsection 4.1.3
$q_{(i=1),t}^{Grid}$	Reactive grid power in p.u. at hour t
q_i^{Invt}	Reactive power output of the smart inverter in p.u. at bus i
$\boldsymbol{q}^{\text{Invt}}$	A vector that contains all q_i^{Invt}
$q_{i,t}^{L}$	Reactive load in p.u. at bus i at hour t
QCQP	Quadratically constrained quadratic programming
r_{ij}	Resistance in p.u. of branch ij
RLT	Reformulation-linearization technique

RDG	Renewable distributed generation
R2LI	Rank-2 linear inequalities
S_i^{Invt}	A real value denoting the rating of the smart inverter in p.u. at bus i
$\boldsymbol{S}^{\text{Invt}}$	A vector that contains all S_i^{Invt}
S_{LE1}	The first set of linear equality constraints
S_{LE2}	The second set of linear equality constraints
S_{LI}	The set of linear inequality constraints
S_{QE}	The set of quadratic equality constraints
S_{QI}	The set of quadratic inequality constraints
$\bar{\boldsymbol{S}}$	The assumed optimal solution of the convexified problem that is not located on the SOC boundary
$\bar{S}_{ij}$	A real value denoting the MVA limit in p.u. of branch ij
$\hat{\boldsymbol{S}}$	A constructed feasible solution which is closer to the SOC boundary and has a smaller objective value than $\bar{S}$
SDP	Semidefinite programming
SIOP	Smart inverter optimal placement
SOCC	Second order cone constraint
SOCCNL	Second order cone constraint neighboring linear constraint
C	
SOCP	Second order cone programming
T	Time. In the dispatch problem T usually equals to 24, while T equals to 24×(number of days) in the allocation problem.

$T(D,t)$	A binary function of D and t that denotes the period in which there exists system constraint violations
t	A variable that denotes the t^{th} hour of a day
t_{mc}	The time instant with the worst system constraint violations
$tr(\cdot)$	Trace of a matrix
$u_{i,t}$	Auxiliary variable
$\boldsymbol{u}_t$	A vector that contains all $u_{i,t}$
$v_{i,t}$	Square of magnitude of voltage at bus i at hour t
$\boldsymbol{v}_t$	A vector that contains all $v_{ij,t}$
VLE	Valid linear equalities
$\boldsymbol{x}$	Vector of intermediate variables in the SDP relaxation
$\boldsymbol{X}$	Auxiliary semidefinite positive matrix in the SDP relaxation
x_{ij}	Reactance of branch ij
$\ell_{ij,t}$	Square of magnitude of current in branch ij at hour t
$\boldsymbol{\ell}_t$	A vector that contains all $\ell_{ij,t}$
$\ell_{ij,\max}$	The limit of the current square in p.u. of branch ij
α_i	The i^{th} binary variable
$\boldsymbol{\alpha}$	A vector that contains all α_i
γ	An arbitrary positive scalar
ε	An arbitrarily small positive value. It may be marked with a subscript in different contents

Φ_i	The *i*th subset of descent directions of the objective function that will result in exactness of the SOCP relaxation
Ω	Feasible set of a given problem.
$\succeq$	$\boldsymbol{A} \succeq 0$ means matrix $\boldsymbol{A}$ is positive semidefinite

Chapter 1 INTRODUCTION

1.1 Potential Issues in Distribution Systems with High Penetration PV

Photovoltaic (PV) resources connected to distribution systems and referred to as renewable distributed generation (RDG) have experienced a rapid growth in the past decades. PV resources provide an alternative to fossil fuel generation. However, operational issues have been widely reported in distribution systems as the penetration of PV resources has increased. The operational issues observed include over loading in conductors and voltage limit violation. Therefore, new techniques are required to mitigate the operational issues arising due to the high penetration of PV.

A typical daily PV generation curve measured at a real world feeder location in Arizona is shown in Figure 1.1 at a time resolution of one minute. The forecasted PV generation curve for this day is depicted by the dashed line as shown in Figure 1.1. By subtracting the forecasted PV generation value from the measured value, the uncertain PV generation (error in PV power) curve can be obtained as the solid line shown in Figure 1.1.

It can be observed from Figures 1.3 and 1.4 that, when the penetration of PV is high, at the time resolution of 1 minute the main operational problem observed is fast voltage fluctuations caused by short-duration (lasting 1 second to 1 minute) variation of PV output. Note that the example given in Figure 1.3 and 1.4 is different from that in Figure 1.1 and 1.2. And, the operational problem caused by the forecast component of PV generation is system constraint violations at the time resolution of 15 minute – 1 hour.

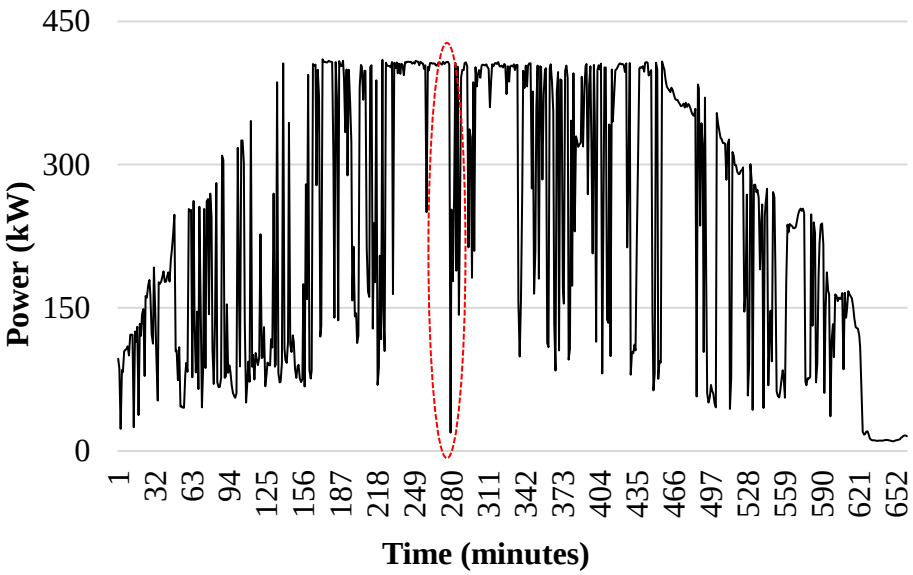

Figure 1.1 Actual Measured PV Production of A Selected Day (from 6:00 to 19:00) [1]

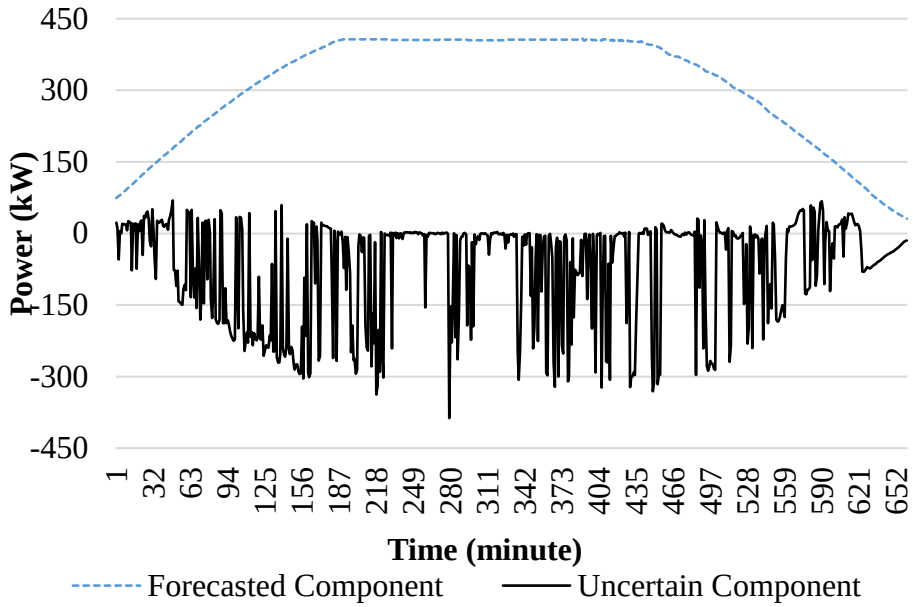

Figure 1.2 Decomposition of Actual Measured PV Production of A Selected Day (from 6:00 to 19:00) [1]

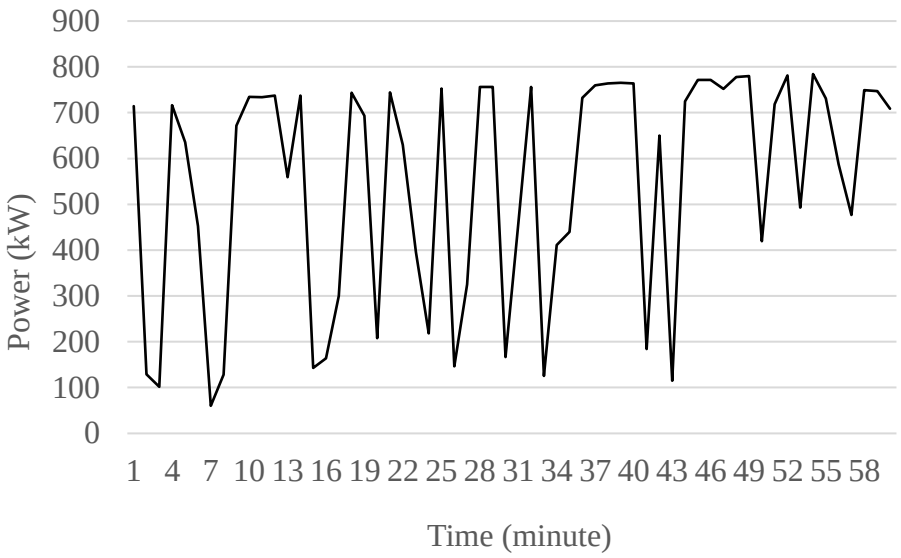

Figure 1.3 A 1-hour Example of PV Output Fluctuation [1]

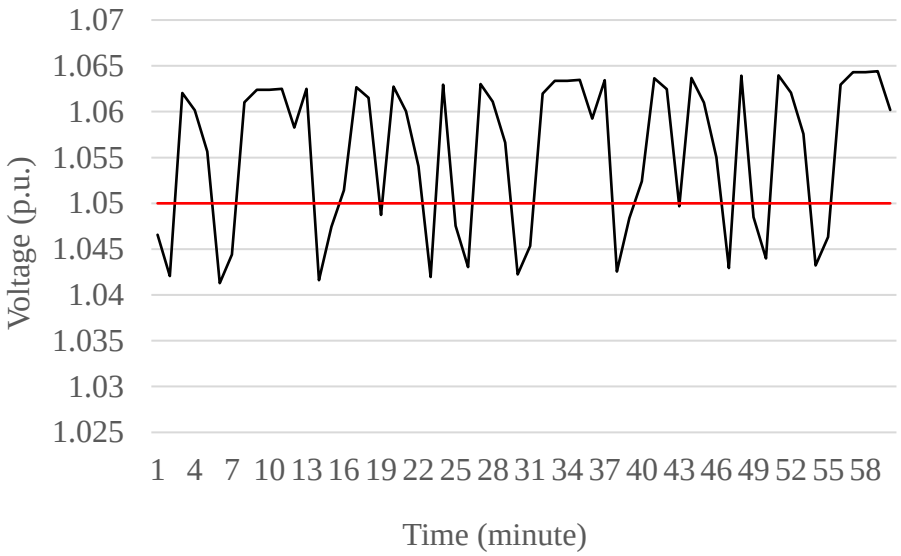

Figure 1.4 The Corresponding Voltage Profile of the 1-hour Example Where the Voltage Base is 12.47 kV.

This research studies the detrimental impacts caused by high penetration PV at mainly two time resolutions – one hour at which optimization techniques can be applied

and one minute at which the effects of short-term PV output uncertainty with high ramp rates can be properly observed. The feasibility of utilizing distributed energy storage (DES) and smart PV inverters to mitigate the adverse effects caused by PV is estimated. Novel techniques are developed for implementing the DES and smart PV inverters in distribution systems with integration of high penetration PV at both of planning and operation stages.

1.2 Capability of the DES and Smart PV Inverters in Mitigating the PV Issues

1.2.1 Distributed Energy Storage

It is a consensus among energy specialists that energy storage (ES) systems will play a significant role in modern and future power systems with integrated renewable sources [1] – [7]. For the distribution system integrated with distributed generation, battery or ultra-capacitor ES units which are referred to as distributed ES (DES) in [2] are important. In this research, the DES is used to alleviate detrimental impacts of high penetration photovoltaic (PV) resources on distribution systems. The analysis is carried out at mainly two time resolutions - one hour at which optimization techniques can be applied and one minute at which the effects of short-term PV output uncertainty with high ramp rates can be properly observed. To achieve this objective, methods for sizing, allocation and operation of DES based on different time horizons are proposed.

Most power system components like capacitors [8] and [9], distribution transformers [10] and FACTS devices [11], [12], can be sized based on economic criteria, namely minimizing the cost of losses and investments over a period of time (e.g. 1-10 years). However, unit costs of DES are still very high compared with the savings [3]. As a result, this objective is not suitable to be directly applied to the sizing of DES. Under the condition

that the cost of DES is high, it is advisable to design the DES based on accommodating the PV power and energy that cause system constraint (voltage limits, feeder line ampacity limits and reverse power flow limit) violations [4]. High-energy storage systems are usually required for this application. In this report, the spilled PV power and energy are determined by a proposed approach based on OpenDSS [13], [14] where the entire feeder (including the single-phase system) is modeled. Once the total power rating and energy capacity of the DES are determined, optimization techniques are used to obtain the optimal locations. As a result, at the time resolution of 1 hour, the planning stage of DES is divided into two steps: i) determine the total size of the battery or supercapacitor and the converter which are required to avoid spilling power and energy output of the given PV sources (Section 2.1); ii) then choose the optimal sites to locate the DES units along the feeder with system limits as constraints that each optimal solution should satisfy and minimizing operational costs or power losses as objective (Section 3.1).

At the time resolution of 1 minute the main operational problem is fast voltage fluctuations caused by short-duration (lasting 1 sec to 1 min) variation of PV output [3]. To reduce the short-duration output uncertainty, megawatt-scale photovoltaic installations may require high-power, low-energy storage systems [3]. To avoid unacceptably high investment, a probabilistic method is proposed to size DES for this application (see Section 2.2). As a result, the operational strategy for DES should contain two sub-strategies, one is based on the time resolution of 1 hour while the other is based on the time resolution of 1 minute (see Section 2.3).

1.2.2 Smart PV inverters

As stated above, integration of high penetration PV may cause various operational issues in power systems. Among these problems, voltage regulation issues have been widely reported [15] - [18]. The smart inverter is a promising resource of volt/VAr control for integration of high penetration of PV [16]. In 2009, a photovoltaic and storage integration research program conducted by EPRI has identified common measures by which smart inverters may be integrated into utility systems [19]. The smart inverter volt/VAr control strategies for high penetration of PV on distribution systems were studied in [16] - [18]. The smart inverters are usually more expensive than the conventional ones due to the extra capability to provide reactive power support and the communication functions. The utilization of smart inverters in power systems raises an interesting issue: how to obtain the minimum investment of smart inverters to meet the volt/VAr control requirement.

This dissertation designs an optimization model for smart inverter placement minimizing the total investment of inverters. The designed optimization model is a MIQCQP problem taking into account the AC power flow constraints. MIQCQP problems are hard to solve since they contain two kinds of non-convexities: integer variables and non-convex quadratic constraints (i.e. AC power flow equations) [20].

1.3 State of Art of Convex Optimization Techniques in Power Systems

To obtain the best performance of the distribution system from the given assets, various decision-making processes are involved. The optimal allocation and optimal scheduling of DES, and the optimal placement of smart PV inverters in distribution systems are problems of highly non-convex. This property will result in a locally optimal solution that

may be far away from the global optimal when conventional nonlinear programming algorithms are used. Such non-convex problems are also difficult to solve due to the NP-hardness [21], [22]. Some research efforts have used heuristic algorithms, like genetic algorithm [3], [23] and [24] bee colony algorithm [25] and firefly algorithm [26], to deal with the NP-hard problem. The heuristic algorithms are good methods to remedy the local solution problem. However, as stated in literature, the drawbacks of such approaches are obvious: 1) rely heavily on a good initial population; 2) choice of some parameters depend on experience; 3) converge prematurely to a local minimum and 4) heavy computational burden.

Compared with approaches of solving the power system optimization problem in its original non-convex form, solving these problems through convex relaxation provides several advantages. First, as aforementioned, the solutions obtained by nonlinear algorithms are just locally optimal solutions without guarantee of the quality of the solutions. Second, with convex relaxation, NP-hardness is largely avoided. These features make the convexified algorithms adaptable to larger systems or faster control in the future.

1.3.1 A Conventional Convexification: Linearization

A simple but effective convexification of the AC power flow is called DC power flow which has been since the 1970s [27]. The DC power flow is a linear approximation of the AC power flow. The accuracy of the DC power flow relies heavily on a low r/x-ratio of the circuit branches. However, the r/x-ratio of feeders in distribution systems is high. The DC power flow is hence unsuitable for the DES and smart inverter optimizations studied in this research. Another popular linearization technique is the first-order Taylor series expansion. The accuracy of the first-order Taylor series expansion relies on a requirement

that the operating point should be close to the original operating point, which is hard to satisfy in power systems. Consequently, nonlinear convex relaxations are needed.

1.3.2 State of the Art of Nonlinear Convex Relaxation

As alternatives to the DC power flow, some nonlinear convex relaxations have been applied to various optimization problems in power systems, e.g. optimal power flow (OPF) [28]-[30] transmission system expansion planning [31], transmission optimal switching [32], distribution system reconfiguration [33], security-constrained unit commitment [34] and reactive power planning [35]. What these problems have in common is that the AC power flow equalities are considered as constraints. All the non-convexity or at least a significant portion of the non-convexity of these problems comes from the power flow constraints. These convex relaxations are semidefinite programming (SDP) [28], second order cone programming (SOCP) [31], quadratic convex (QC) [32] and moment-based relaxations [36].

There are mainly two types of mathematical models that can be used to describe the AC power flow. They are the branch flow models (BFM) and the bus injection models (BIM) [21]. The BFMs are preferred for radial networks since they are exact for radial networks and contain fewer non-convex equalities [37]. However, the BFMs are not exact for meshed networks. In radial networks, the SOCP relaxation is tighter than the basic form of the SDP relaxation when BFMs are used [38]. However, the SOCP relaxation may be inefficient when some objective functions other than the objective function of minimizing generation cost are adopted. For the DES optimal scheduling cases where the SOCP relaxation is not exact, this research proposes the enhanced SDP relaxations in the non-iterative

computing framework. In meshed networks where the power flow is described by BIMs, the SDP relaxation dominates the SOCP relaxation regarding the tightness [21]. In fact, the QC relaxation is equivalent to the SOCP relaxation for power flow in BIMs if the range of angle differences is not subjectively tightened [39]. Overall, the SDP relaxation is still preferred for convexifying the power flow equations described by the BIM (generally in meshed networks), even though it performs unsatisfactorily for a number of OPF cases [40] and [41].

Several references have tried to strengthen the convex relaxations of OPFs in iterative computing structures. For example, [42] applied a penalty method to the SDP relaxation to enforce the rank of its solution to become nearly 1 based on a premise that the rank of the solution for the basic SDP (BSDP) relaxation is low. Iteratively generated linear cuts are added to tighten the SOCP relaxation for OPFs in [43]. Interesting results have been reported with these iterative methods. However, some issues still exist with the iterative methods. For instance, an iterative procedure usually solves a problem repeatedly, which results in high computational burden. Moreover, the convergence of most of these iterative methods is not well studied. In reference [40], non-iterative linear cuts are proposed based on the SOCP formulation of OPF to provide a tight root node for solving the relaxed OPF problem in BARON [54], where the relaxed OPF problem is still non-convex.

The topology of distribution systems is usually radial. Hence, a BFM is used to describe the AC power flow in radial networks in the DES and smart inverter optimization models since the BFMs are exact for radial networks and contain fewer non-convex constraints [37]. The DistFlow model and the modified power flow model proposed in [44] and [45] respectively are representatives of BFMs. They are equivalent since there is a

bijection between them. The DistFlow model proposed in [44] is used in this research. As an alternative, this research looks for computationally effective convex constraints that are valid for tightening the basic SDP relaxation of the DES and smart inverter optimization problems in a non-iterative framework. Moreover, the convex hull or quasi-convex hull of these non-convex constraints in AC power flow constraints are studied in this thesis.

1.4 Thesis Organization

Work in this thesis mainly aims at proposing tighter convex relaxations for the DES and smart PV inverter optimizations. A brief introduction with a concise literature review has been presented in Chapter 1. A framework of the approaches studied in this report is shown in Figure 1.5.

The remainder of this report is organized as follows.

In Chapter 2, methods of DES sizing are proposed to meet the operational requirements at two time resolutions respectively, which provides the basis for the optimal allocation and scheduling of DES studied in later chapters.

In Chapter 3, optimization models for the optimal allocation and operation of DES, and the optimal placement of smart PV inverters in radial distribution systems are established respectively.

Chapter 4 examines limitations of existing convex relaxation techniques, e.g. the SOCP relaxation, to reveal some inherent properties of the convex relaxations for the AC branch power flow. Then, some convex constraints proposed in the analytical optimization literature are introduced to construct a tighter convex relaxation known as the enhanced SDP relaxation in a non-iterative framework.

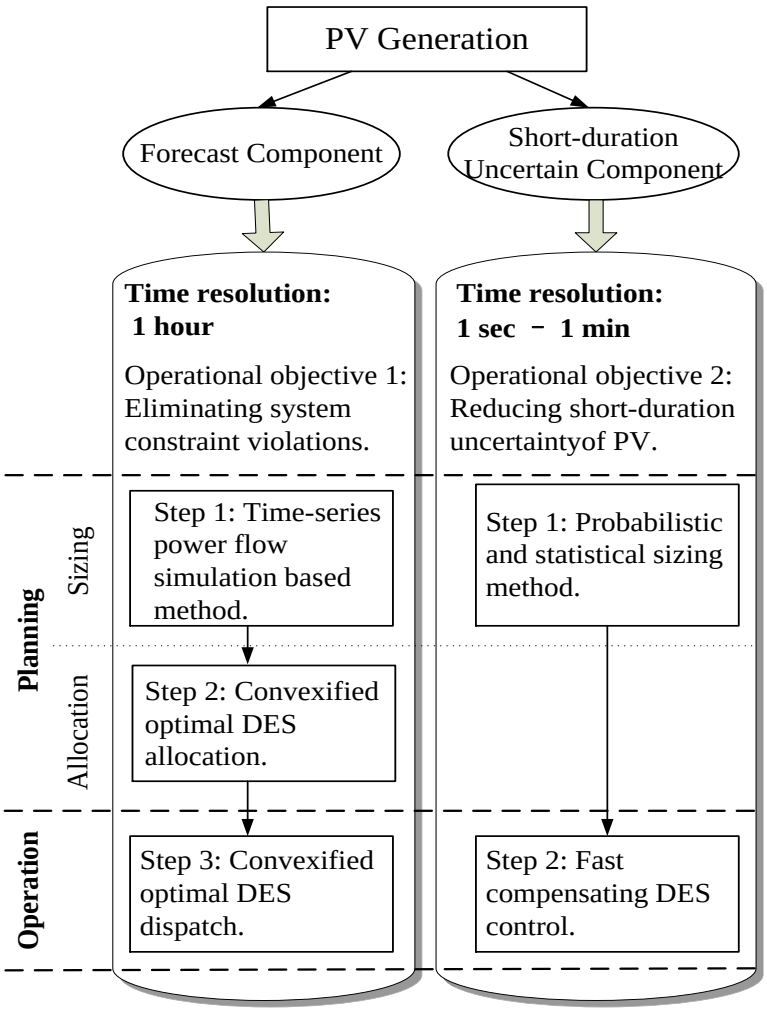

Figure 1.5 Framework of Proposed Approaches in this Report.

Next in Chapter 5, the quasi-convex hull of the quadratic equalities in the AC power bus injection model (BIM) and the exact convex hull of the quadratic equality in the AC power branch flow model (BFM) are proposed respectively. Based on the convex hull of BFM, a novel convex relaxation, called CH relaxation, of the DES optimizations is proposed

Chapter 6 presents the numerical comparisons among the CH, ESDP, SOCP, and the BSDP relaxations on a real-world feeder and several benchmark IEEE radial test feeders.

Finally, the conclusions and contributions of this research are summarized in Chapter 7. In addition, directions for the future work are also provided. The proofs of the theorems and propositions are given in the appendix section.

Chapter 2 SIZING OF DES FOR TWO OPERATIONAL REQUIREMENTS

2.1 Sizing DES for Eliminating System Constraint Violations

When the PV penetration is high, system constraint violations may occur due to the instantaneous imbalance of power and energy. Hence, it is important to size the DES according to the power and energy imbalance. However, the definition of unbalance power and energy in some previous references, e.g. [5], is not suitable for this application scenario. To determine the exact amount of power and energy that causes system constraint violations, the network structure and system constraints of a distribution system should be taken into account.

The authors of [4] used an OPF to determine the maximum amount of wind power and energy that can be absorbed by the distribution system without violating any system constraint. The ES systems were then designed to accommodate the spilled wind power and energy. However, an actual feeder usually contains a number of single-phase nodes and branches. If the single-phase system is fully modeled, the resulting time-coupled OPF may be intractable. If the single-phase system is simply neglected, the designed size of the DES is most likely to be inaccurate, since the system constraint violations occur in the single-phase system more frequently [37]. To achieve a balance, this report divides the planning stage into two steps as introduced in Chapter 1. In the first step, the PV power and energy imbalance that causes system violations is calculated by OpenDSS, where the entire feeder is modeled, to determine the total size of DES required. Second, the optimal sites are chosen to allocate the DES units determined in the previous step using the convex optimization techniques introduced in Chapter 3 with system limits as constraints and three objective functions. Note that, the number of storage units is not restricted to 1. There may

be multiple units at multiple locations respectively. The number of units required depends on the result of the optimization. However, the summation of the ratings of all the units should equal to the total rating determined. Moreover, the method proposed in [4] has a limitation that the potential locations of ES units are restricted to the wind power sites. This limitation may shrink the physically feasible set of the allocation problem.

In OpenDSS, the proposed approach for determining the spilled PV power and energy uses the measured historical yearly load shapes along the feeder and the measured PV outputs of all the PV systems on the feeder. The size of DES determined by the proposed procedure is believed to be more accurate than that determined by OPF in which the single-phase system is simply dropped. The detailed procedure of the proposed method is as follows:

1) Run hourly time series power flow simulations with the actual operating conditions in OpenDSS and check whether there exists system constraints violations over a time period;

2) From the various cases at which constraint violations occur, denote t_{mc} as the instant in time at which the worst system constraint violation occurs in terms of the chosen constraint. Define the PV generation at this instant as $P_{t_{mc}}^{PV,lmt}$;

3) Define the PV generation at a desired penetration level at t_{mc} to be $P_{t_{mc}}^{PV,desired}$;

4) The total power rating of the DES is then given by (2.1),

$$P^{ES} = P_{t_{mc}}^{PV,desired} - P_{t_{mc}}^{PV,lmt} \tag{2.1}$$

5) The energy capacity is given by (2.2),

$$E^{ES} = \max_{D} \left\{ \int_0^{23} \left(P_{D,t}^{PV,desired} - P_{D,t}^{PV,lmt} \right) T\left(D,t\right) dt \right\} \tag{2.2}$$

where D and t (t=0, …, 23) represent days of the considered historical data and hours in a day respectively; $T(D, t)$, which is a binary function of D and t, denotes the period at which there exists system constraint violations. When there exists a system constraint violation, T equals to 1, otherwise, T equals to 0. Note that P^{ES} and E^{ES} do not necessarily occur on the same day. P^{ES} and E^{ES} will be used as inputs to the optimal allocation problem introduced in Section 3.1 (see constraints (3.16) and (3.17)).

2.2 Sizing DES for Reducing Short-duration Uncertainty of PV

Simulation results obtained from OpenDSS show that severe drops in PV output cause fast voltage sags. The historical minute by minute and second by second data (an example is given in Figure 1.1) shows that, in the worst case, the PV output dropped from the rated value to almost zero within one second due to cloud effects [3], implying that if one wants to completely smooth the power injection from a PV system into the distribution system, a large DES system is needed. However, this is not necessary since the feeder itself has sufficient capability to handle small variations in power injections from a PV system [46]. For instance, when the PV penetration is low, the PV output uncertainty will not be a problem. As a result, it is essential to determine the proper size of the DES that can reduce the short-duration uncertainty of PV output to an acceptable level (an example is shown in Section 2.4). A probabilistic method is suitable for sizing the DES to meet this requirement while taking care of the short-duration uncertainty. Furthermore, the short-duration uncertainty of PV generation should be determined by removing the periodic effect of the annual position of the sun [47].

The detailed procedure for DES sizing based on the proposed probabilistic and statistical method is given as:

1) Use (2.3) and (2.4) to obtain the maximum error (ME) in power and energy outputs of each day in the considered operating year and form a maximum error power set $P^{ME} = \left\{ P_D^{ME} \right\}$ and a maximum error energy set $E^{ME} = \left\{ E_D^{ME} \right\}$ respectively,

$$P_D^{ME} = \max_t \left\{ \left| P_{D,t}^{PV} - P_{D,t}^{F} \right| \right\} \tag{2.3}$$

$$E_D^{ME} = \max_t \left\{ \left| \int_0^{1439} \left(P_{D,t}^{PV} - P_{D,t}^{F} \right) dt \right| \right\} \tag{2.4}$$

2) Use $\left\{ P_D^{ME} \right\}$ and $\left\{ E_D^{ME} \right\}$ as the statistical sample sets to obtain the cumulative distribution functions (CDF) of the daily maximum error in power $f_P\left(P^{ME} \right)$ and energy $f_E\left(E^{ME} \right)$ respectively;

3) Equations (2.5) and (2.6) can be used to calculate the power rating and energy capacity of DES respectively,

$$P^{ES} = \underset{P^{ME}}{Arg} \left\{ f_P\left(P^{ME} \right) = p\% \right\} \tag{2.5}$$

$$E^{ES} = \underset{E^{ME}}{Arg} \left\{ f_E\left(E^{ME} \right) = e\% \right\} \tag{2.6}$$

where $P_{D,t}^{PV}$ and $P_{D,t}^{F}$ represent the measured and forecast PV power at the t^{th} minute of the D^{th} day respectively; *Arg* is an argument function; *p* and *e* are constants given by the operators. It means that the DES determined by (2.5) can manage the errors in power and energy of at least *p*% and *e*% of the cases occurring in the operation year respectively.

With the designed DES of which the power rating is determined by equation (2.5) and a properly designed DES controller (see Section 2.3), the output curves of the PV plant

in *p*% of the cases can be completely smoothed. In the rest (1-*p*)% of the cases, the fast variations of PV power cannot be eliminated, however the magnitude of the short-duration PV power swings can be reduced to a small amount. Therefore, it does not necessarily mean that there will be system violations for these cases. Similar conclusion can be made to the energy rating determined by equation (2.6). Generally, the minimum operation cycle of ES is a day. Hence, it is proper to use 1 day as the minimum period to determine the size of DES.

2.3 Operational Strategy of DES

The first sub-strategy is aimed at mitigating the problem caused by the uncertain component of PV power within a timescale of seconds to minutes. A mathematical representation of the charging and discharging rate of the DES is given as

$$P_{D,t}^{ES} = \left\{ P_{D,t}^{F} - P_{D,t}^{PV} \,\middle\|\, P_{D,t}^{F} - P_{D,t}^{PV} \right| \geq K \right\} \tag{2.7}$$

where K is a chosen value to prevent the DES from frequently charging and discharging. By implementing this sub-strategy, the power injected into the distribution system from the PV and DES is nearly equal to the forecast power which has already been considered in the day-ahead scheduling.

For better control performance, some potential advanced control strategies can be incorporated, like open-loop based optimal control [48], feed-back-based optimal control [49], model predictive control [50], fuzzy control [51] and artificial neural network (ANN) control [51].

The second operational sub-strategy for the DES is the optimal scheduling. The convexified optimization models can also be applied to the operation problem. The optimal

allocation model can be used as the dispatch model with constraints (3.16) and (3.17) omitted. P_i^{ES} and E_i^{ES} ($i \in N$) are outputs of the allocation problem and parameters of the dispatch problem. The parameter T in the dispatch problem is usually 24 hours.

2.4 Results of the DES Sizing

The DES sizing methods are tested on an actual feeder located in Arizona. The three-phase trunk for this system is shown in Figure 2.1. In this system, there are two commercial PV plants, about 200 residential PV systems, and over 3000 nodes (including the single-phase system). The rated power of PV plants 1 and 2 are 600 kW and 400 kW respectively. The total capacity of the residential PV systems is about 500 kW. The yearly peak load is 8.05 MW while the lowest load throughout the year is 1.83 MW. The test bed feeder is fully modeled in OpenDSS.

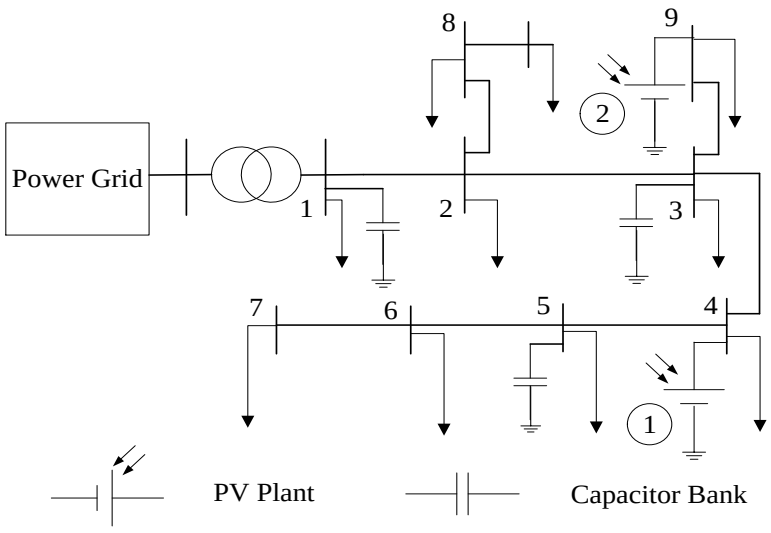

Figure 2.1 The Real-world Test Feeder in Southwest U.S.

To support this study, a data acquisition platform was developed to obtain the required field data (as shown in Figure 1.1 and Figure 2.4). This platform consists of Automated Meter Infrastructure (AMI), weather stations and some advanced metering systems, e.g. Schweitzer Engineering Laboratories SEL-734, 735 systems.

As the basic level of the data acquisition platform, AMI meters collect 15-min interval load and PV generation data for all customer sites. SEL-734 metering systems collect additional power quality information every 1 second for a selected number of PV installations. The weather and irradiance data are sampled and stored by the weather station prototype at 1-second intervals. Electrical parameters relating to the distribution feeder are collected via six utility pole-mounted power quality meters (SEL-735).

At the present PV penetration level, no system constraint violation is observed in the real-world feeder. Therefore, the rated power of the PV plants is doubled to create a case with high penetration of PV resources. In this case, the unbalance power at t_{mc} is 1000 kW. On the worst case day, the unbalance energy is 5500 kWh. Hence, the values of the power and energy unbalance can be used to determine the size of DES for the first operational objective.

Applying the method proposed in Section 2.2, CDF curves as shown in Figure 2.3 are obtained. In (2.5) and (2.6), if both p and e are set to be 80, then DES systems with power ratings of 475 kW and 300 kW and energy ratings of 275 kWh (35 minutes of storage) and 200 kWh (40 minutes of storage) are chosen for PV plants 1 and 2 respectively. These results are reasonable according to a statement made in [3]: larger megawatt-scale PV installations will need energy storage, which would generally be in the size range of

500 kW to 1 MW or larger with 15 minutes to 1 hour of storage, due to the occurrence of large power output variation.

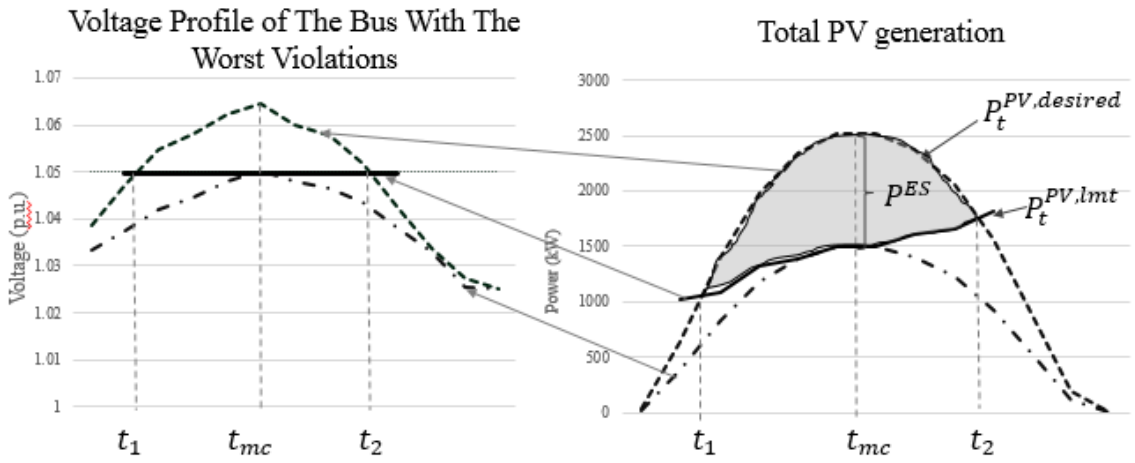

Figure 2.2 Result of DES Sizing for the First Operational Objective

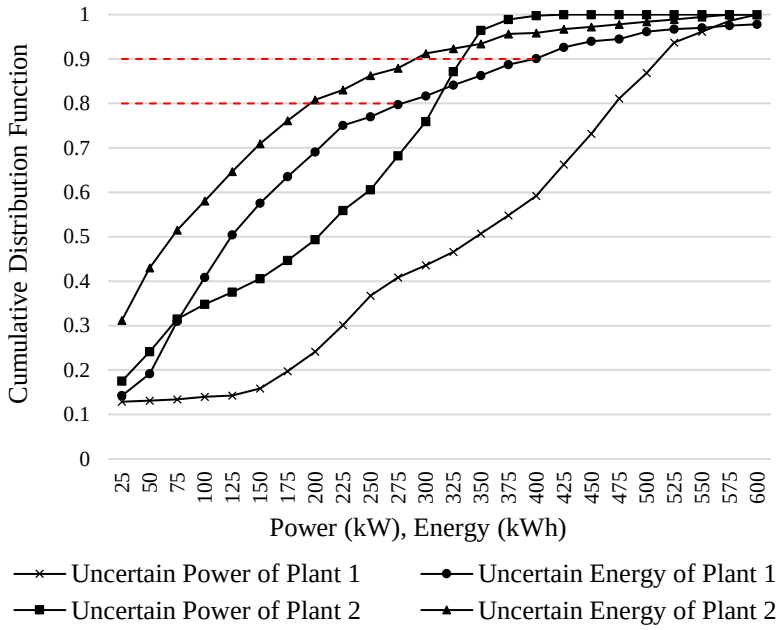

Figure 2.3 CDF Curves of the Uncertain Power and Energy

In fact, this is not the only information provided by the CDF curves. Take PV plant 2 for example, if e = 90 in (2.6), a battery with capacity of 300 kWh is needed. Compared with the case of e = 80, the effectiveness is only increased by about 12%. However, the capacity of the battery needs to be increased by 50%. This kind of information can help the planner make suitable tradeoffs.

With the chosen DES (275 kW, 200 kWh) and a properly designed DES controller at PV plant 2, the uncertainty of active power output on Jan. 11th, 2013 is significantly reduced (as shown in Figure 2.4).

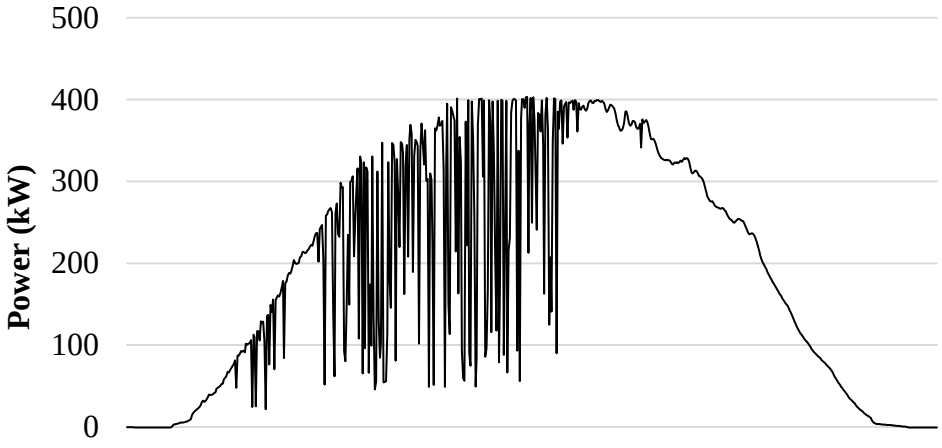

(a) PV Output Curve Without DES

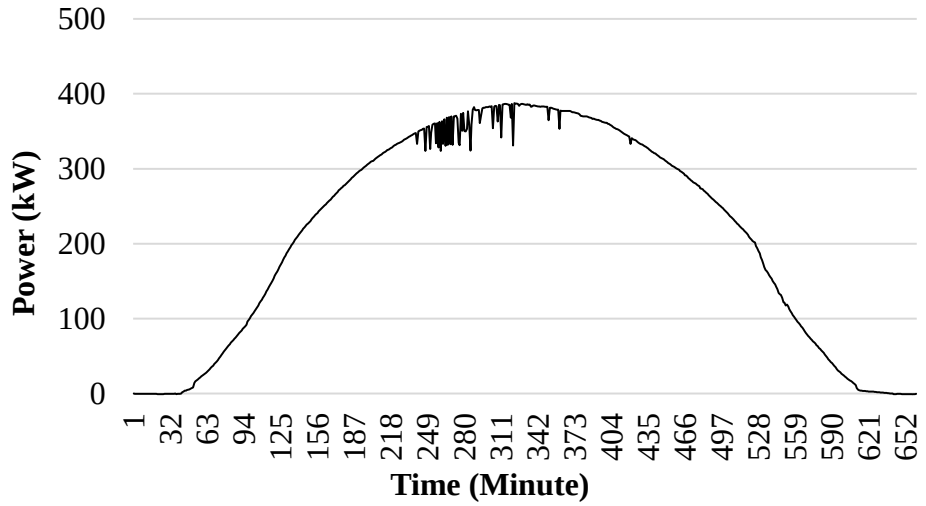

(b) PV Output Curve with DES

Figure 2.4 Active Power Output of PV Plant 2 on Jan. 11th [1].

Chapter 3 MODELING AND NON-CONVEXITY OF THE OPTIMIZATION PROBLEMS

Three decision-making problems are considered in this research. They are the DES optimal allocation (DESOA), the DES optimal scheduling (DESOS), and the smart inverter optimal placement (SIOP). Since the sizing of DES has been completed independently, the resulting DESOA problem is a continuous problem (further explanation is given in Section 2.1). Obviously, the DESOS is a continuous problem while the SIOP is studied as an example of a mixed-integer problem. Therefore, the first two problems are continuous QCQPs while the third one is an MIQCQP.

3.1 Optimal Allocation and Dispatch of DES

The topology of distribution systems is usually radial. Hence, the branch flow model (BFM) where the phase angles of the voltages and currents are ignored is used to describe the AC power flow in radial networks in the optimization model since the BFMs are exact for radial networks [37]. The BFMs proposed in [44] and [45] are equivalent since there is a bijection between them. Bijection means there is a one-to-one correspondence between the solution sets of the two BFMs. Using the branch flow model proposed in [44], the DESOA is described by (3.1)-(3.17) while the DESOS is represented by (3.1)-(3.15),

(**DESOA/DESOS**) $$\min \quad F_1 = \sum_t^T \sum_i^N c_t p_t^{Grid} \tag{3.1}$$

$$\min \quad F_2 = \sum_t^T \left(\sum_i^M r_i \ell_{i,t} + \sum_i^{N_T} k_i v_{i,t} + \sum_i^{N_S} p_{i,t}^{DESloss} \right) \tag{3.2}$$

$$\min \quad F_3 = \sum_t^T \sum_i^N \left(\left| v_{i,t} - v_i^{set} \right| + \varepsilon \sum_i^{NS} p_{i,t}^{DESloss} \right) \tag{3.3}$$

$$\text{s.t.} \quad p_{i,t}^{DCH} + p_{i,t}^{CH} + p_{(i=1),t}^{Grid} + p_{i,t}^{PV} - p_{i,t}^{L} = \sum_{k:i\to k} P_{ik,t} - \left(P_{ji,t} - r_{ij} \ell_{ji,t} \right) \tag{3.4}$$

$$q_{i,t}^{DCH} + q_{i,t}^{CH} + q_{(i=1),t}^{Grid} - q_{i,t}^{L} = \sum_{k:i\to k} Q_{ik,t} - \left(Q_{ji,t} - x_{ij} \ell_{ji,t} \right) \tag{3.5}$$

$$v_{i,t} = v_{j,t} + 2\left(r_{ij} P_{ij,t} + x_{ij} Q_{ij,t} \right) - \left(r_{ij}^2 + x_{ij}^2 \right) \ell_{ij,t} \tag{3.6}$$

$$v_{i,t} \ell_{ij,t} = P_{ij,t}^2 + Q_{ij,t}^2 \tag{3.7}$$

$$0 \le E_i^{spl} - \sum_{t=1}^{t'} \left(\eta_c p_{i,t}^{CH} + p_{i,t}^{DCH} / \eta_d \right) \Delta t \le E_i^{DES} \tag{3.8}$$

$$-P_i^{DES} \le p_{i,t}^{CH} \le 0 \tag{3.9}$$

$$0 \le p_{i,t}^{DCH} \le P_i^{DES} \tag{3.10}$$

$$p_{i,t}^{DESloss} = \left(1/\eta_d - 1 \right) p_{i,t}^{DCH} + \left(1 - \eta_c \right) p_{i,t}^{CH} \tag{3.11}$$

$$P_{ij,t}^2 + Q_{ij,t}^2 \le \overline{S}_{ij}^2 \tag{3.12}$$

$$0 \le \ell_{ij,t} \le \overline{\ell}_{ij} \tag{3.13}$$

$$\underline{v_i} \le v_{i,t} \le \overline{v}_i \tag{3.14}$$

$$-0.6R \le p_t^{Grid}, q_t^{Grid} \le R \tag{3.15}$$

$$\sum_{i=1}^{N} P_i^{ES} = P^{ES} \tag{3.16}$$

$$\sum_{i=1}^{N} E_i^{ES} = E^{ES} \tag{3.17}$$

where $i \in N$, $ij \in E$ and $t \in T$ in (3.4)-(3.7) and (3.12)-(315) while $i \in N$ and $t \in T$ in (3.8)-(3.11), and $t' = 1, ..., 24$. Quantity P^{ES} in (3.16) and E^{ES} in (3.17) are calculated by (2.1)

and (2.2) respectively. Quantities P_i^{ES} and E_i^{ES} ($i \in N$) are variables in the DESOA and they are parameters in DESOS. Quantity ε is an arbitrarily small positive value. The MVA limits of the DES units can be expressed in exactly the same form as (3.12). Hence, (3.12) represents MVA limits of both the feeders and the DES units.

Constraints (3.4)-(3.7) denote the branch flow constraints; (3.4)-(3.6) are linear while (3.7) is quadratic; (3.8)-(3.10) represent the state and rate of charging/discharging constraints of the DES respectively [52]; (3.11) captures the active power losses in the DES units; and (3.12)-(3.15) denote the system constraints. Note that, in the above model, one of (3.12) and (3.13) is redundant due to the relation described in (3.7). However, the equality in (3.7) may not hold in an optimal solution of a convex relaxation. Thus, both (3.12) and (3.13) are retained. (3.16) and (3.17) guarantee that the summation of the ratings of all the units should equal to the total ratings determined in Chapter 2.

Objective function (3.1) represents minimizing purchase cost of grid energy which is analogous to the objective function of minimizing generation cost in OPF problems. Objective functions (3.2) and (3.3) minimize network losses and voltage magnitude deviation respectively. These objective functions are frequently used in reactive power optimization problems [53] and play important roles in distribution system operations. In the variable space, (3.1) and (3.2) are monotonic over the feasible set while (3.3) is not. Based on the operational requirement, only one of the functions in (3.1)-(3.3) will be chosen as the objective function of the required optimization model for the DESOA or the DESOS.

Both (3.1) and (3.2) are linear, and (3.3) which contains the absolute value sign is not. Therefore, before applying the convex relaxations to the DESOS or DESOA problem,

(3.3) needs to be pre-processed to facilitate the convexification. Introducing auxiliary variables $u_{i,t}$ ($i \in Ns$, $t \in T$) which are positive, (3.3) can be reformulated as

$$\min \quad F_3 = \sum_t^T \left(\sum_i^N u_{i,t} + \varepsilon \sum_i^{N_S} p_{i,t}^{DESloss} \right) \tag{3.18}$$

$$-u_{i,t} \le v_{i,t} - v_i^{set} \le u_{i,t} . \quad (i \in N, t \in T) \tag{3.19}$$

Three reformulated DESOA and DESOS models for which the details are given in Table 3.1 and 3.2 respectively are obtained.

Table 3.1 The Reformulated DESOA Models

Notation	DESOA 1	DESOA 2	DESOA 3
Objective function	(3.1)	(3.2)	(3.18)
Constraints	(3.4) - (3.17)	(3.4) - (3.17)	(3.4) - (3.17) and (3.19)

Table 3.2 The Reformulated DESOS Models

Notation	DESOS 1	DESOS 2	DESOS 3
Objective function	(3.1)	(3.2)	(3.18)
Constraints	(3.4) - (3.15)	(3.4) - (3.15)	(3.4) - (3.15) and (3.19)

For the above DESOS models, note the following:

i) In any optimal solution of (**DESOA 2/DESOS 2**), $p_{i,t}^{DCH}$ and $p_{i,t}^{CH}$ cannot be non-zero simultaneously. Suppose that $\bar{\boldsymbol{z}}$ is an optimal solution of (**DESOA 2/DESOS 2**) where both $\bar{p}_{i,t}^{DCH}$ and $\bar{p}_{i,t}^{CH}$ are non-zero and $\bar{p}_{i,t}^{DCH} + \bar{p}_{i,t}^{CH} = K > 0$ ($\bar{p}_{i,t}^{DCH} + \bar{p}_{i,t}^{CH} = K < 0$). There always exists another solution $\hat{\boldsymbol{z}}$ where $\hat{p}_{i,t}^{DCH} = K$ and $\hat{p}_{i,t}^{CH} = 0$ ($\hat{p}_{i,t}^{DCH} = 0$ and $\hat{p}_{i,t}^{CH} = K$). It is easy to show that $\hat{\boldsymbol{z}}$ satisfies (3.4), (3.8)-(3.10) and $\hat{p}_{i,t}^{DESloss} \le \bar{p}_{i,t}^{DESloss}$ which

means $\hat{f}_2 \le \overline{f}_2$. Hence $\hat{\boldsymbol{z}}$ is the optimal solution rather than $\overline{\boldsymbol{z}}$.

ii) In any optimal solution of (**DESOA 1/DESOS 1**), $p_{i,t}^{DCH}$ and $p_{i,t}^{CH}$ also cannot be non-zero simultaneously. From i), it can be observed that the term $\sum_i^{N_S} p_{i,t}^{DESloss}$ in the objective function forces at most one of $p_{i,t}^{DCH}$ and $p_{i,t}^{CH}$ to be non-zero in a specific time interval. In fact, $\sum_i^{N_S} p_{i,t}^{DESloss}$ is concealed in the objective function (3.1) since higher DES losses increase the grid energy consumption. With the second term in (3.18), this conclusion is also valid for (**DESOA 3/DESOS 3**) no matter how small ε is.

iii) Objective function (3.18) is equivalent to (3.3) from an engineering point of view if ε is small enough. Therefore, one can choose an arbitrarily small value for ε so that (3.18) is equivalent to (3.3) in engineering applications.

3.2 Optimal Placement of the Smart Inverter

To determine the minimum total investment of inverters to meet the requirement of volt/VAr regulation, an optimization model is proposed as shown in (3.20)-(3.30) where the AC power flow constraints are considered and the objective function as well as some constraints contain binary variables. This problem is also studied in radial distribution systems. Hence, the BFM proposed in [44] is used to describe the AC power flow,

(**SIOP**)
$$\min \ F_4 = \sum_i \left[c_s S_i^{Invt} + (1-\alpha_i) c_c S_i^{PV} \right] \tag{3.20}$$

$$\text{s.t.} \quad p_{(i=1)}^{Grid} + p_i^{PV} - p_i^L = \sum_{k:i\to k} P_{ik} - \left(P_{ji} - r_{ij} l_{ji} \right) \tag{3.21}$$

$$q_{(i=1)}^{Grid} - q_i^L + q_i^{Invt} = \sum_{k:i\to k} Q_{ik} - \left(Q_{ji} - x_{ij} l_{ji} \right) \tag{3.22}$$

$$v_i = v_j + 2\left(r_{ij}P_{ij} + x_{ij}Q_{ij}\right) - \left(r_{ij}^2 + x_{ij}^2\right)\ell_{ij} \tag{3.23}$$

$$v_i \ell_{ij} = P_{ij}^2 + Q_{ij}^2 \tag{3.24}$$

$$\left(q_i^{Invt}\right)^2 + \left(p_i^{PV}\right)^2 \le \left(S_i^{Invt}\right)^2 + (1-\alpha_i)\left(S_i^{PV}\right)^2 \tag{3.25}$$

$$-S_i^{Invt} \le q_i^{Invt} \le S_i^{Invt} \tag{3.26}$$

$$\alpha_i S_i^{PV} \le S_i^{Invt} \le \alpha_i M \tag{3.27}$$

$$P_{ij,t}^2 + Q_{ij,t}^2 \le \bar{S}_{ij}^2 \tag{3.28}$$

$$0 \le \ell_{ij,t} \le \bar{\ell}_{ij} \tag{3.29}$$

$$\underline{v}_i \le v_{i,t} \le \bar{v}_i \tag{3.30}$$

$$-0.6R \le p_t^{Grid}, q_t^{Grid} \le R \tag{3.31}$$

where the objective function represents minimizing the total investment of inverters in the system (including smart inverters and regular inverters); (3.21)-(3.24) denote the branch flow constraints where (3.21)-(3.23) are linear and (3.24) is quadratic; (3.25) and (3.26) represent the reactive capability constraints for the smart inverters which are quadratic inequalities and it is designed based on the research result of [18]; (3.27) is the yes/no constraints for installing a smart PV inverter; (3.28)-(3.31) denote the system constraints. (3.26) is dominated by (3.25) when $\alpha_i = 1$ and conversely dominates (3.25) when $\alpha_i = 0$. The SIOP is an MIQCQP problem.

3.3 Analysis of the Non-convexity

In the DESOA/DESOS, the non-convexity comes from the quadratic equality (3.7). The non-convexity of the SIOP stems from the quadratic equality (3.24) and inequality (3.25), and the integer variable α_i. In this report, the non-convexity caused by the integer

variables is handled by the branch and bound (B&B) algorithm where the integer variables are treated as certain values in each node problem. The node problems of a B&B algorithm are continuous, which means the non-convexity caused by the integer variables is avoided. This research mainly aims at eliminating the non-convexity introduced by the non-convex quadratic constraints, especially the AC power flow constraint (3.7)/(3.24).

Chapter 4 NON-ITERATIVE ENHANCED SDP RELAXATIONS

Limitations of the existing convex relaxation techniques, e.g. the SOCP relaxation are studied in this chapter. Then, some convex constraints proposed in the analytical optimization literature are introduced to construct a tighter convex relaxation named as the enhanced SDP (ESDP) relaxation in a non-iterative framework.

4.1 Second Order Cone Programming Relaxation

To convexify constraint (3.7)/(3.24) which is an equality constraint, a crucial step is to relax it into an inequality constraint (4.1). However, (4.1) is still non-convex. By re-arranging (4.1), one can obtain a second order cone constraint (SOCC) as shown in (4.2). The idea of relaxing the quadratic equality constraints in a branch flow model to inequality constraints to yield an SOCC was first proposed in [55],

$$v_{i,t}\ell_{(i,j),t} \geq P^2_{(i,j),t} + Q^2_{(i,j),t} \tag{4.1}$$

$$\left\| \begin{matrix} \sqrt{2}P_{ij,t} \\ \sqrt{2}Q_{ij,t} \\ v_{i,t} \\ \ell_{ij,t} \end{matrix} \right\|_2 \leq \begin{bmatrix} 0 & 0 & 1 & 1 \end{bmatrix} \begin{bmatrix} \sqrt{2}P_{ij,t} \\ \sqrt{2}Q_{ij,t} \\ v_{i,t} \\ \ell_{ij,t} \end{bmatrix}. \tag{4.2}$$

In a similar way, (3.12)/(3.28) can be rearranged as

$$\left\| \begin{matrix} P_{ij,t} \\ Q_{ij,t} \end{matrix} \right\|_2 \leq \bar{S}_{ij} \tag{4.3}$$

which is also an SOCC.

It is difficult to reformulate (3.25) which is a non-convex quadratic equality as an SOCC. Consequently, the SOCP relaxation is not applicable to the SIOP. This section only addresses the application of the SOCP relaxation to the DESOA/DESOS problems.

4.1.1 Discussion on Sufficient Condition for Exactness of the SOCP Relaxation

***Proposition 4.1* (*sufficient condition*):** The SOCP relaxation for **DESOA_1/ DESOA_2** is exact if there is sufficient controllable injection at each bus.

Under the condition stated in the above proposition, one can prove by contradiction that optimal solutions of the SOCP relaxation for DESOA_1/DESOA_2 are located on the boundary of SOCC using the procedure shown in Figure 4.1. In other words, the SOCP relaxation for optimization problems of DESOA_1/DESOA_2 is exact. The equalities $h_i(\boldsymbol{\varepsilon}) = 0$ ($i = 1, \ldots, n$) and inequalities $g_i(\boldsymbol{\varepsilon}) \geq 0$ 0 ($i = 1, \ldots, m$) reflect a property that $\boldsymbol{x}'$ is closer to the boundary of SOCC than $\boldsymbol{x}^*$ in the feasible set of solutions for the SOCP problem. $f(\boldsymbol{x}') < f(\boldsymbol{x}^*)$ means that $\boldsymbol{x}^*$ is not the optimal solution of the SOCP. For a given solution $\boldsymbol{x}^*$, one can always find a better solution $\boldsymbol{x}'$ which is closer to the boundary of the SOCC until $\boldsymbol{x}^*$ locates on the boundary of SOCC, if the conditions shown in Figure 4.1 hold. A complete proof of Proposition 4.1 is given in Appendix A. In parallel, a similar conclusion to Proposition 4.1 has been obtained in [56] by using the injection region method.

Obviously, the optimal allocation problem of DES satisfies the condition in proposition 4.1 since it is assumed that there is DES, which is a controllable injection, at each bus. In the optimal dispatch problem, the locations of DES are obtained by solving the allocation problem. It means that there may not be controllable injection at some of the buses, namely, the condition does not hold. The simulation results (see Section 6.1) show

that the SOCP relaxation for some cases of DESOS_1/ DESOS_2 is also exact, even though the condition in proposition 4.1 is not satisfied.

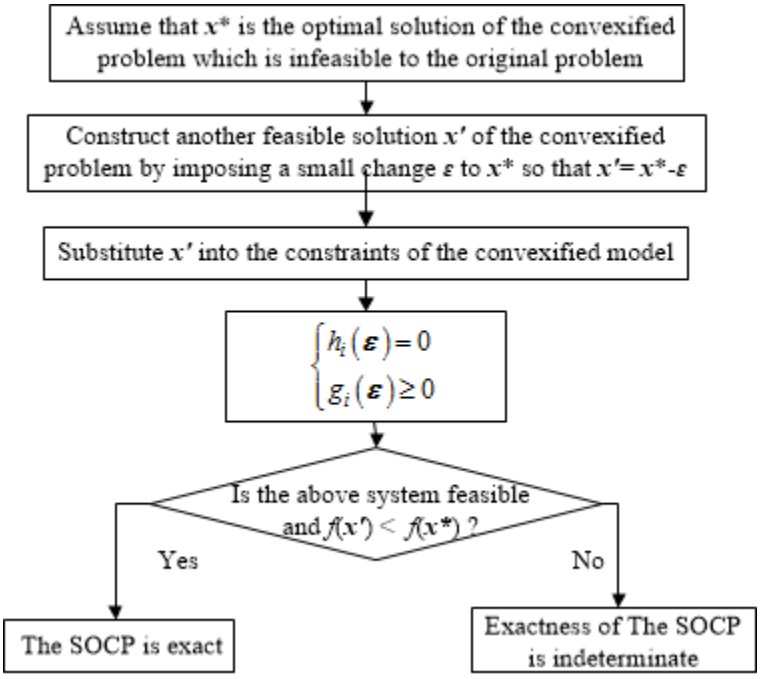

Figure 4.1 Flow Charts for Verifying the Exactness of the SOCP Relaxation

4.1.2 The Necessary and Sufficient Condition for Exactness

Like proposition 4.1, in [21], [22], [56] and the references therein, the authors provided their own sufficient conditions for exactness of the SOCP relaxation in terms of their chosen objective functions. These sufficient conditions are based on network assumptions which are basically not practical for most of the actual power systems. In fact, it is still very hard to analytically verify the exactness of the SOCP relaxation under actual network conditions. To deepen the understanding of the SOCP relaxation, the necessary and sufficient condition for the exactness of SOCP relaxation is discussed in this subsection.

Definition 4.1: among the linear constraints that form the boundary of the feasible

set of the SOCP problem under study, those that intersect the second order cone constraints are defined as the second order cone constraint neighboring linear constraint (SOCCNLC, as shown in Figure 4.2).

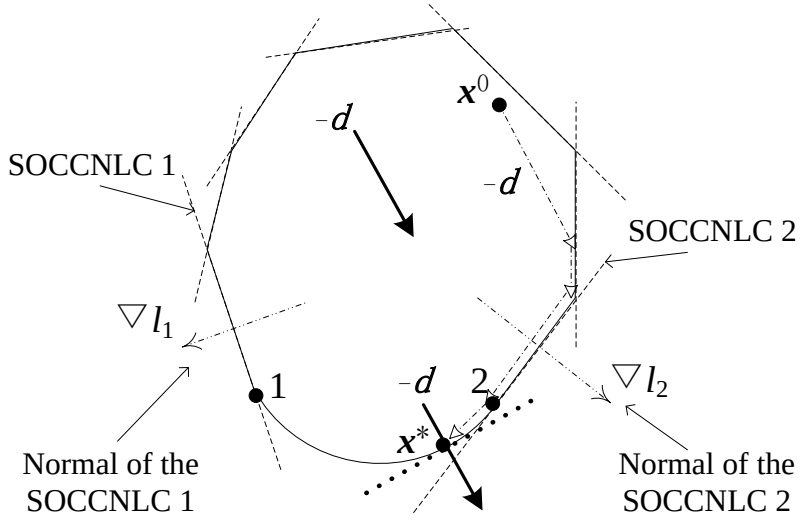

Figure 4.2 An Example of the Sufficient and Necessary Condition.

If the objective function is nonlinear, it should at least be convex and monotone in the feasible set so that the optimization problem can be converted to the standard SOCP where the objective function is linear. A linear objective function $\boldsymbol{d}^T\boldsymbol{x}$ specifies a vector field $-\boldsymbol{d}$ in the variable space.

***Proposition 4.2 (Necessary and sufficient condition)*:** the SOCP relaxation is exact, if and only if $\boldsymbol{d}$ satisfies

$$\Phi_i = \left\{-\gamma_0 \nabla s(\boldsymbol{x}_i) - \sum\nolimits_j \gamma_j \nabla l_j \,\middle|\, s(\boldsymbol{x}_i) = 0, \forall \boldsymbol{x}_i \in \Omega, \forall j\right\} \text{ and } \boldsymbol{d} = \left\{\boldsymbol{d} \,\middle|\, \boldsymbol{d} \in \bigcup\nolimits_{\forall i} \Phi_i\right\}, \quad (4.4)$$

where $s(\boldsymbol{x}) = 0$ represents the equation of SOCC and $l_j(\boldsymbol{x})$ is the expression of the jth active SOCCNLC for a given feasible solution $\boldsymbol{x}_i$. $l_j(\boldsymbol{x})$ is active for $\boldsymbol{x}_i$ means $l_j(\boldsymbol{x}_i) = 0$. Ω is the feasible set of the SOCP. γ_0 is an arbitrary positive scalar. γ_j is an arbitrary positive scalar

(zero) when $\nabla l_j(\boldsymbol{x}_i) = 0$ ($\nabla l_j(\boldsymbol{x}_i) \neq 0$). ∇l_j and $\nabla s(\boldsymbol{x})$ which are normal vectors of SOCCNLCs and SOCC respectively point out of the feasible set.

The proof of Proposition 4.2 is given in Appendix B. Note that, for the SOCP relaxation of a power system optimization problem, there always exist SOCCNLCs in (4.4) due to the existence of linear equality constraints in BFM. Generally, there are multiple SOCCs in a SOCP relaxation for a power system optimization and each SOCC relates to only a small portion of the variables. For instance, (4.2) is an SOCC that is about only four of the variables. In the sub-space of the variables which are contained in an SOCC, the SOCC can be used independently in (4.4) to determine the feasible direction of the corresponding portion of $\boldsymbol{d}$. For example, let $\boldsymbol{d}_1$ be the portion of $\boldsymbol{d}$ that relates to sub-variable space in (4.2), then $s(\boldsymbol{x})$ in (4.4) is (4.2) which can be used to determine the feasible direction of $\boldsymbol{d}_1$. For a given $\boldsymbol{d}$ that is required to make the SOCP relaxation exact, all of its portions should satisfy (4.4) determined by their corresponding SOCCs respectively.

Proposition 4.2 reveals an inherent limitation of the SOCP relaxation. In other words, the objective function should: 1) be convex and monotone over the feasible set; 2) satisfy (4.4). For a given system, the selected objective function may not satisfy these conditions, for instance the objective function (14) in [53] which minimizes the deviation of voltage profiles. In this case, the SOCP relaxation is invalid. Figure 4.2 provides an intuitive understanding of the sufficient and necessary condition. However, it is still inconvenient to use this condition to verify exactness of the SCOP relaxation since it is very hard to figure out the SOCCNLCs for a system whose bus number is higher than 3.

4.1.3 An Illustrative Example of DESOS

This subsection studies the impact of objective functions on the efficiency of the SOCP relaxations for the DESOS problems through an illustrative example. A 2-bus, 1-line, three-phase system as shown in Figure 4.3 is designed, where bus 1 is assumed to be an infinite bus. The variables and parameters of this simple system are defined in Table IV. For the sake of simplicity, the charging/discharging efficiency are considered to be 100% and the charging/discharging power are represented by one variable in this simple example.

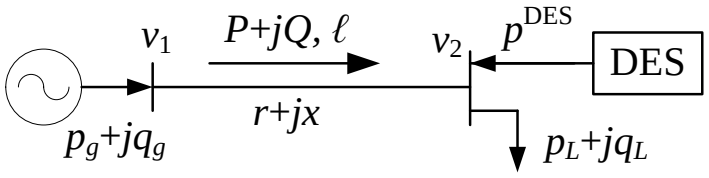

Figure 4.3 Topology of the Simple System.

The branch AC power flow model of this system is given as:

$$\begin{cases} p_g = P, q_g = Q \\ p_L - p^{DES} = P - r\ell, q_L = Q - x\ell \\ v_1 - v_2 = 2rP + 2xQ - \left(r^2 + x^2\right)\ell \\ P^2 + Q^2 = v_1\ell \end{cases}. \tag{4.5}$$

Eliminating the branch powers P and Q, the projections of the feasible set of (4.5) onto the (p_g, p^{DES}), (ℓ, p^{DES}) and (v_2, p^{DES}) spaces are shown in Figure 4.4, Figure 4.5 and Figure 4.6 respectively.

In the following figures, the feasible sets of the SOCP relaxation are described by the shaded regions. The black boundaries of these shaded regions are the feasible sets of the original DESOS problem. The curves are marked with the constraints they represent.

The optimal solutions of the SOCP relaxation and the original problem are denoted by a circle and a solid diamond respectively in the figures. In Figure 4.4, a case of negative LMPs is taken into account since negative LMPs may occur due to some reasons in actual power systems, for example congestion on transmission lines.

Table 4.1 The Parameters of the 2-bus System.

Type	Symbol	Bounds/Values
Variable	ℓ	0 to 0.22 p.u.
Variable	v_2	0.9 to 1.1 p.u.
Variable	p_g	-12 MW to 20 MW
Variable	q_g	-9 MVAr to 15 MVAr
Variable	p^{DES}	-10 MW to 10 MW
Parameter	v_1	1.04^2=1.0816 p.u.
Parameter	$r+jx$	10+j4 ohm
Parameter	p_L+jq_L	10+j6 MVA
Parameter	Nominal voltage	12.47 kV
Parameter	Power base	100 MVA

In Figure 4.4, when the LMP is positive, the descent direction of objective function F_1 is denoted by the black arrow. In this case, the optimal solutions of the SOCP relaxation and the original problem are identical, which means the SOCP relaxation is exact. When the LMP is negative, the SOCP relaxation of this case is not exact.

In Figure 4.5, since the charging/discharging efficiency of the DES are assumed to be 100% and no transformers are taken into account, the only term in objective function F_2 is $r\ell$ whose descent direction is denoted by the grey arrow. The SOCP relaxation of this case is exact.

In Figure 4.6, Objective function F_3 is not monotonic over the feasible set, hence its descent directions are represented by the grey arrows. The optimal solution of the original problem is denoted by the grey diamond while that of the SOCP relaxation is not unique and denoted by the grey cylinder. Therefore, the SOCP relaxation of this case is most likely not exact.

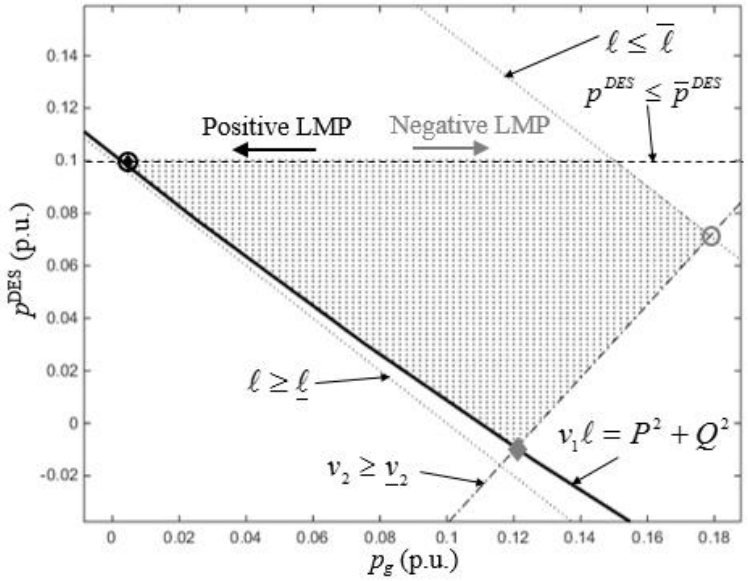

Figure 4.4 The Projection of the Feasible Set of (4.5) onto the (p_g, p^{DES})-space.

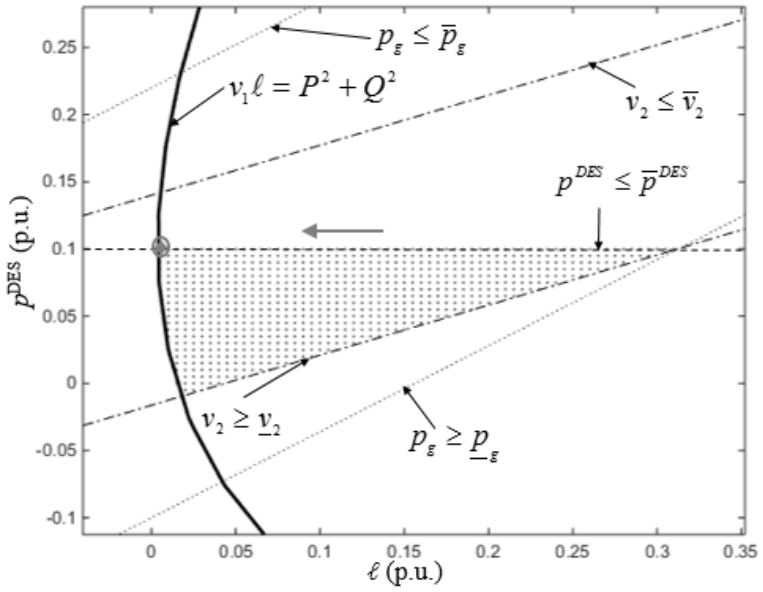

Figure 4.5 The Projection of the Feasible Set of (4.5) onto the (ℓ, p^{DES})-space.

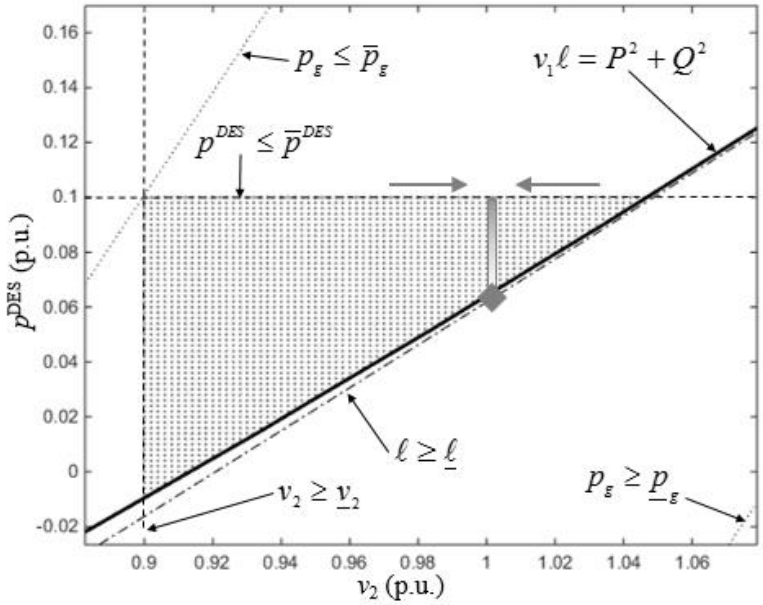

Figure 4.6 The Projection of the Feasible Set of (4.5) onto the (v_2, p^{DES})-space.

4.1.4 Observation and Discussion

From this illustrative example, the following observations are made:

a) The SOCP relaxation offers a convex superset, a portion of whose boundaries is the feasible set of the original non-convex problem. An exact globally optimal solution of the original problem can be achieved if the objective function is monotonic over the feasible set and its descent direction points to this part of boundaries. For a given DESOS problem, there is a specific range of descent directions under which its SOCP relaxation is exact. A mathematical description of such a range of descent directions is given in Proposition 4.2.

b) For an objective function which does not satisfy Proposition 4.2, an unsatisfactory solution may result, e.g. the negative LMP case in Figure 4.4. The bounds of some variables also affect the exactness of the SOCP relaxation, for more details please refer to [40]. In fact, the state of charging/discharging constraint (3.8) may also affect the exactness of the SOCP relaxation for the DESOS problems.

c) The feasible set of the original non-convex problem is not necessarily a part of the boundaries of the convex superset offered by the basic SDP relaxation. As shown in [38], the SOCP relaxation of the branch AC power flow equalities (3.7)/(3.24) (as shown in (4.2)) is tighter than the basic SDP relaxation (please see the next section). As a result, for some potential objective functions of the DESOS problems for which the SOCP relaxation does not work well, the basic SDP relaxation may also be ineffective. Alternative convex relaxations are required to achieve a better solution when these objective functions are adopted to meet some specific operational requirements.

4.2 Basic Semidefinite Programming Relaxation

The SDP relaxation is a promising convex relaxation that has been successfully

applied to some large-scale OPF problems [57]. Many well-known algorithms with uniform frameworks have been exploited [58]. It is adopted to convexify the DESOS cases for which the SOCP relaxation is not exact and the SIOP. Note that, in this report, a convex relaxation for a non-convex problem is defined to be exact if the optimal solution obtained by solving the convexified problem is a feasible solution of the original non-convex problem. This section introduces the basic SDP relaxation for the DESOS and SIOP algorithms in radial networks.

For the DESOS cases, let $\boldsymbol{x}_t := [\boldsymbol{P}_t^{\mathrm{T}}\ \boldsymbol{Q}_t^{\mathrm{T}}\ \boldsymbol{v}_t^{\mathrm{T}}\ \boldsymbol{\ell}_t^{\mathrm{T}}]^{\mathrm{T}}$ and $\boldsymbol{y}_t := [\boldsymbol{p}_t^{\mathrm{DCH\ T}}\ \boldsymbol{p}_t^{\mathrm{CH\ T}}\ \boldsymbol{p}_t^{\mathrm{DESloss\ T}}\ p_t^{\mathrm{Grid}}\ q_t^{\mathrm{Grid}}\ \boldsymbol{u}_t^{\mathrm{T}}]^{\mathrm{T}}$ ($t \in T$). And, for the SIOP case, let $\boldsymbol{x}_t := [\boldsymbol{P}_t^{\mathrm{T}}\ \boldsymbol{Q}_t^{\mathrm{T}}\ \boldsymbol{v}_t^{\mathrm{T}}\ \boldsymbol{\ell}_t^{\mathrm{T}}\ \boldsymbol{S}^{\mathrm{Invt\ T}}\ \boldsymbol{q}^{\mathrm{Invt\ T}}]^{\mathrm{T}}$ and $\boldsymbol{y}_t := [p_t^{\mathrm{Grid}}\ q_t^{\mathrm{Grid}}\ \boldsymbol{\alpha}^{\mathrm{T}}]^{\mathrm{T}}$ ($t = 1$). The auxiliary semidefinite variables $\boldsymbol{X}_t$ are defined in terms of $\boldsymbol{x}_t$. A general formulation which can be used to describe the BSDP relaxation for all DESOS and SIOP models is given as follow ($t \in T$):

(**BSDP**)

$$\min\ F(\boldsymbol{x}_t, \boldsymbol{y}_t) = \boldsymbol{c}_0^T \boldsymbol{x}_t + \boldsymbol{d}_0^T \boldsymbol{y}_t \tag{4.6}$$

$$\text{s.t. } tr(\boldsymbol{Q}_i \boldsymbol{X}_t) = 0\ \ (i \in S_{\mathrm{QE}}) \tag{4.7}$$

$$tr(\boldsymbol{Q}_i \boldsymbol{X}_t) \le b_i\ \ (i \in S_{\mathrm{QI}}) \tag{4.8}$$

$$\boldsymbol{c}_i^T \boldsymbol{x}_t = b_i\ \ (i \in S_{\mathrm{LE1}}) \tag{4.9}$$

$$\boldsymbol{c}_i^T \boldsymbol{x}_t + \boldsymbol{d}_i^T \boldsymbol{y}_t = b_i\ \ (i \in S_{\mathrm{LE2}}) \tag{4.10}$$

$$\boldsymbol{c}_i^T \boldsymbol{x}_t + \boldsymbol{d}_i^T \boldsymbol{y}_t \le b_i\ \ (i \in S_{\mathrm{LI}}) \tag{4.11}$$

$$\left(\max\{0, \underline{x}_i\}\right)^2 \le X_{ii,t} \le \max\left\{\underline{x}_i^2, \bar{x}_i^2\right\} \tag{4.12}$$

$$\begin{bmatrix} 1 & \boldsymbol{x}_t^T \\ \boldsymbol{x}_t & \boldsymbol{X}_t \end{bmatrix} \succeq 0 \tag{4.13}$$

where $tr(\cdot)$ denotes the trace of a matrix, (4.12) are valid bounds on the diagonal entries of

$\boldsymbol{X}_t$, and (6h) is the well-known Shor's inequality [58]. S_{QE}, S_{QI} and S_{LI} denote the sets of quadratic equalities, quadratic inequalities and linear inequalities respectively. S_{LE1} and S_{LE2} are the first and second sets of linear equalities respectively. The correspondence between the constraints in (BSDP) and those in (DESOA), (DESOS) and (SIOP) are given in Table 4.2, Table 4.3 and Table 4.4 respectively.

Table 4.2 The Correspondence between Constraints in (BSDP) and (DESOA).

In (BSDP)	In (DESOA)
(4.6)	(3.1), (3.2) or (3.18)
(4.7)	(3.7)
(4.8)	(3.12)
(4.9)	(3.4) and (3.5) for the buses which are not the substation bus or the DES-connected buses, and (3.6)
(4.10)	(3.4) and (3.5) for the substation bus and the DES-connected buses, (3.11), (3.16) and (3.17)
(4.11)	(3.8)-(3.10), (3.13)-(3.15) and (3.19)

Table 4.3 The Correspondence between Constraints in (BSDP) and (DESOS).

In (BSDP)	In (DESOS)
(4.6)	(3.1), (3.2) or (3.18)
(4.7)	(3.7)
(4.8)	(3.12)
(4.9)	(3.4) and (3.5) for the buses which are not the substation bus or the DES-connected buses, and (3.6)
(4.10)	(3.4) and (3.5) for the substation bus and the DES-connected buses, and (3.11)
(4.11)	(3.8)-(3.10), (3.13)-(3.15), and (3.19)

Table 4.4 The Correspondence between Constraints in (BSDP) and (SIOP).

In (BSDP)	In (SIOP)
(4.6)	(3.20)
(4.7)	(3.24)
(4.8)	(3.25) and (3.28)
(4.9)	(3.21) and (3.22) for the buses which are not the substation bus or the DES-connected buses, and (3.23)
(4.10)	(3.21) and (3.22) for the substation bus and the DES-connected buses, (3.11), (3.16) and (3.17)
(4.11)	(3.26), (3.27) and (3.29)-(3.31)

4.3 Non-iterative Enhanced SDP Relaxations

In this section, some convex constraints which can be used to approximate the rank-1 constraint $\boldsymbol{X} = \boldsymbol{x}\boldsymbol{x}^{\mathrm{T}}$ are introduced to construct ESDP relaxations in the non-iterative framework for the DESOS problems. One primary objective of this research is to obtain, through numerical comparison, tighter but computationally effective non-iterative ESDP relaxations for the DESOS problems.

4.3.1 Rank-2 Linear Inequalities

Stemming from pairwise products of the linear inequalities in (4.11) where $\boldsymbol{d}_i^{\mathrm{T}} = \boldsymbol{0}$, the following relations are implicit in problems (DESOA), (DESOS) and (SIOP),

$$\begin{cases} (x_i - \underline{x}_i)(x_j - \underline{x}_j) \geq 0 \\ (x_i - \underline{x}_i)(x_j - \overline{x}_j) \leq 0 \\ (x_i - \overline{x}_i)(x_j - \underline{x}_j) \leq 0 \\ (x_i - \overline{x}_i)(x_j - \overline{x}_j) \geq 0 \\ (x_i - \underline{x}_i)(\boldsymbol{c}_j^T \boldsymbol{x} - b_j) \leq 0 \\ (x_i - \overline{x}_i)(\boldsymbol{c}_j^T \boldsymbol{x} - b_j) \geq 0 \\ (\boldsymbol{c}_i^T \boldsymbol{x} - b_i)(\boldsymbol{c}_j^T \boldsymbol{x} - b_j) \geq 0 \end{cases} . \tag{4.14}$$

Rearranging (4.14) and replacing the quadratic terms $x_i x_j$ with X_{ij} results in

$$\begin{cases} \boldsymbol{X} \geq \boldsymbol{x}\overline{\boldsymbol{x}}^{\mathrm{T}} + \overline{\boldsymbol{x}}\boldsymbol{x}^{\mathrm{T}} - \overline{\boldsymbol{x}}\overline{\boldsymbol{x}}^{\mathrm{T}} \\ \boldsymbol{X} \geq \boldsymbol{x}\underline{\boldsymbol{x}}^{\mathrm{T}} + \underline{\boldsymbol{x}}\boldsymbol{x}^{\mathrm{T}} - \underline{\boldsymbol{x}}\underline{\boldsymbol{x}}^{\mathrm{T}} \\ \boldsymbol{X} \leq \boldsymbol{x}\underline{\boldsymbol{x}}^{\mathrm{T}} + \overline{\boldsymbol{x}}\boldsymbol{x}^{\mathrm{T}} - \underline{\boldsymbol{x}}\overline{\boldsymbol{x}}^{\mathrm{T}} \end{cases}, \tag{4.15}$$

$$\begin{cases} \boldsymbol{X}\boldsymbol{c}_i - b_i\boldsymbol{x} + b_i\underline{\boldsymbol{x}} - \underline{\boldsymbol{x}}\boldsymbol{x}^T\boldsymbol{c}_i \leq 0 \\ \boldsymbol{X}\boldsymbol{c}_i - b_i\boldsymbol{x} + b_i\overline{\boldsymbol{x}} - \overline{\boldsymbol{x}}\boldsymbol{x}^T\boldsymbol{c}_i \geq 0 \\ \boldsymbol{c}_i^T\boldsymbol{X}\boldsymbol{c}_j - (b_i\boldsymbol{c}_j^T + b_j\boldsymbol{c}_i^T)\boldsymbol{x} + b_i b_j \geq 0 \end{cases} . \tag{4.16}$$

Constraints (4.15) and (4.16) are often referred to as valid rank-2 linear inequalities [60]. (4.15) are the well-known “reformulation-linearization technique” (RLT) [61] which

originate from pairwise products of the bound constraints. In fact, the RLT stems from replacing the quadratic terms in the McCormick inequalities [62] with $\boldsymbol{X}$, where the McCormick inequalities are pairwise products of the bound constraints on $\boldsymbol{x}$. The RLT itself is a convex relaxation of a QCQP problem. The matrix $\boldsymbol{X}$ is not required to be positive semidefinite in a pure RLT relaxation. Note that, (4.12) is redundant when the R2LIs are used, since (4.12) are the diagonal minors of (4.15). There exist bound constraints on $\boldsymbol{x}$ in (DESOA), (DESOS) and (SIOP) hence, the RLTs are valid for generating the non-iterative ESDP relaxation of (DESOA), (DESOS) and (SIOP).

4.3.2 Valid Linear Equalities

Pre-multiplying the linear equalities in (4.9) by $\boldsymbol{x}$ and replacing the quadratic terms with $\boldsymbol{X}$ results in

$$\boldsymbol{X}\boldsymbol{c}_i = b_i\boldsymbol{x} \qquad (1 \le i \le n). \tag{4.17}$$

Replacing the quadratic terms in the pairwise products of the linear equalities in (4.9) with $\boldsymbol{X}$, the following valid linear equalities (VLE) are obtained.

$$\boldsymbol{c}_i^T\boldsymbol{X}\boldsymbol{c}_j - \left(b_i\boldsymbol{c}_j^T + b_j\boldsymbol{c}_i^T\right)\boldsymbol{x} + b_ib_j = 0 \quad (1 \le i \le j \le n) \tag{4.18}$$

$$\boldsymbol{c}_i^T\boldsymbol{X}\boldsymbol{c}_j = b_ib_j \quad (1 \le i \le j \le n). \tag{4.19}$$

Linear equalities (4.17)-(4.19) have been used to tighten the SDP relaxation for small-scale general quadratically constrained quadratic programming (QCQP) problems which contain linear equality constraints [63] and [64]. Constraint (4.18) is equivalent to (4.19) and tighter than (4.17) since (4.18) and (4.19) are equivalent to (4.17) when $i = j$. When $i = j$, constraint (4.18) becomes $\boldsymbol{c}_i^{\mathrm{T}}\boldsymbol{X}\boldsymbol{c}_i - 2b_i\boldsymbol{c}_i^{\mathrm{T}}\boldsymbol{x} + b_i^2 = 0$. Due to the Shor's inequality in (4.13), $0 = \boldsymbol{c}_i^{\mathrm{T}}\boldsymbol{X}\boldsymbol{c}_i - 2b_i\boldsymbol{c}_i^{\mathrm{T}}\boldsymbol{x} + b_i^2 \ge \boldsymbol{c}_i^{\mathrm{T}}\boldsymbol{x}\boldsymbol{x}^{\mathrm{T}}\boldsymbol{c}_i - 2b_i\boldsymbol{c}_i^{\mathrm{T}}\boldsymbol{x} + b_i^2 = (\boldsymbol{c}_i^{\mathrm{T}}\boldsymbol{x} - b_i)^2$, which means $\boldsymbol{c}_i^{\mathrm{T}}\boldsymbol{x}$

- $b_i = 0$. Thus, (4.9) is redundant if (4.18) is adopted in the ESDP relaxation of (DESOA), (DESOS) and (SIOP).

Proposition 4.3. The ESDP relaxation including (4.18) for (DESOA), (DESOS) and (SIOP) is equivalent to the original problems respectively if matrix $\boldsymbol{C}$ which consists of the coefficient vector $\boldsymbol{c}_i$ ($i \in S_{\mathrm{LE}}$) of the linear equalities is a full-rank matrix.

The proof of Proposition 4.3 is given in Appendix C. Note that, usually, the matrices $\boldsymbol{C}$s for the DESOA, DESOS and SIOP problems is not full-rank since $|S_{\mathrm{LE}}| < n$. Generally, the higher the rank of $\boldsymbol{C}$, the tighter the resulting ESDP relaxation is. In general, (4.18) is preferred for obtaining tight convex relaxations for (DESOA), (DESOS) and (SIOP).

4.3.3 Semidefinite Inequality_1

Constraint (3.12)/(3.28) is a convex quadratic which can be rewritten in the following general form

$$\boldsymbol{x}_t^T \boldsymbol{A}_{ij,t} \boldsymbol{x}_t \le \bar{\boldsymbol{S}}_{ij}^2 \quad (ij \in M,\, t \in T) \tag{4.20}$$

where $\boldsymbol{A}_{ij,t}$ is an $n \times n$ matrix (n is the size of the vector $\boldsymbol{x}_t$ defined in Section 4.2) and the only non-zero entries of $\boldsymbol{A}_{ij,t}$ are the two diagonal entries corresponding to $P_{ij,t}$ and $Q_{ij,t}$. Based on the Schur complement condition for positive definiteness [65], (4.20) can be further reformulated as

$$\begin{bmatrix} & & P_{ij,t} \\ & \boldsymbol{I}_2 & Q_{ij,t} \\ P_{ij,t} & Q_{ij,t} & \bar{S}_{ij}^2 \end{bmatrix} \succeq 0\,, \; (ij \in M,\, t \in T) \tag{4.21}$$

where $\boldsymbol{I}_2$ is a 2×2 identity matrix.

4.3.4 Semidefinite Inequality_2

The constraints in (3.13)/(3.29) and (3.14)/(3.30) can be reformulated as

$$\begin{cases} v_{i,t} - \underline{v}_i \geq 0 \\ \overline{v}_i - v_{i,t} \geq 0 \\ \ell_{ij,t} - \underline{\ell}_{ij} \geq 0 \\ \overline{\ell}_{ij} - \ell_{ij,t} \geq 0 \end{cases} \quad (i \in N,\ ij \in M). \tag{4.22}$$

Multiplying (4.21) by the first term of (4.22) for instance, the following semidefinite inequality is obtained

$$\begin{bmatrix} v_{i,t} - \underline{v}_i & 0 & P_{ij,t} v_{i,t} - P_{ij,t} \underline{v}_i \\ 0 & v_{i,t} - \underline{v}_i & Q_{ij,t} v_{i,t} - Q_{ij,t} \underline{v}_i \\ P_{ij,t} v_{i,t} - P_{ij,t} \underline{v}_i & Q_{ij,t} v_{i,t} - Q_{ij,t} \underline{v}_i & \overline{S}_{ij}^2 v_{i,t} - \overline{S}_{ij}^2 \underline{v}_i \end{bmatrix} \succeq 0 \text{ , } (i \in N,\ ij \in M,\ t \in T). \tag{4.23}$$

Replacing the quadratic terms in (4.23) with the corresponding entries of $\boldsymbol{X}_t$ yields

$$\begin{bmatrix} v_{i,t} - \underline{v}_i & 0 & X_{(P_{ij,t} v_{i,t})} - P_{ij,t} \underline{v}_i \\ 0 & v_{i,t} - \underline{v}_i & X_{(Q_{ij,t} v_{i,t})} - Q_{ij,t} \underline{v}_i \\ X_{(P_{ij,t} v_{i,t})} - P_{ij,t} \underline{v}_i & X_{(Q_{ij,t} v_{i,t})} - Q_{ij,t} \underline{v}_i & \overline{S}_{ij}^2 v_{i,t} - \overline{S}_{ij}^2 \underline{v}_i \end{bmatrix} \succeq 0 \text{ , } (i \in N,\ ij \in M,\ t \in T). \tag{4.24}$$

For a general description of the semidefinite inequalities in (4.24), please refer to [66]. In fact, inequalities (4.23) are implicitly contained in (DESOA), (DESOS) and (SIOP) since a given ($P_{ij,t}$, $Q_{ij,t}$, $v_{ij,t}$) that satisfies (3.13)/(3.29) and (3.14)/(3.30) will also satisfy (4.23). As a result, (4.24) in conjunction with (3.14)/(3.30) and (4.21) which is equivalent to (3.12)/(3.28) offers strong approximations to the relations that $X_{(Pij,tvij,t)} = P_{ij,t}v_{ij,t}$ and $X_{(Qij,tvij,t)} = Q_{ij,t}v_{ij,t}$.

The left hand side of (4.24) includes 3×3-dimensional matrices which make constraints (4.24) easy to handle computationally. Note that each term in (4.22) can be multiplied by (4.21) to generate a semidefinite inequality which is similar to (4.24). Therefore, the complete form of (4.24) can impact every entry of $\boldsymbol{X}_t$, by which one can expect a tight SDP relaxation with (4.24) imposed.

4.4 Geometric Interpretation

To provide a geometric interpretation of the convex constraints introduced above, the following 2-dimensional system, whose feasible set is given in Figure 4.7, is studied in this subsection. Note that the feasible set of the SDP relaxation for a system whose dimension is higher than 2 is hard to visualize,

$$\begin{cases} x^2+3xy+2y^2=0.5 \\ x-y=1 \\ x^2+y^2\le 1.5 \\ 0\le x\le 1 \\ -1\le y\le 1 \end{cases}. \tag{4.25}$$

The BSDP relaxation of system (4.25) is

$$\begin{cases} X_{11}+3X_{12}+2X_{22}=0.5 \\ x-y=1 \\ X_{11}+X_{22}\le 1.5 \\ 0\le X_{11},X_{22}\le 1 \\ 0\le x\le 1,-1\le y\le 1 \\ \boldsymbol{X}=\begin{bmatrix} X_{11} & X_{12} \\ X_{12} & X_{22} \end{bmatrix}\succeq 0 \end{cases}, \tag{4.26}$$

whose feasible region is described in Figure 4.8. The feasible set of (4.26) is the region on the plane $X_{11}+3X_{12}+2X_{22}=0.5$ that is enclosed by the surface $X_{11}X_{22} = X_{21}^2$ and the plane

$X_{11}+X_{22}=1.5$.

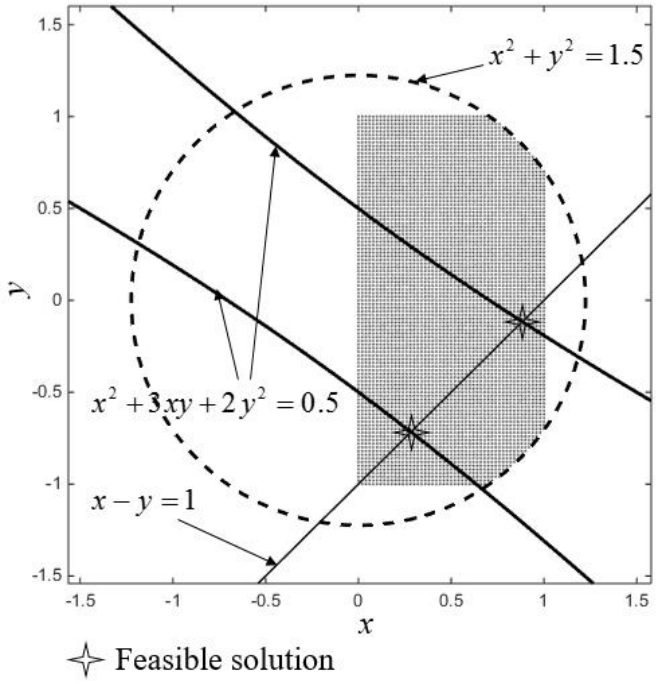

Figure 4.7 Feasible Set of System (4.25).

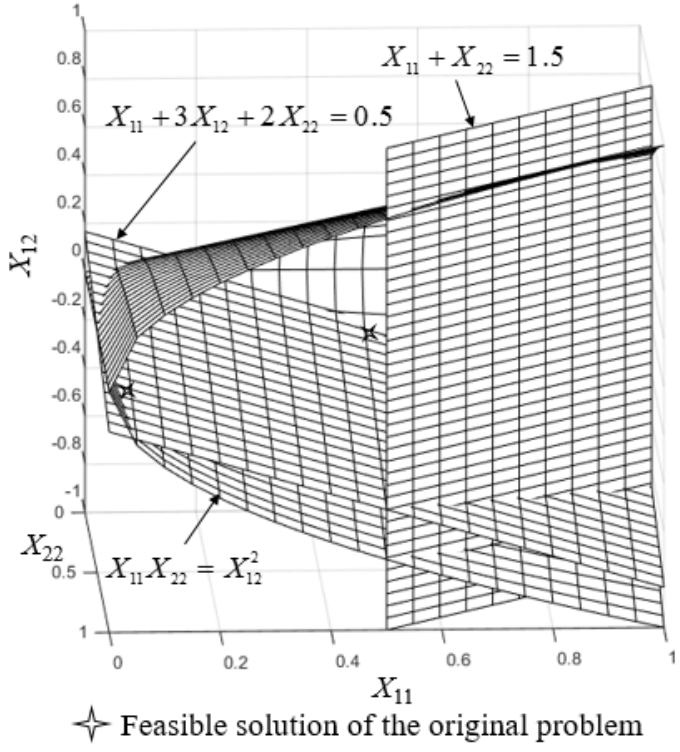

Figure 4.8 Feasible Set of System (4.26) in the (X_{11}, X_{22}, X_{12})-space.

Following the steps introduced in Subsection 4.3.1, the following RLT constraints for this system are obtained

$$\begin{cases} \max\{2x-1,0\} \le X_{11} \le x \\ \max\{2y-1,-2y-1\} \le X_{22} \le 1. \\ \max\{x+y-1,-x\} \le X_{12} \le 0 \end{cases} \tag{4.27}$$

The first constraint in (4.27) demonstrates that, for a non-negative variable, the RLT constraint on the diagonal entry of $\boldsymbol{X}$ corresponding to this variable dominates that in (4.12). The efficiency of the bound constraint $X_{12} \le 0$ which is one of the RLT constraints in (4.27) is illustrated in Figure 4.9. The projection of the feasible set of (4.26) onto the (X_{11}, X_{22})-plane is the meshed region to the left of line $X_{11}+X_{22}=1.5$. The dashed line is the projection of the intersection of $X_{11}+3X_{12}+2X_{22}=0.5$ and $X_{12} = 0$ onto the (X_{11}, X_{22})-plane. The triangular area to the left of the dashed line is cut off when $X_{12} \le 0$ is added.

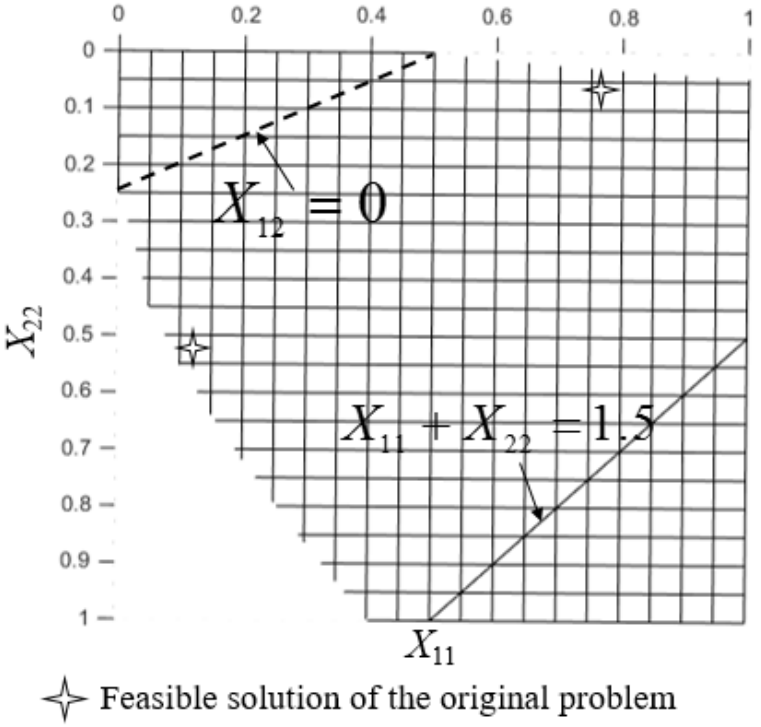

Figure 4.9 Geometric Interpretation of RLT.

Based on the linear equality $x - y = 1$, the following VLE ((4.17)) is obtained for this system

$$\begin{bmatrix} X_{11} & X_{12} \\ X_{12} & X_{22} \end{bmatrix} \begin{bmatrix} 1 \\ -1 \end{bmatrix} = 1 \times \begin{bmatrix} x \\ y \end{bmatrix}, \tag{4.28}$$

which is equivalent to (combining $x - y = 1$)

$$X_{11} - 2X_{12} + X_{22} = 1. \tag{4.29}$$

The feasible set of the SDP relaxation of (4.25) with (4.29) imposed is given in Figure 4.10, which becomes as tight as a line segment. The line segment $2.5X_{11}+3.5X_{22}=2$ is the projection of the intersection of $X_{11}+3X_{12}+2X_{22}=0.5$ and (4.29) onto the (X_{11}, X_{22})-plane within the feasible set. This line segment is exactly the resulting feasible set after imposing (4.29) on system (4.26). This example numerically demonstrates that the VLE is effective if there exists a considerable number of linear equality constraints in the original problem. Another important reason why the BFM is preferred to formulate the AC power flow is that most constraints in the BFM are linear equalities.

Based on the convex quadratic constraint in (4.25) and (4.21), the semidefinite inequality in (4.30) is obtained. Since the link between $\boldsymbol{X}$ and [x, y] is very weak in the BSDP relaxation (4.26), it is hard to obtain the geometric figure for semidefinite inequality_1. However, the efficiency of the SI_1 has been verified by numerical studies in power systems given in Section V,

$$\begin{bmatrix} 1 & 0 & x \\ 0 & 1 & y \\ x & y & 1.5 \end{bmatrix} \succeq 0. \tag{4.30}$$

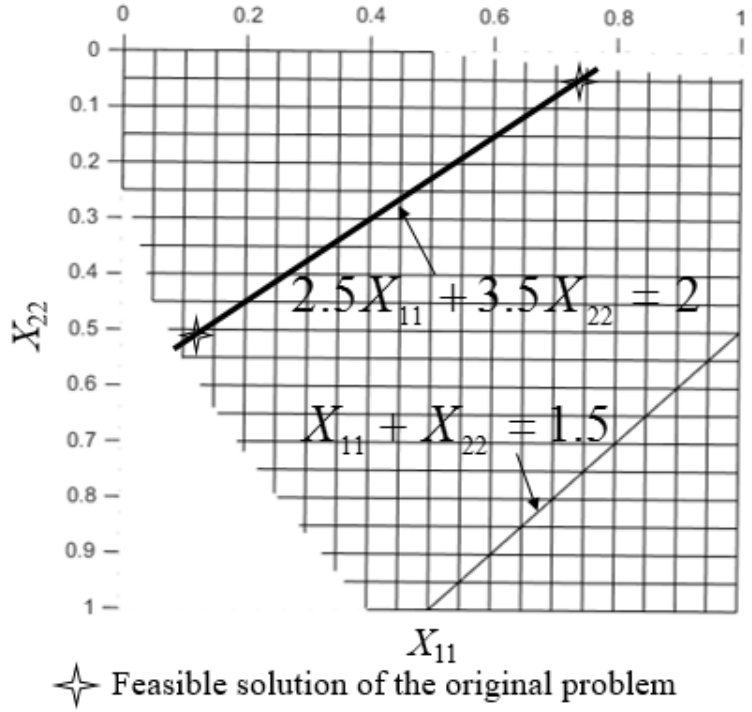

Figure 4.10 Geometric Interpretation of VLE.

Multiplying (4.30) by the lower bound constraint on x and replacing the quadratic terms with the corresponding entries in $\boldsymbol{X}$ yields the following semidefinite inequality

$$\begin{bmatrix} x & 0 & X_{11} \\ 0 & x & X_{12} \\ X_{11} & X_{12} & 1.5x \end{bmatrix} \succeq 0, \tag{4.31}$$

which implies that

$$X_{11}^2 + X_{12}^2 \le 1.5x^2 \le 1.5. \tag{4.32}$$

Adding (4.32) to the BSDP relaxation (4.26), the resulting feasible set is plotted in

Fig. 4.11. A portion of the feasible set of (4.26) is cut off by (4.32). The SI_2 constraint in (4.31) will cut off a bigger portion of the feasible set since (4.32) is looser than (4.31).

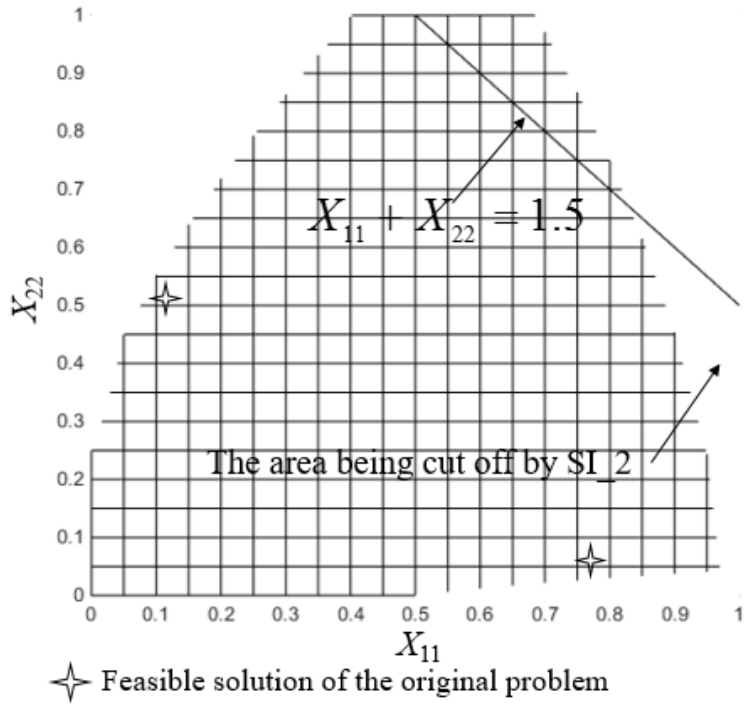

Figure 4.11 Geometric Interpretation of SI_2.

4.5 Non-iterative Enhanced SDP relaxations

The non-iterative enhanced SDP relaxations are constructed by imposing one or some of the above convex constraints to the basic SDP relaxation in (BSDP). The designed ESDP relaxations are listed in Table 4.5. Even in an iterative framework, the computations can also benefit from the non-iterative constraints since they are valid for the sub-problem at each iteration. This merit motivates researchers to develop techniques to lift valid cuts obtained at a node of the branch and bound tree to the entire tree [67] and [68].

Table 4.5 The Enhanced SDP Relaxations of (DESOA), (DESOS) and (SIOP)

ESDP#	Constraints
1	(4.6)-(4.13) and (4.15)
2	(4.6)-(4.13) and (4.18)
3	(4.6)-(4.13) and (4.21)
4	(4.6)-(4.13), (4.21) and (4.24)
5	(4.6)-(4.13), (4.18) and (4.21)
6	(4.6)-(4.13), (4.15) and (4.18)

4.6 Comparison of Tightness

Combining the results obtained in this report and those reported in literature, a hypothesis on the tightness of the SOCP, BSDP as well as the ESDP relaxations for the DESOA, DESOS and SIOP problems in radial networks is illustrated in Figure 4.7. Let $\Omega(\cdot)$ denotes a feasible set. The set Ω(DESOA/DESOS/SIOP) is denoted by the black thick curve. The set Ω(SOCP) is the shaded region while Ω(BSDP) and Ω(ESDP) are the regions enclosed by the dotted-dashed curve and the dotted curve respectively.

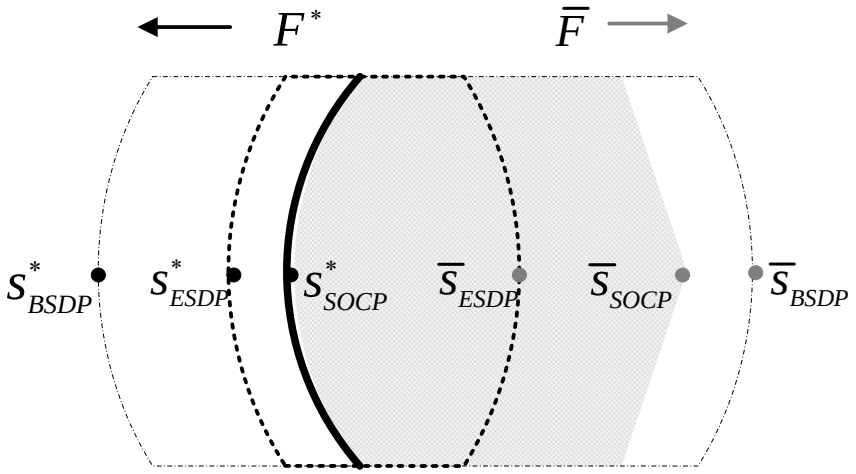

Figure 4.12 Hypothesis about the Tightness of the Convex Relaxations for the (DESOA), (DESOS) and (SIOP) Problems in Radial Networks.

Chapter 5 CONVEX HULL OF THE AC POWER FLOW

Both BIMs and BFMs contain non-convex constraints whose convex relaxations have been widely studied in literature. The convex hull or quasi-convex hull of these non-convex constraints are studied in this chapter. Convex hull is defined as the tightest convex set that contains a non-convex set, which makes the convex hull or quasi-convex hull attractive compared with other kinds of convex relaxations. Following the previous analysis, BIM and BFM are used to formulate the AC power flow in meshed and radial networks respectively.

5.1 AC Power Flow in Meshed Networks

5.1.1 Revisit the BIM in Rectangular Coordinates

A typical formulation of the AC power flow model in rectangular coordinates is given as

1. Power flow equations:

$$\begin{cases} \sum_j \left(G_{ij} e_i e_j - B_{ij} e_i f_j + B_{ij} f_i e_j + G_{ij} f_i f_j \right) - P_i^G + p_i^L = 0 \\ \sum_j \left(-B_{ij} e_i e_j - G_{ij} e_i f_j + G_{ij} f_i e_j - B_{ij} f_i f_j \right) - Q_i^R + q_i^L = 0 \end{cases} \quad (i \in N) \tag{5.1}$$

2. Constraints of the reference bus:

$$e_r = 1.05 \text{ p.u. and } f_r = 0 \tag{5.2}$$

3. System constraints:

$$\underline{P}_i^G \le P_i^G \le \bar{P}_i^G \qquad (i \in N_G) \tag{5.3}$$

$$\underline{Q}_i^R \le Q_i^R \le \bar{Q}_i^R \qquad (i \in N_R) \tag{5.4}$$

$$\underline{V}_i^2 \le e^2 + f^2 \le \overline{V}_i^2 \ (i \in N) \tag{5.5}$$

$$\begin{cases} P_{ij}^2 + Q_{ij}^2 \le \overline{S}_{ij}^2 \\ P_{ij} = G_{ij} e_i e_j - B_{ij} e_i f_j + B_{ij} f_i e_j + G_{ij} f_i f_j \quad (ij \in E) \\ Q_{ij} = -B_{ij} e_i e_j - G_{ij} e_i f_j + G_{ij} f_i e_j - B_{ij} f_i f_j \end{cases} \tag{5.6}$$

The 2nd and 3rd equalities in (5.6) are non-convex quadratic equalities which are in the same form as (5.1). The above AC power flow model is also called the bus injection model (BIM) in some references [21]. To facilitate the analysis, a compact formulation of the power flow equations (5.1) and the 2nd and 3rd equalities in (5.6) is developed in this subsection. Let $\boldsymbol{x} = [\boldsymbol{e}^{\mathrm{T}}\ \boldsymbol{f}^{\mathrm{T}}]^{\mathrm{T}}$ and $\boldsymbol{y} = [\boldsymbol{P}^{G\mathrm{T}}\ \boldsymbol{Q}^{R\mathrm{T}}\ \boldsymbol{P}^{\mathrm{T}}\ \boldsymbol{Q}^{\mathrm{T}}]^{\mathrm{T}}$, the compact formulation is

$$\boldsymbol{x}^{\mathrm{T}} \boldsymbol{A}_i^k \boldsymbol{x} + \boldsymbol{c}_i^{k\mathrm{T}} \boldsymbol{y} + b_i^k = 0 \quad (i \in N, k = 1, \ldots, 4) \tag{5.7}$$

where $\boldsymbol{A}_i^k$ is the corresponding admittance matrix.

5.1.2 Convex Hull of the Non-convex Quadratic Inequalities in BIM

First, consider the following decomposition scheme for (5.7)

$$\boldsymbol{x}^{\mathrm{T}} \left(\boldsymbol{A}_i^k + \boldsymbol{M}_i^k \right) \boldsymbol{x} + \boldsymbol{c}_i^{k\mathrm{T}} \boldsymbol{y} + b_i^k = \boldsymbol{x}^{\mathrm{T}} \boldsymbol{M}_i^k \boldsymbol{x} \tag{5.8}$$

where $\boldsymbol{M}_i^k$ is a constructed positive definite matrix such that $(\boldsymbol{A}_i^k + \boldsymbol{M}_i^k)$ is positive semidefinite. The step from (5.7) to (5.8) is analogous to the D.C. decomposition of a non-convex quadratic objective function introduced in [69]. Then, by introducing an auxiliary scalar variable z_i^k, (5.8) is equivalent to

$$\begin{cases} \boldsymbol{x}^{\mathrm{T}} \left(\boldsymbol{A}_i^k + \boldsymbol{M}_i^k \right) \boldsymbol{x} + \boldsymbol{c}_i^{k\mathrm{T}} \boldsymbol{y} + b_i^k - z_i^k = 0 \\ \boldsymbol{x}^{\mathrm{T}} \boldsymbol{M}_i^k \boldsymbol{x} - z_i^k = 0 \end{cases}, \tag{5.9}$$

which can be further decomposed into

$$\begin{cases} \boldsymbol{x}^{\mathrm{T}}\left(\boldsymbol{A}_i^k + \boldsymbol{M}_i^k\right)\boldsymbol{x} + \boldsymbol{c}_i^{k\mathrm{T}}\boldsymbol{y} + b_i^k - z_i^k \le 0 \\ \boldsymbol{x}^{\mathrm{T}}\left(\boldsymbol{A}_i^k + \boldsymbol{M}_i^k\right)\boldsymbol{x} + \boldsymbol{c}_i^{k\mathrm{T}}\boldsymbol{y} + b_i^k - z_i^k \ge 0 \\ \boldsymbol{x}^{\mathrm{T}}\boldsymbol{M}_i^k\boldsymbol{x} - z_i^k \le 0 \\ \boldsymbol{x}^{\mathrm{T}}\boldsymbol{M}_i^k\boldsymbol{x} - z_i^k \ge 0 \end{cases}. \tag{5.10}$$

Obviously the 1st and 3rd terms in (5.10) are convex constraints while the 2nd and 4th terms are not. Since both of $(\boldsymbol{A}_i^k + \boldsymbol{M}_i^k)$ and $\boldsymbol{M}_i^k$ are positive semidefinite, it is possible to reformulate the non-convex quadratic inequalities, i.e. the 2nd and 4th terms in (5.10), as

$$\begin{cases} \boldsymbol{x}^{\mathrm{T}}\boldsymbol{a}_i^k\boldsymbol{a}_i^{k\mathrm{T}}\boldsymbol{x} \ge z_i^k - b_i^k - \boldsymbol{c}_i^{k\mathrm{T}}\boldsymbol{y} \\ \boldsymbol{x}^{\mathrm{T}}\boldsymbol{m}_i^k\boldsymbol{m}_i^{k\mathrm{T}}\boldsymbol{x} \ge z_i^k \end{cases} \tag{5.11}$$

where $\boldsymbol{a}_i^k$ and $\boldsymbol{m}_i^k$ are lower triangular matrices with nonnegative diagonal entries such that $\boldsymbol{A}_i^k + \boldsymbol{M}_i^k = \boldsymbol{a}_i^{k\mathrm{T}}\boldsymbol{a}_i^k$ and $\boldsymbol{M}_i^k = \boldsymbol{m}_i^{k\mathrm{T}}\boldsymbol{m}_i^k$ [70]. Using a new vector $\boldsymbol{u}$ to represent $\boldsymbol{a}_i^{k\mathrm{T}}\boldsymbol{x}$ or $\boldsymbol{m}_i^{k\mathrm{T}}\boldsymbol{x}$, and a new scalar v to represent the right hand side of (5.11), then (5.11) can be represented by

$$\boldsymbol{u}^{\mathrm{T}}\boldsymbol{u} \ge v\,. \tag{5.12}$$

Now the convex hull of inequality (5.12) is explored. Suppose that $\boldsymbol{u}$ is an n-dimensional vector and define $\boldsymbol{w}$ as $[\boldsymbol{u}^{\mathrm{T}}\ v]^{\mathrm{T}}$; let $f(\boldsymbol{u}) \coloneqq \boldsymbol{u}^{\mathrm{T}}\boldsymbol{u}$; $\tilde{w}^t$ (t = 1, …, 2^n) denote 2^n points in the $\boldsymbol{w}$-space, where

Element	$\tilde{w}_1^t$	$\tilde{w}_2^t$	…	$\tilde{w}_n^t$	$\tilde{w}_{n+1}^t$
Value	$\underline{u}_1$ or $\bar{u}_1$	$\underline{u}_2$ or $\bar{u}_2$	…	$\underline{u}_n$ or $\bar{u}_n$	$f\left(\tilde{\boldsymbol{u}}^t\right)$

.

Actually, $\tilde{w}^t$ (t = 1, …, 2^n) are the vertices of the feasible set in the $\boldsymbol{w}$-space, if there is valid "box" bound on $\boldsymbol{u}$. With the above definitions, the following theorem is proposed.

Theorem 5.1

$$CONV\left(\{\boldsymbol{u} \mid (5.12) \text{ holds and } \underline{\boldsymbol{u}} \le \boldsymbol{u} \le \bar{\boldsymbol{u}}\}\right) = \left\{\boldsymbol{w} \middle| \boldsymbol{B}^{\mathrm{T}}\boldsymbol{w} \le d,\ \underline{\boldsymbol{u}} \le \boldsymbol{u} \le \bar{\boldsymbol{u}}\right\},$$

where $\boldsymbol{B}$ is an (n+1)-dimensional vector, $\boldsymbol{B}^{\mathrm{T}}\boldsymbol{w} = d$ represents a hyperplane that crosses all the $\tilde{w}$ points, and $CONV(\cdot)$ denotes the convex hull of a set.

$\boldsymbol{B}^{\mathrm{T}}\boldsymbol{w} = d$ can be obtained by using anyone of the bases of $\tilde{w}^t$ ($t = 1, \ldots, 2^n$). Theorem 5.1 is true for the cases where there are valid "box" bounds for $\boldsymbol{u}$., i.e. $\underline{\boldsymbol{u}} \le \boldsymbol{u} \le \bar{\boldsymbol{u}}$. However, there are no valid "box" bounds for $\boldsymbol{x}$ defined in Subsection III-B. Hence, virtual "box" bounds for $\boldsymbol{x}$ are required. Fortunately, it is not difficult to obtain such "box" bounds for $\boldsymbol{x}$ based on the operating experience of a specific power system. Since the convex hull of the BIM is based on virtual "box" bounds for $\boldsymbol{x}$, it is called the quasi-convex hull of the BIM in this thesis.

5.1.3 An Illustrative Example

To provide an intuitive understanding of Theorem 5.1, the convex hull of the following non-convex quadratic inequality is plotted in a 3-dimensional space, as shown in Figure 5.1.

$$\begin{bmatrix} x & y \end{bmatrix} \begin{bmatrix} x \\ y \end{bmatrix} \ge z \quad (-4 \le x \le 8,\ -5 \le y \le 3), \tag{5.13}$$

where $\begin{bmatrix} \tilde{\boldsymbol{w}}^1 \\ \tilde{\boldsymbol{w}}^2 \\ \tilde{\boldsymbol{w}}^3 \\ \tilde{\boldsymbol{w}}^4 \end{bmatrix} = \begin{bmatrix} -4 & -5 & 41 \\ -4 & 3 & 25 \\ 8 & -5 & 89 \\ 8 & 3 & 73 \end{bmatrix}$, $\boldsymbol{B} = \begin{bmatrix} 4 \\ -2 \\ -1 \end{bmatrix}$ and d = -47. The convex hull of system (5.13) is the space enclosed by $4x - 2y - z \ge -47$, $-4 \le x \le 8$, and $-5 \le y \le 3$.

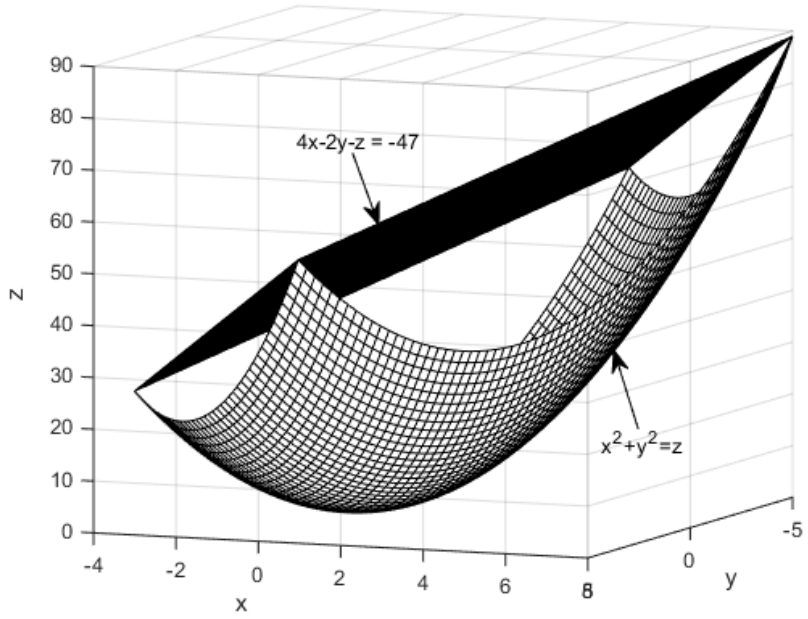

Figure 5.1 Feasible Set of System (5.13) is the Space below the Surface and within the Box Constraints.

5.2 AC Power Flow in Radial Networks

5.2.1 Revisit the Branch Flow Model

In this research, the adopted BFM is the DistFlow model proposed in [44] which is given as

$$p_i = \sum_k P_{ik} - \left(P_{ji} - r_{ij}\ell_{ji}\right) \tag{5.14}$$

$$q_i = \sum_k Q_{ik} - \left(Q_{ji} - x_{ij}\ell_{ji}\right) \tag{5.15}$$

$$v_i = v_k + 2\left(r_{ik}P_{ik} + x_{ik}Q_{ik}\right) - \left(r_{ik}^2 + x_{ik}^2\right)\ell_{ik} \tag{5.16}$$

$$v_i\ell_{ik} = P_{ik}^2 + Q_{ik}^2 \tag{5.17}$$

where $k \in N_i$, $i \in N$, j is the upstream bus of i. Since the network structure is radial, for each bus i, there is only one upstream bus. The feasible set of (5.14)-(5.17) is also subjected to

$$0 \le \ell_{ik} \le \overline{\ell}_{ik} \tag{5.18}$$

$$\underline{v}_i \le v_{ik} \le \overline{v}_i \tag{5.19}$$

$$P_{ik}^2 + Q_{ik}^2 \le \overline{S}_{ik}^2 \tag{5.20}$$

where both $\overline{\ell}_{ik}$ and $\overline{S}_{ik}$ are related to the thermal limit of a feeder line. Note that an analogous AC power flow model was proposed in [45]. In the scope of this thesis, they are equivalent. Therefore, they are called branch flow model (BFM) in this thesis.

5.2.2 Geometric Understanding of the Convex Hull of BFM

In the modified DistFlow model, the only non-convex constraints are those in (5.17). Each equality in (5.17) is a quadratic function of three independent variables and the 4th variable can be regarded as dependent variable. It is not possible to plot the feasible set of (5.17), Ω_0, in the (P_{ik} Q_{ik} ℓ_{ik} v_i)-space which is a 4-dimensional space. To provide a geometric understanding of the convex hull of constraint (5.17) in the DistFlow model, its feasible set is projected to all the 3-dimensional sub-spaces. For example, the projection of Ω_0 onto the **(P_{ik} Q_{ik} ℓ_{ik})**-space is denoted as $\Omega_{PQ\ell}$. Note that all the quantities in this subsection are in p.u.

Projection In the (P_{ik} Q_{ik} ℓ_{ik})-space

Considering v_i as a parameter, equality (5.17) can be rewritten as

$$\ell_{ik} = g_1\left(P_{ik}, Q_{ik}\right) = \left(P_{ik}^2 + Q_{ik}^2\right)/v_i\,, \tag{5.21}$$

which is subjected to constraints (5.18)-(5.20). The feasible set of (5.21), $\Omega_{PQ\ell}$, is sketched in Figure 5.2. By observation, $CONV(\Omega_{PQ\ell})$ can be formulated as

$$P_{ik}^2 + Q_{ik}^2 \le \overline{v}_i \ell_{ik} \le \overline{v}_i \overline{S}_{ik}^2 / \underline{v}_i \,. \tag{5.22}$$

Consequently, $\overline{\ell}_{ik}$, the upper bound of ℓ_{ik}, needs to be updated as

$$\overline{\ell}_{ik} = \overline{S}_{ik}^2 / \underline{v}_i \tag{5.23}$$

In fact, constraint (5.23) is an inherent property of the original problem, which is not considered in many SOCP relaxations in literature.

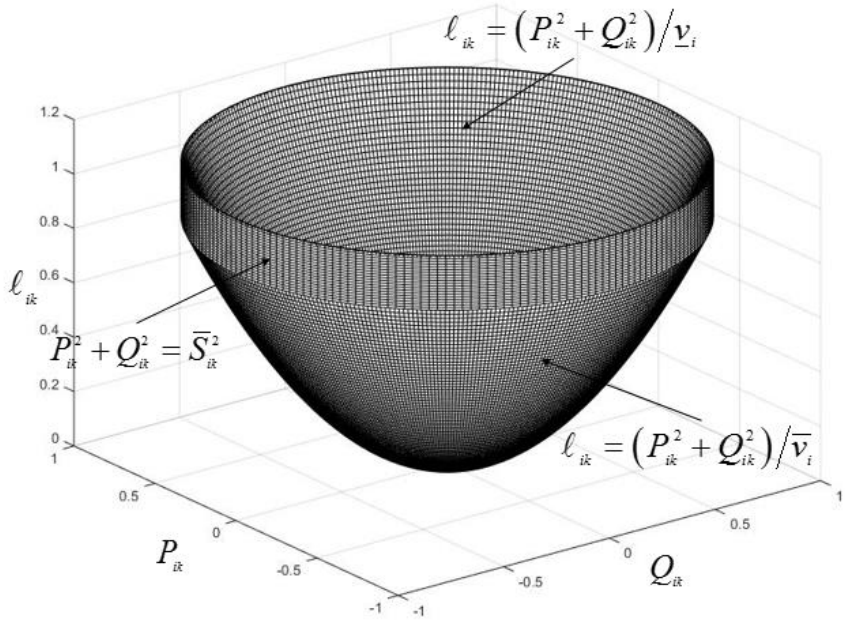

Figure 5.2 Feasible Set of System (5.21).

Projection in the (P_{ik} Q_{ik} v_i)-space

Consdiering ℓ_{ik} as a parameter, equality (5.17) can be rewritten as

$$v_i = g_2\left(P_{ik}, Q_{ik}\right) = \left(P_{ik}^2 + Q_{ik}^2\right)/\ell_{ik}\ , \tag{5.24}$$

which is subjected to constraints (5.18)-(5.20). The feasible set of (5.24), Ω_{PQv}, is sketched in Figure 5.3. By observation, $CONV(\Omega_{PQv})$ can be formulated as

$$P_{ik}^2 + Q_{ik}^2 \le \overline{\ell}_{ik} v_i \tag{5.25}$$

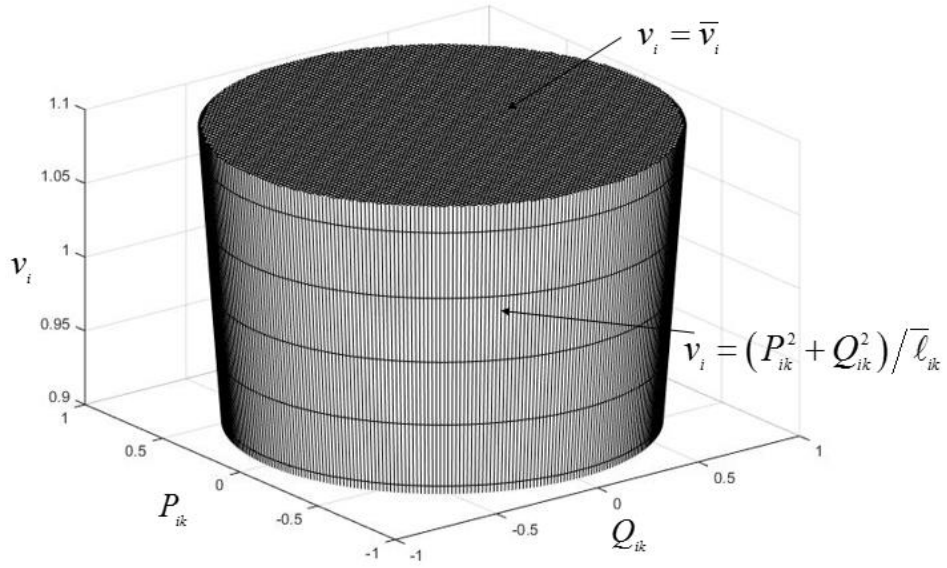

Figure 5.3 Feasible Set of System (5.24).

Projection in the (P_{ik} ℓ_{ik} v_i)-space and the (Q_{ik} ℓ_{ik} v_i)-space

In the variable space, the positions of P_{ik} and Q_{ik} are completely symmetrical. As a result, the formulation of $\Omega_{\ell vP}$ can be directly applied to obtain $\Omega_{\ell vQ}$ by replacing P_{ik} with Q_{ik}. Considering Q_{ik} as a parameter, equality (5.17) can be rewritten as

$$P_{ik} = g_3\left(\ell_{ik}, v_i\right) = \pm\sqrt{v_i \ell_{ik} - Q_{ik}^2}\ , \tag{5.26}$$

which is subjected to constraints (5.18)-(5.20). The feasible set of (5.26), $\Omega_{\ell vP}$, is sketched in Figure 5.4. $\Omega_{\ell vP}$ is the space that is enclosed by the bounding planes described by (5.18) and (5.19), and the two surfaces in Figure 5.4. By observation, *CONV*($\Omega_{\ell vP}$) can be formulated as

$$\begin{cases} \left\| \begin{matrix} P_{ik} \\ v_i - \ell_{ik} \end{matrix} \right\|_2 \le v_i + \ell_{ik} \\ \underline{v}_i \overline{v}_i \ell_{ik} + \overline{S}_{ik}^2 v_i \le \overline{S}_{ik}^2 \left(\overline{v}_i + \underline{v}_i \right) \end{cases} \tag{5.27}$$

Consequently, CONV($\Omega_{\ell vQ}$) can be expressed as

$$\begin{cases} \left\| \begin{matrix} Q_{ik} \\ v_i - \ell_{ik} \end{matrix} \right\|_2 \le v_i + \ell_{ik} \\ \underline{v}_i \overline{v}_i \ell_{ik} + \overline{S}_{ik}^2 v_i \le \overline{S}_{ik}^2 \left(\overline{v}_i + \underline{v}_i \right) \end{cases} . \tag{5.28}$$

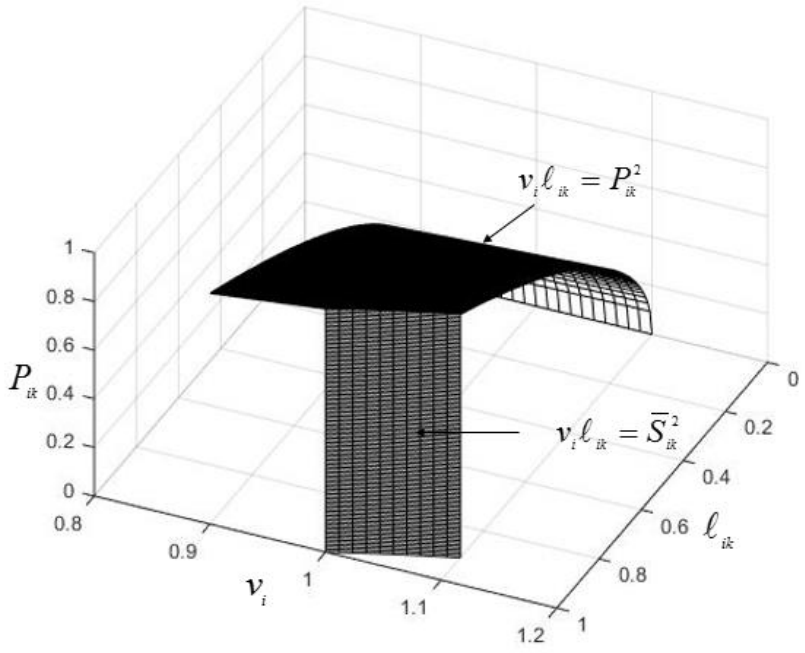

Figure 5.4 Feasible Set of System (5.26).

5.2.3 Mathematical Formulation of the Convex Hull of DistFlow

Let $\boldsymbol{x}_{ik} = [P_{ik}\ Q_{ik}\ \ell_{ik}\ v_i]^{\mathrm{T}}$ ($ik \in M$) and define $\Omega_0 = \{\boldsymbol{x}_{ik} \mid (5.17)\ –(5.20)\ \text{hold.}\}$. Following the analysis given in the above subsection, we have the Proposition 1.

Theorem 5.2. The convex hull of Ω_0 can be formulated as

$$CONV(\Omega_0) = \Omega_1 = \left\{ \boldsymbol{x}_{ik} \left| \begin{array}{c} \overline{\ell}_{ik} = \overline{S}_{ik}^2 / \underline{v}_i \\ \left\| \begin{array}{c} P_{ik} \\ Q_{ik} \\ v_i - \ell_{ik} \end{array} \right\|_2 \le v_i + \ell_{ik} \\ \underline{v}_i \overline{v}_i \ell_{ik} + \overline{S}_{ik}^2 v_i \le \overline{S}_{ik}^2 \left(\overline{v}_i + \underline{v}_i \right) \\ \boldsymbol{x}_{ik} \in (2) \end{array} \right. \right\}. \tag{5.29}$$

The proof of Theorem 5.2 is given in Appendix E. It is easy to figure out that

$$\begin{cases} (\Omega_1)_{PQ\ell} = CONV\left(\Omega_{PQ\ell}\right) \\ (\Omega_1)_{PQv} = CONV\left(\Omega_{PQv}\right) \\ (\Omega_1)_{\ell vP} = CONV\left(\Omega_{\ell vP}\right) \\ (\Omega_1)_{\ell vQ} = CONV\left(\Omega_{\ell vQ}\right) \end{cases},$$

where $(\Omega_1)_{PQ\ell}$ means the projection of Ω_1 onto the $(P_{ik}\ Q_{ik}\ v_i)$-space. Without the 1st and 3rd constraints, Ω_1 is exactly the SOCP relaxation of Ω_0. With the 1st constraint, the 3rd constraint is a valid inequality which intersects the original feasible set, Ω_0, on the exact "edges". Hence, including these constraints results the convex hull of Ω_0. This is the primary contribution and novelty compared with the valid inequalities proposed in literature.

Based on the convex hull formulation (5.29) of the non-convex constraints in the DistFlow model, a novel convex relaxation of the DESOSs is proposed in this thesis which is named CH relaxation. The details are given in Table 5.1.

Table 5.1 The CH Relaxations for the DESOSs

Notation	CH 1	CH 2	CH 3
Objective function	(3.1)	(3.2)	(3.18)
Constraints	(3.4) - (3.6), (3.8) - (3.17), and (5.29)	(3.4) - (3.6), (3.8) - (3.17), and (5.29)	(3.4) - (3.6), (3.8) - (3.17), (3.19), and (5.29)

Chapter 6 CASE STUDY

This chapter consists of three sections. The case study in section 6.1 is a continuation of that in Section 2.4 and shows the efficiency of the proposed methods from a perspective of power system engineering. The effectiveness of the non-iterative enhanced SDP relaxations in improving the tightness of convex relaxation for the DESOS (a continuous case) and SIOP (a mixed-integer case) is demonstrated in the sections 6.2 and 6.3 respectively.

6.1 Efficiency from a Perspective of Power System Engineering

This section focuses on applying the proposed approaches to the real-world feeder in Arizona as shown in Figure 2.1. Since the DES optimization problems are time-coupled, modeling the full feeder will result in intractable optimization problems. Thus, only the three-phase trunk of this system is considered in the optimization computation which is implemented in YALMIP [71] by calling the solver SDPT3 [72]. YALMIP is a MATLAB toolbox for optimization while SDPT3 is a solver that can handle SOCP problems. The charging efficiency η_c and the discharging efficiency η_d are set to be 90% and 95% respectively. Following Section 2.4, the results of optimal allocation are tabulated in Table 6.1 (the 2nd and 3rd columns).

As a comparison, the optimal allocation of DES obtained by solving the non-convex model using KNITRO [73] solver in AMPL [74] is given in the 4^{th} and 5^{th} columns of Table 6.1. Note that an initial solution is usually needed when solving a non-convex problem. The initial solution shown in the 6^{th} and 7^{th} columns of Table 6.1 was used when solving the non-convex model in AMPL.

Table 6.1 Optimal Allocation of DES Units when Objective Function (3.1) is Chosen.

Bus #	Convex optimization		Non-convex optimization		Initial solution of the Non-convex optimization	
	Power rating (kW)	Energy rating (kWh)	Power rating (kW)	Energy rating (kWh)	Power rating (kW)	Energy rating (kWh)
1	0.00186	0.09751	0.0008	87.5701	111.11	611.11
2	0.03439	0.18645	0.0016	87.5735	111.11	611.11
3	0.04792	0.28553	0.0024	87.5768	111.11	611.11
4	318.160	1257.59	376.53	1669	111.11	611.11
5	121.408	765.451	103.52	522.365	111.11	611.11
6	133.057	823.638	104.42	526.171	111.11	611.11
7	84.9874	519.655	68.453	386.972	111.11	611.11
8	0.21194	1.12923	0.0018	87.5742	111.11	611.11
9	342.092	1632.05	347.05	1545.2	111.11	611.11

The two operational strategies introduced in Section 2.3 are implemented in OpenDSS with the DES systems designed from the previous steps. It can be observed from Figure 6.1 that, with the chosen DES systems and the proposed operational strategy, the voltage profile of the bus with the worst voltage violation on the worst case day is maintained within the limit and the short-duration voltage fluctuations are significantly reduced. These voltage profiles shown in Figure 6.1 are at a time resolution of 1 minute. Note that the bus with the worst voltage violation is not necessarily the terminal bus of one of the PV plants. Fast voltage fluctuations at the buses that are close to the PV plants are more severe than what is observed in this figure. Hence, the application of reducing the short-duration PV output uncertainty makes more sense to the buses which are nearby the PV plants. This plot is obtained by simulations in OpenDSS.

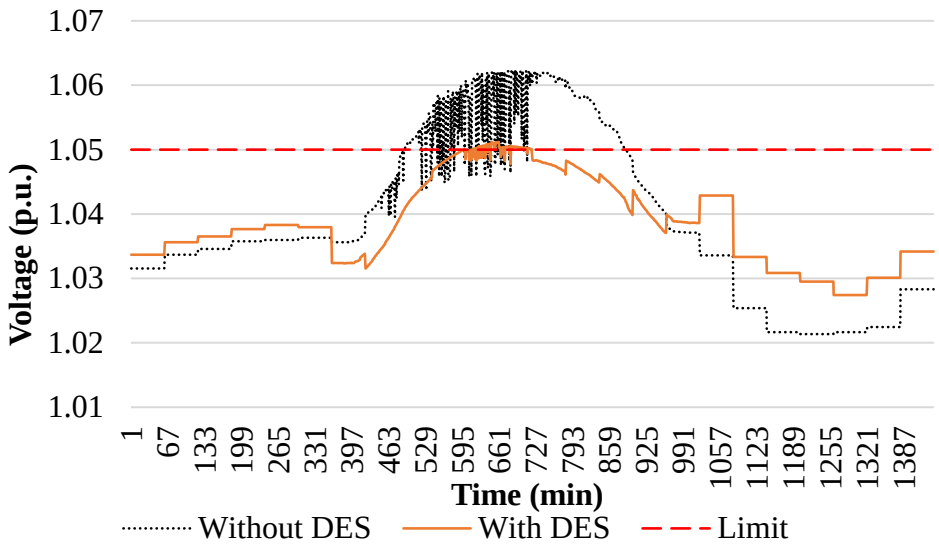

Figure 6.1 Voltage Profiles of the Bus with the Worst Violation on the Worst Case Day.

To verify the exactness of the SOCP relaxation when the aforementioned objective functions are used, an index is proposed to quantify the error between the right-hand side and left-hand side of (4.1). This index is given as

$$e_{\max} = \max \left| v_{i,t} \ell_{(i,j)t} - P^2_{(i,j),t} - Q^2_{(i,j),t} \right| \tag{6.1}$$

Since the SOCP is not exact for the DESOA when the objective function (3.3) is selected. The maximum errors of two cases of the allocation problem with both objective functions are tabulated in Table 6.2. The small errors indicate that the SOCP relaxation is exact for optimal allocation of the DES with the chosen objective functions.

Table 6.2 Maximum Errors of the SOCP Relaxation for DESOAs in p.u.

	Objective Function (3.1)	Objective Function (3.2)
Max. Error	0.00031617	0.00017096

To verify the effectiveness of the SOCP relaxation, the solutions obtained by solving the problem as convex and nonconvex optimization are compared. In this subsection, five operating cases are studied with objective function (3.1) and five cost curves chosen (shown in Figure 6.2). The cost curves used in cases 1 and 2 are assumed while those in cases 3-5 are actual ones for the feeder considered. The results given in Table 6.3 clearly demonstrate that the solution of the DES optimization as a convex problem is more effective than solving it as a non-convex problem. In Table 6.3, the convex problem is solved by SDPT3 through YALMIP while the non-convex problem is solved by KNITRO solver through AMPL. Table 6.3 in conjunction with Figure 6.1 demonstrates that the convex method is able to obtain lower costs/losses solutions without voltage violations.

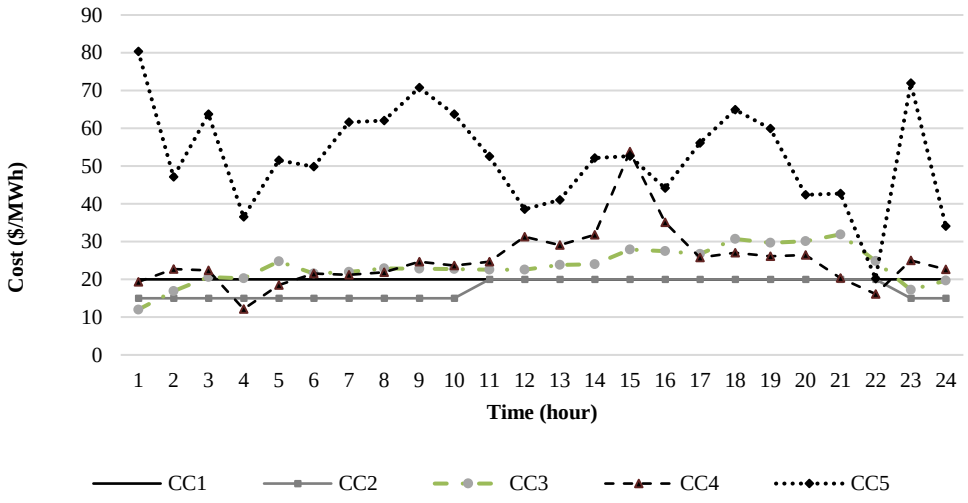

Figure 6.2 Cost Curves Used in the Case Study.

Table 6.3 Operational Costs in p.u.

# of the cost curve	1	2	3	4	5
Convex	1314.8	1517.7	1797.8	1840.6	3908.6
Non-convex	1393.4	1602.8	1903.2	1963.5	4120.0

6.2 DESOS: Tightness of the ESDP Relaxations for Continuous Cases

6.2.1 Test System and Case Design

With objective function (3.1) or (3.2) selected, the SOCP relaxation for DESOA is exact. For the DESOS, the SOCP relaxation is only occasionally exact no matter which objective function is selected. Hence, the effectiveness of the ESDP relaxations is verified for the DESOS where the SOCP relaxation works unsatisfactorily. The convex relaxations of the DESOS algorithm are tested on the 9-bus real-world feeder (Figure 2.1) and the IEEE 13, 37, 123-bus feeders [75] assuming that there is high penetration of PV resources respectively. The three-phase topologies of the three networks are shown in Figure 6.3. The capacities of both PV and DES systems for all the test systems are listed in Table 6.4. The convex problems are solved by the solver MOSEK [76] through the MATLAB toolbox YALMIP. A computer with a 64-bit Intel i5-3230M dual core CPU at 2.60 GHz and 4 GB of RAM was used to run the test cases.

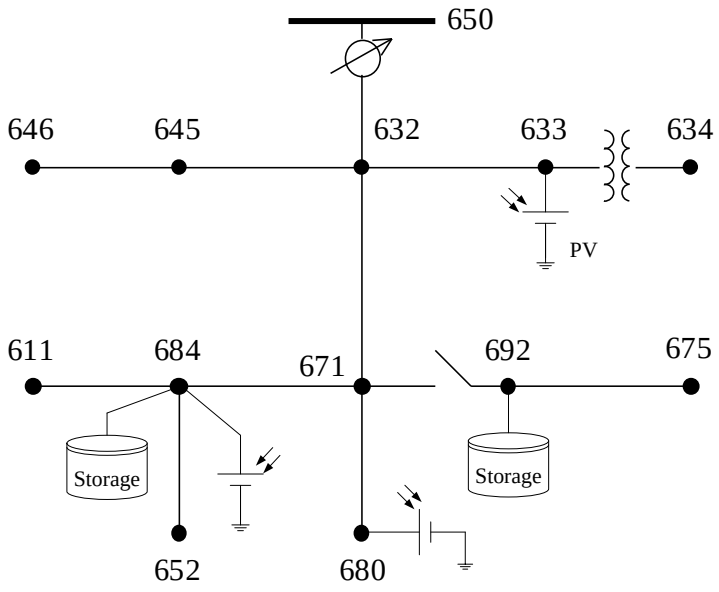

(a) IEEE 13-bus Feeder.

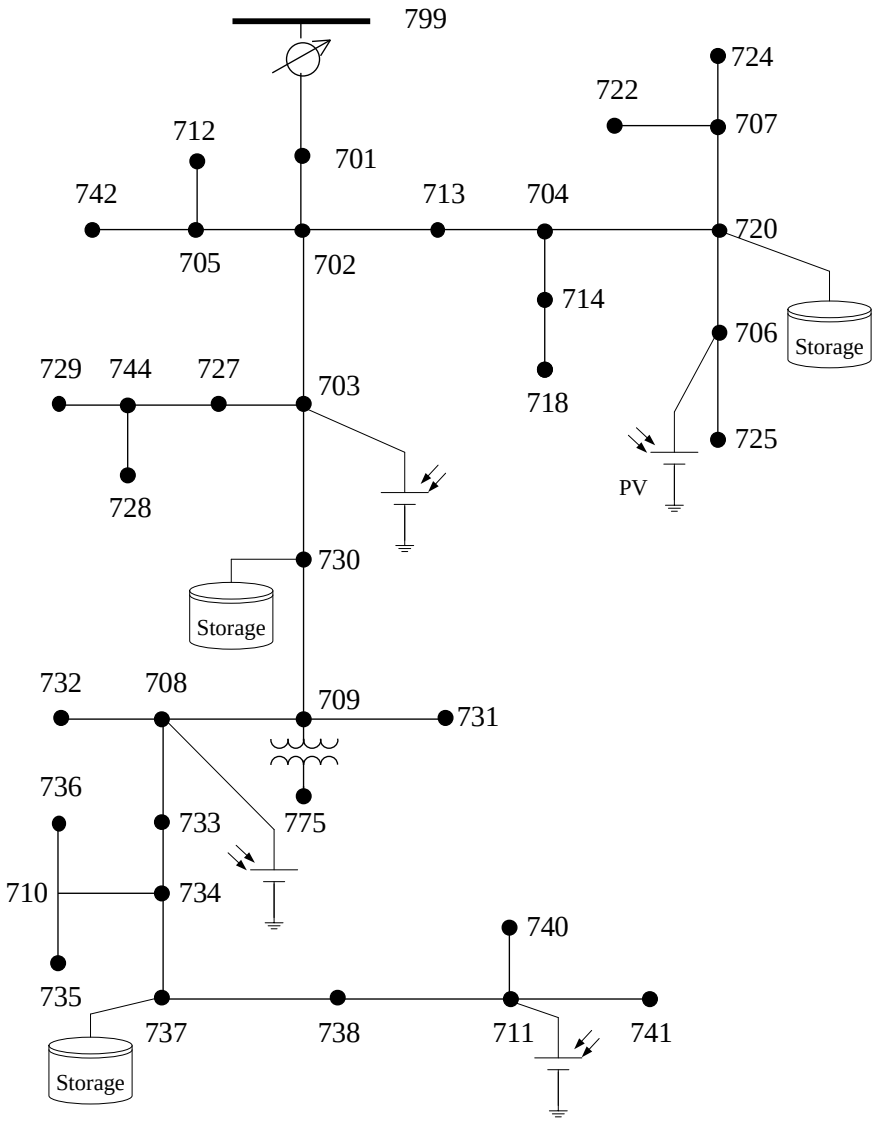

(b) IEEE 37-bus Feeder.

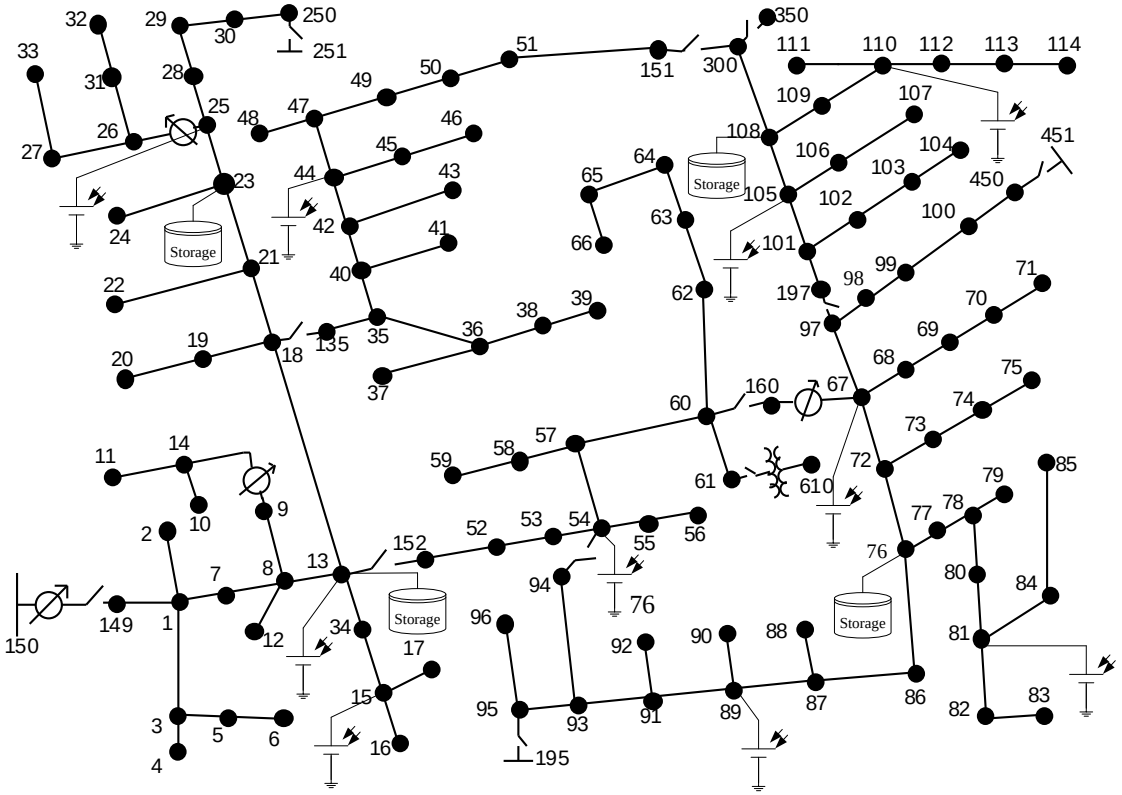

(c) IEEE 123-bus Feeder.
Figure 6.3 Topologies of the IEEE Test Systems.

Table 6.4 PV System and DES Unit Locations and Capabilities

Test system	PV location (bus #) and capacity	penetration
9-bus	4 (0.85 MW), 9 (0.65 MW)	30.5%
13-bus	633 (0.5 MW), 680 (0.2 MW), 684 (0.5 MW)	36.7%
37-bus	703 (0.3 MW), 706 (0.3 MW), 708 (0.3 MW), 711 (0.3 MW)	48.8%
123-bus	8, 15, 25, 44, 54, 67, 81, 89, 105, 110 (all PV systems have the same size of 0.2 MW)	57.3%
Test system	DES location (bus #) and capacity	
9-bus	4 (0.4 MW, 2 MWh), 9 (0.3 MW, 1.5 MWh)	
13-bus	684 (0.6 MW, 2.4 MWh), 692 (0.8 MW, 3.2 MWh)	
37-bus	720 (0.3 MW, 1.2 MWh), 730 (0.3 MW, 1.2 MWh), 737 (0.3 MW, 1.2 MWh)	
123-bus	13 (0.3 MW, 1.2 MWh), 23 (0.3 MW, 1.2 MWh), 76 (0.3 MW, 1.2 MWh), 108 (0.3 MW, 1.2 MWh)	

Multi-period demand and PV generation profiles are available only for the real-world feeder. Hence, in the real-world feeder cases, 24-hour data is used. The DES dynamic constraint (3.8) is omitted and only a snapshot power flow is considered in each of the IEEE feeder cases. When objective function (3.1) is chosen, an actual 24-hour LMP curve (CC4 in Figure 6.2) from the website of the ISO New England is used. The coefficient c in objective function (3.1) is set to be -30 $/MWh for the IEEE cases. For all cases, the charging efficiency η_c and the discharging efficiency η_d are set to be 90% and 95% respectively.

The optimal objective values (OOV) of the solutions are compared to quantify the tightness of the convex relaxations as people did in the literature. As reported widely in literature, the SOCP relaxation outperforms the SDP relaxation in terms of computational efficiency. There is no surprise, that the CPU times of the SOCP relaxation for the DESOS problems, are less than those of the SDP relaxations. This report aims at finding computationally inexpensive convex constraints that can tighten the basic SDP relaxation. Therefore, the CPU time of the ESDP is displayed in per unit with the runtime of the BSDP as the base. In this way, it is more convenient to observe how much the runtime of the BSDP relaxation increases with a convex constraint added (see Table 6.5).

For the cases where the convex relaxations are exact, two nonlinear solvers, IPOPT and KNITRO are used to obtain feasible solutions. In Table 6.5, KNITRO_1 and KNITRO_2 represent the scenarios where the multi-start option is off and on respectively. In the scenario of KNITRO_2, the number of starting points is set to be 10.

6.2.2 Remarks

Some remarks regarding the results shown in Table 6.5 are provided as follows:

a) In the IEEE feeder cases which are single-period cases, when objective function (3.1) with positive LMPs is selected, the SOCP relaxation is exact. In the cases with negative LMPs, the SOCP relaxation is not exact.

Table 6.5 Results of DESOS

System	Relaxation	Objective Function (3.1)		Objective Function (3.2)		Objective Function (3.3)	
		OOV ($)	CPU time (s)	OOV (p.u.)	CPU time (s)	OOV (p.u.)	CPU time (s)
9-bus real-world feeder	SOCP	1231.20	0.84	0.5832*	0.44	13.5148	0.50
	BSDP	1230.50	3.28	0.2822	2.68	13.4025	4.04
	ESDP1	1236.00	11.25	0.5769	5.82	13.4025	14.63
	ESDP2	1236.10	3.58	0.3350	2.86	14.2875	5.56
	ESDP3	1231.40	3.68	0.3369	3.21	13.4267	4.12
	ESDP4	1244.60	6.05	0.4235	4.25	13.4394	7.45
	ESDP5	1236.80	4.66	0.3350	3.46	14.4720	6.24
	ESDP6	1240.90	12.33	0.5792	6.62	14.2876	15.89
	CH	1239.4	0.69	0.5832*	0.57	15.8133	0.64
	IPOPT	1263.5	1.551	–	–	16.7597	2.424
	KNITRO_1	1263.5	22.359	–	–	16.7583	114.203
	KNITRO_2	Out of memory		–	–	Out of memory	
IEEE 13-bus feeder	SOCP	-28.887	0.28	0.1276*	0.39	0.3933	0.36
	BSDP	-29.331	1.31	0.0485	1.40	0.3752	1.43
	ESDP1	-28.188	3.58	0.1201	3.75	0.4040	3.87
	ESDP2	-27.708	1.73	0.0558	1.53	0.4347	1.69
	ESDP3	-27.786	1.36	0.0534	1.40	0.4248	1.52
	ESDP4	-26.372	2.12	0.0597	2.13	0.4418	2.08
	ESDP5	-27.708	1.89	0.0565	1.74	0.4347	1.88
	ESDP6	-27.381	3.26	0.1256	3.39	0.4349	3.90
	CH	-23.973	0.41	0.1276*	0.46	0.4363*	0.33
	IPOPT	-22.449	0.103	–	–	–	–
	KNITRO_1	-23.707	1.188	–	–	–	–
	KNITRO_2	-23.815	72.984	–	–	–	–
IEEE 37-bus feeder	SOCP	-71.727	0.45	0.0469*	0.47	0.6206	0.30
	BSDP	-72.213	6.81	0.0098	6.23	0.6039	1.000
	ESDP1	-72.192	24.02	0.0455	17.91	0.6206	3.087
	ESDP2	-69.303	12.69	0.0153	7.38	0.6165	1.930

	ESDP3	-70.421	7.60	0.0118	6.27	0.6239	1.039
	ESDP4	-66.697	8.74	0.0143	8.10	0.6559	1.479
	ESDP5	-69.303	13.02	0.0159	7.63	0.6248	2.046
	ESDP6	-68.670	19.22	0.0469	13.06	0.6394	3.612
	CH	-64.071*	0.36	0.0469*	0.41	1.0785	0.45
	IPOPT	–	–	–	–	1.1307	0.132
	KNITRO_1	–	–	–	–	1.1307	0.703
	KNITRO_2	–	–	–	–	1.1307	6020.06
IEEE 123-bus feeder	SOCP	-43.851	0.58	0.0306*	0.52	2.9345	0.56
	BSDP	-44.910	110.49	0.0106	103.93	2.7832	118.69
	ESDP1	-43.857	273.90	0.0296	315.32	2.9313	375.89
	ESDP2	-43.596	149.27	0.0145	129.91	3.0272	165.34
	ESDP3	-42.594	145.74	0.0127	118.06	3.1559	151.21
	ESDP4	-41.988	186.84	0.0140	175.95	3.2576	230.26
	ESDP5	-42.375	152.81	0.0152	141.76	3.1567	179.46
	ESDP6	-43.509	305.62	0.0305	328.31	3.1348	390.02
	CH	-39.582	0.39	0.0306*	0.43	3.6629	0.45
	IPOPT	–	–	–	–	–	–
	KNITRO_1	Out of memory		–	–	Out of memory	
	KNITRO_2	Out of memory		–	–	Out of memory	

The results marked with "*" are the exact globally optimal solutions to the corresponding cases.

b) Several 24-hour LMP curves (all positive, as shown in Figure 6.2) have been tested on the 9-bus feeder. The SOCP relaxation for the cases with some LMP curves is exact, while for the other cases it is not. Generally, with objective function (3.1), the SOCP relaxation is only occasionally exact even when all values on the LMP curves are positive.

c) When objective function (3.2) is chosen, the SOCP relaxation is in general exact. Because, minimizing $r\ell$ usually leads to a situation that constraint (4.1) is binding, which means (3.7) is satisfied. However, it does not necessarily mean the SOCP relaxation is exact for all the DESOS cases where objective function (3.2) is adopted.

d) The SOCP relaxation is generally not exact when objective function (3.3) is selected, since it is strictly non-monotonic in the feasible set.

e) Dropping constraint (3.8), the DESOS with objective function (3.1) and the 4th LMP curve in Figure 6.2 is decomposed into 24 OPF problems. The SCOP relaxation for these 24 OPFs is exact. However, it is not for the 24-hour DESOS problem.

6.2.3 Observations and Discussions

From the results shown in Table 6.5, one can observe that:

1) The exactness of the SOCP relaxation for the DESOS problems is sensitive to the descent direction of the chosen objective function. Moreover, it is also sensitive to some set-tings, for instance some bound values (see Sections III and IV in [38]).

2) Adding a linear constraint (e.g. the state of charging/discharging constraint (3.8)) to an OPF problem may change the exactness of the SOCP relaxation for this problem. The effect of adding a linear constraint on exactness of the SOCP relaxation is similar to that of changing some bounds as shown in [38]. Please refer to Remark e) in Subsection 6.2.2.

3) The statements in observations 1) and 2) actually reveal several aspects that may determine whether a DESOS problem satisfies the conditions in Proposition 4.2, i.e. the conditions for exactness of the SOCP relaxation, or not. It implies, on the other hand, the exactness of the SOCP relaxation for the DESOSs is determined by various factors.

4) The ESDP relaxations, especially ESDP4 and ESDP5, are attractive alternatives for the DESOS cases where the SOCP relaxation is not exact, since one can usually find an ESDP relaxation that can provide a much tighter solution than SOCP relaxation do in these cases. The convex constraints introduced in Section 4.3 do not considerably increase the computational burden of the BSDP relaxation except for the RLT. It has been reported in [57] that the solution time for solving the basic SDP relaxation in an OPF problem for

the IEEE 300-bus system has been reduced to 5.7s by exploiting the sparsity. This makes the ESDP relaxations valuable in application.

5) The CH relaxation dominates other convex relaxations except for the 9-bus cases. With the CH relaxation whose computational efficiency is close to that of the SOCP relaxation, the possibility of exactness is increased.

6) KNITRO obtains similar locally optimal solutions as the IPOPT does to most of the cases. However, its computational efficiency is much lower than IPOPT in some cases. When the multi-start option is enabled, the effectiveness of optimal solutions to some cases are increased while to the others are not. Nevertheless, the CPU times increase rapidly as the number of starting point in KNITRO increases. In some cases, the CPU times of KNITRO with multi-start option enabled are unacceptably high.

6.3 SIOP: Tightness of the ESDP Relaxations for Discrete Cases

The SOCP relaxation is not valid for the SIOP cases. Consequently, the comparison between the ESDP and BSDP relaxation for the SIOP is offered in this section.

6.3.1 Solution Method

A branch and bound algorithm is used to solve the convex relaxations of the SIOP so that the node-problems in the branch and bound tree are convex. When a B&B algorithm is used to solve an integer programming problem, some settings may affect the computational performance drastically [77]. These settings include node selecting strategy (i.e. depth-first search plus backtracking and breadth-first search) and strategy for branching variable selection (i.e. choosing the next integer variable on which to branching) [78]. Users can choose these strategies based on the problem they need to solve. However, there is

no universal rule for making the choices. Some may select the branching variable with the lowest or highest objective value [77] while others may choose the smallest or largest fraction value [79].

Solvers that can reliably solve a mixed-integer semidefinite programming problem are not currently available. In this subsection, a standard B&B algorithm provided by a built-in solver of MATLAB, BNB, is used. With BNB, one can choose the node selecting strategy efficiently. For further information about BNB, please refer to the help text of MATLAB and [80]. At each node, the SDP solver, MOSEK, is called to obtain the bounds for the corresponding sub-problem. The above solution procedure is implemented in YALMIP.

6.3.2 Results and Analysis

In this case study, the proposed approach is tested on the power systems mentioned in the previous section. The unit price of the smart PV inverter is considered to be twice that of the conventional PV inverter. The test results are tabulated in Table 6.6, which demonstrate: 1) the non-iterative ESDP relaxations are valid for the SIOP problems which are mixed-integer problems when a B&B method is used; 2) the ESDP relaxations dominate the BSDP relaxation which has been used in literature; 3) in some cases, the ESDP relaxations may not provide tighter solutions. However, the computational efficiency of the B&B algorithm is improved since the feasible sets of the node-problems is tightened by the added convex constraints.

Table 6.6 Results of SIOP in p.u.

System	Relaxation	OOV	CPU time
9-bus feeder	BSDP	2.000	1.000
	ESDP1	2.288	2.364
	ESDP2	2.120	1.091
	ESDP3	2.045	1.045
	ESDP4	2.426	1.182
	ESDP5	2.131	1.227
	ESDP6	2.297	2.636
13-bus feeder	BSDP	3.970	1.000
	ESDP1	4.202	2.045
	ESDP2	4.238	1.354
	ESDP3	3.970	1.122
	ESDP4	3.970	1.221
	ESDP5	4.238	1.112
	ESDP6	4.249	1.970
37-bus feeder	BSDP	3.000	1.000
	ESDP1	4.200	2.087
	ESDP2	3.600	0.672
	ESDP3	3.000	0.804
	ESDP4	3.000	1.663
	ESDP5	3.600	0.895
	ESDP6	4.800	2.244
123-bus feeder	BSDP	4.000	1.000
	ESDP1	5.367	2.286
	ESDP2	4.877	1.071
	ESDP3	4.205	1.036
	ESDP4	5.748	1.143
	ESDP5	4.967	1.179
	ESDP6	5.369	2.786

Chapter 7 CONCLUSIONS AND FUTURE WORK

7.1 General Summary

This thesis develops technologies for utilizing distributed energy storage as well as smart PV inverters to mitigate the detrimental impacts of high penetration PV resources on distribution systems. As a matter of fact, an actual feeder usually contains considerable numbers of single-phase nodes and branches. If the single-phase system is fully modeled, the resulting time-coupled OPF may be intractable. If the single-phase system is simply neglected, the designed size of the DES is most likely to be inaccurate, since the system constraint violations occur in the single-phase system more frequently. To achieve a balance, this thesis divided the planning stage of DES into two steps. In the first step, the PV power and energy imbalance that causes system violations is calculated by OpenDSS, where the entire feeder is modeled, to determine the total size of DES required. Second, the optimal sites are chosen to allocate the DES determined in the previous step using convex optimization techniques with system limits as constraints and minimizing operational costs or power losses as objective.

The research work in this thesis is mainly concerned with constructing tighter convex relaxations for the optimal allocation and scheduling of DES units, and the optimal placement of smart PV inverters in radial distribution systems. First, all the optimization models are built based on a branch flow model. Then, the limitations of the SOCP relaxation which is a well-recognized convex relaxation for the BFM in radial networks are studied. This study reveals the reasons why the SOCP relaxation works unsatisfactorily for a number of the (DESOA), (DESOS) and (SIOP) cases. To obtain better global solutions of the (DESOA), (DESOS) and (SIOP) cases for which the SOCP relaxation is not exact, the

enhanced SDP relaxations are proposed. The enhanced SDP relaxations are constructed by imposing one or some convex constraints that have good approximation to the rank-1 constraint on the BSDP relaxation. Most of these convex constraints are proposed in the references of analytical optimization and have not been used in power systems.

To further tighten the convex relaxation of the AC power flow, convex hull formulations of both BIM and BFM are proposed in this research. The convex hull is the tightest convex relaxation of a non-convex set. Based on the convex hull formulation of the DistFlow model, a novel convex relaxation for optimization problems, e.g. DESOA, DESOS, SIOP, OPF, in power systems is proposed.

7.2 Contributions and Findings

As an innovative study on convex relaxations of the optimization problems in distribution systems, the research in this thesis has made the following contributions and findings.

- Identifying the impact of a chosen objective function on the exactness of the convex relaxations.

Convexification of the OPF problem has attracted substantial research efforts. In OPF problems, researchers usually consider an objective function which is a linear or a convex nonlinear function in terms of the outputs of the various generators and represents the generation cost. However, the objective function of a (DESOA/DESOS/SIOP) problem may vary due to the needs for DES/smart inverters to meet various operational requirements. As a result, some conclusions on the convex relaxations for OPFs may not be valid for the (DESOA), (DESOS) and (SIOP) problems. This research finds that the descent

direction of a selected objective function in the feasible set plays an important role in the exactness of the convex relaxations for the (DESOA), (DESOS) and (SIOP) problems.

- Proposing a mathematical description of the necessary and sufficient condition for the exactness of the SOCP relaxation.

Although the SOCP relaxation is good convex relaxation for the BFM in radial networks, the case study in Section 6.2 shows that the exactness of the SOCP relaxation for the DESOSs is determined by various factors, which means the sufficient conditions studied in literature are not clear enough to reveal the true properties of the SOCP relaxation. The necessary and sufficient condition proposed in this report provides an insight into the inherent nature of the SOCP relaxation.

- Construction of the non-iterative enhanced SDP relaxations

To avoid the limitations of the SOCP relaxation and achieve better globally optimal solutions for the cases for which the SOCP relaxation is not exact, the ESDP relaxations in the non-iterative computing framework are proposed by imposing convex constraints to the BSDP relaxation. The introduced convex constraints can offer strong links between the auxiliary semidefinite matrix $\boldsymbol{X}$ and the rank-1 matrix $\boldsymbol{x}^{\mathrm{T}}\boldsymbol{x}$. Most of these convex constraints are first applied in power systems in this report. The results of the case study elucidate that they work effectively in the power system cases.

- Proposed a novel convex relaxation for decision-making processes in power systems based on the convex hull formulation of the AC power flow equations in radial networks

Although a large number of research efforts have been directed towards the SOCP relaxation and SDP relaxation, there is still a strong desire to obtain tighter relaxations for

the AC power flow. In this thesis, the properties of the non-convex quadratic equalities in two typical AC power flow models, i.e. the BIM and BFM, are fully studied, following which the quasi-convex hull of the quadratic equalities in the AC power bus injection model (BIM) and the exact convex hull of the quadratic equality in the AC power branch flow model (BFM) are proposed respectively. Based on the exact convex hull formulation of non-convex quadratic constraint in BFM, a novel convex relaxation for many decision-making processes, like the DESOA, DESOS and SIOP problems are proposed.

- Sizing method of DES based on time resolutions

The DES has multiple functions, e.g. time-shifting of energy supplied and fast-ramping. These functions work at different time resolutions respectively. Time resolution based sizing methods of DES are proposed in this report. The proposed sizing method are implemented in the OpenDSS platform which can model the entire feeder more precisely so that over-sizing is largely avoided.

7.3 Suggested Future Work

Interesting approaches for convexifying the (DESOA), (DESOS) and (SIOP) algorithms have been proposed and compared with the existing methods in this thesis. To make these novel methods practical, work that needs to be conducted in the future includes:

- Exploit sparsity in the ESDP relaxations

The computational burden of solving the ESDP relaxations of the (DESOA), (DESOS) and (SIOP) problems is still a concern, even though [57] has reported that the solution time for solving the basic SDP relaxation in an OPF problem for the IEEE 300-bus system has been reduced to 5.7s by exploiting the sparsity. One still needs to confirm that the existing dimension reduction techniques are valid for the ESDP relaxations of the

(DESOA), (DESOS) and (SIOP) problems. If not, novel techniques need to be developed to reduce the CPU times of solving the ESDP relaxations.

- Advanced modeling of DES

The DES model presented in Chapter 3 has been widely adopted in related references since it is simple and does not increase the overall complexity of the optimization model. However, a more accurate DES model is desired in the future application in power systems. An advanced DES model means a mathematical model of DES that does not introduce much complexity to the overall optimization model but can accurately capture the performance of both batteries and converters.

REFERENCES

[1] D. Narang, R. Ayyanar, P. Gemin, M. Baggu and D. Srinivasan, "High penetration of photovoltaic generation study - Flagstaff community power," Ariona Public Service Company, Pheonix, AZ, Feb. 2015.

[2] G. Carpinelli, G. Celli, S. Mocci, F. Mottola, F. Pilo, and D. Proto, "Optimal integration of distributed energy storage devices in smart grids," *IEEE Trans. Smart Grid*, vol. 4, no. 2, pp. 985–995, Jun. 2013.

[3] D. Rastler, "Electricity energy storage technology options: a white paper primer on applications, costs, and benefits," Electric Power Research Institute, Palo Alto, CA, December 2010.

[4] Y. M. Atwa and E. F. El-Saadany, "Optimal allocation of ESS in distribution systems with a high penetration of wind energy," *IEEE Trans. Power Syst.*, vol. 25, no. 4, pp. 1815–1822, Nov. 2010.

[5] Y. Makarov et al., "Sizing energy storage to accommodate high penetration of variable energy resources", *IEEE Trans. on Sustain. Energy*, vol. 3, no. 1, pp.34-40. Jan. 2012.

[6] M. Ghofrani, A. Arabali, M. Etezadi-Amoli, and M. S. Fadali, "A framework for optimal placement of energy storage units within a power system with high wind penetration," *IEEE Trans. Sustain. Energy*, vol. 4, no. 2, pp. 434–442, Apr. 2013.

[7] M. Nick, R. Cherkaoui, and M. Paolone, "Optimal allocation of dispersed energy storage systems in active distribution networks for energy balance and grid support," *IEEE Trans. Power Syst.*, vol. 29, no. 5, pp. 2300–2310, Sep. 2014.

[8] J. P. Chiou, C. F. Chang, and C. T. Su, "Ant direction hybrid differential evolution for solving large capacitor placement problems*," IEEE Trans. Power Syst.*, vol. 19, no. 4, pp. 1794–1800, Nov. 2004.

[9] R. A. Gallego, A. J. Monticelli, and R. Romero, "Optimal capacitor placement in radial distribution networks," *IEEE Trans. Power Syst.,* vol. 16, no. 4, pp. 630–637, Nov. 2001.

[10] J. J. Wakileh and A. Pahwa, "Distribution system design optimization for cold load pickup," *IEEE Trans. Power Syst.*, vol. 11, pp. 1879–1884, Nov. 1996.

[11] M. Gitizadeh and M. Kalantar, "A novel approach for optimum allocation of FACTS devices using multi-objective function," *Energy Convers. Manage*., vol. 50, no. 3, pp. 682–690, 2009.

[12] S.A. Jumaat, I. Musirin, M. M. Othman, H. Mokhlis, "Optimal location and sizing of SVC using particle swarm optimization technique", *The 1st Int. Conf. Informatics Computational Intelligence (ICI)*, Bandung, Indonesia, 2011, pp: 312 – 317.

[13] R. Dugan, *Reference guide. the open distribution simulator (OpenDSS)*, EPRI, July 2010.

[14] V. Ramachandran. "Modeling of utility distribution feeder in OpenDSS with steady state impact analysis of distributed generation," M.S. Thesis, Lane Dept. Computer Science Electrical Eng., West Virginia Univ., Morgantown, WV, 2011.

[15] A. K. Barnes, J. C. Balda, A. Escobar-Mejia, and S. O. Geurin, "Placement of energy storage coordinated with smart PV inverters," in *Innovative Smart Grid Technologies* (*ISGT*), 2012 IEEE PES, 2012, pp. 1–7.

[16] P. Jahangiri and D. C. Aliprantis, "Distributed volt/VAr control by PV inverters," *IEEE Trans. Power Syst.*, vol. 28, no. 3, pp. 3429–3439, Aug. 2013.

[17] J. W. Smith, W. Sunderman, R. Dugan, and B. Seal, "Smart inverter volt/var control functions for high penetration of PV on distribution systems," in *Proc. 2011 IEEE/PES Power Syst. Conf. and Exposition (PSCE)*, pp. 1-6.

[18] K. Turitsyn, P. Sulc, S. Backhaus, and M. Chertkov, "Distributed control of reactive power flow in a radial distribution circuit with high photovoltaic penetration," in *Proc. IEEE Power and Energy Society General Meeting*, Minneapolis, MN, Jul. 2010, pp. 1–6.

[19] EPRI. Standard language protocols for photovoltaics and storage grid integration: developing a common method for communicating with inverter-based systems. EPRI, Palo Alto, CA, May 2010.

[20] A. Saxena, P. Bonami and J. Lee, "Convex relaxations of non-convex mixed integer quadratically constrained programs: extended formulations." *Math. Program., Ser. B*, vol. 124, pp. 383-411, 2010.

[21] S. H. Low. "Convex relaxation of optimal power flow, I: formulations and equivalence." *IEEE Trans. Control of Network Syst*., vol. 1, no. 1, pp. 15-27, Mar. 2014.

[22] S. H. Low. "Convex relaxation of optimal power flow, II: exactness." *IEEE Trans. Control of Network Syst*., vol. 1, no. 2, pp. 117-189, Jun. 2014.

[23] G. Celli, S. Mocci, F. Pilo, and M. Loddo, "Optimal integration of energy storage in distribution networks," in *Proc. IEEE Power Tech Conf*., Bucharest, Oct. 2009.

[24] M. Ghofrani, A. Arabali, M. Etezadi-Amoli, and M. S. Fadali, "A framework for optimal placement of energy storage units within a power system with high wind penetration," *IEEE Trans. Sustain. Energy*, vol. 4, no. 2, pp. 434–442, Apr. 2013.

[25] T. Chaiyatham and I. Ngamroo, "Bee colony optimization of battery capacity and placement for mitigation of voltage rise by PV in radial distribution network," in *Proc. of Int. Power Energy Conf. (IPEC '12),* pp. 13–18, Ho Chi Minh City, Vietnam, December 2012.

[26] L. A. Wong, H. Shareef, A. Mohamed and A. Ibrahim, "Optimal battery sizing in photovoltaic based distributed generation using enhanced opposition-based firefly algorithm for voltage rise mitigation," *The Scientific World J.*, vol. 2014, pp. 1-7, 2014.

[27] B. Stott, J. Jardim, and O. Alsac¸, "DC power flow revisited," *IEEE Trans. on Power Systems*, vol. 24, no. 3 pp.1290–1300, Aug 2009.

[28] X. Bai, H.Wei, K. Fujisawa, and Y.Wang, "Semidefinite programming for optimal power flow problems," *Int. J. Elect. Power Energy Syst.*, vol. 30, no. 6–7, pp. 383–392, 2008.

[29] J. Lavaei and S. Low, "Zero duality gap in optimal power flow problem," *IEEE Trans. Power Syst.*, vol. 27, no. 1, pp. 92–107, Feb. 2012.

[30] M. Farivar and S. H. Low, "Branch flow model: relaxations and convexification—parts I," *IEEE Trans. Power Syst.*, vol. 28, no. 3, pp. 2554–2564, Aug. 2013.

[31] R. Jabr, "Optimization of ac transmission system planning," *IEEE Trans. Power Syst.*, vol. 28, no. 3, pp. 2779–2787, 2013.

[32] H. Hijazi, C. Coffrin and P. Hentenryck, "Convex quadratic relaxations for mixed-integer nonlinear programs in power systems," Online available at Optimization-online.org.

[33] J. A. Taylor and F. S. Hover, "Convex models of distribution systemreconfiguration," *IEEE Trans. Power Syst.*, vol. 27, no. 3, pp. 1407–1413, Aug. 2012.

[34] X. Bai and H. Wei, "Semi-definite programming-based method for security-constrained unit commitment with operational and optimal power flow constraints," *IET Gen., Transm., Distrib.*, vol. 3, no. 2, pp. 182–197, 2009.

[35] J. Lopez, D. Pozo, J. Contreras and J.R.S. Mantovani, "A convex chance-constrained model for reactive power planning," *Int. J. Elect. Power Energy Syst.*, vol. 71, pp. 403-411, Oct., 2015.

[36] D. Molzahn and I. Hiskens, "Moment-based relaxation of the optimal power flow problem," in *Power Systems Computation Conference (PSCC),* Aug 2014, pp. 1–7.

[37] Q. Li, R. Ayyanar and V. Vittal, "Convex optimization for DES planning and operation in radial distribution systems with high penetration of photovoltaic resources," *IEEE Trans. Sustain. Energ.*, vol. 7, no. 3, pp. 985-995, 2016.

[38] B. Kocuk, S. Dey, and A. Sun, "Strong SOCP relaxations of the optimal power flow problem," available online at: http://arxiv.org/abs/ 1504.06770, 2015.

[39] C. Coffrin, H. Hijazi, and P. Van Hentenryck, "The QC relaxation: theoretical and computational results on optimal power flow," *IEEE Trans. Power Syst.*, to appear.

[40] B. Kocuk, S. Dey and X. Sun, "Inexactness of SDP relaxation and valid inequalities for optimal power flow. *IEEE Trans. Power Syst*. To appear.

[41] B. Lesieutre, D. Molzahn, A. Borden, and C. DeMarco, "Examining the limits of the application of semidefinite programming to power flow problems." in *Proc. 49th Annual Allerton Conf. Communication, Control, and Computing*, Sep. 28–30, 2011.

[42] R. Madani, S. Sojoudi, and J. Lavaei, "Convex relaxation for optimal power flow problem: mesh networks," *IEEE Trans. Power Syst.*, vol. 30, no. 1, pp. 199–211, Jan. 2015.

[43] S. Abdelouadoud, R. Girard, F. Neirac and T. Guiot, "Optimal power flow of a distribution system based on increasingly tight cutting planes added to a second order cone relaxation," *Int. J. Elect. Power Energy Syst.*, vol. 69, pp. 9-17, 2015.

[44] M. E. Baran and F. F.Wu, "Optimal capacitor placement on radial distribution systems," *IEEE Trans. Power Del.*, vol. 4, no. 1, pp. 725–734, Jan. 1989.

[45] A. G. Expósito and E. R. Ramos, "Reliable load flow technique for radial distribution networks," *IEEE Trans. Power Syst.*, vol. 14, no. 3, pp. 1063–1069, Aug. 1999.

[46] R. Shayani and M. de Oliveira, "Photovoltaic generation penetration limits in radial distribution systems," *IEEE Trans. Power Syst.*, vol. 26, no. 3, pp. 1625–1631, Aug. 2011.

[47] M. Fan, V. Vittal, G. T. Heydt, and R. Ayyanar, "Preprocessing uncertain photovoltaic data," *IEEE Trans. Sustain. Energy*, vol. 5, no. 1, pp. 351– 352, Jan. 2014.

[48] S. Teleke, M. E. Baran, A. Huang, S. Bhattacharya, and L. Anderson, "Control strategies for battery energy storage for wind farm dispatching," *IEEE Trans. Energy Convers*., vol. 24, no. 3, pp. 725–732, Sep. 2009.

[49] S. Zhang and V. Vittal, "Design of wide-area power system damping controllers resilient to communication failures," *IEEE Trans. Power Syst*., vol. 28, no. 4, pp. 4292–4300, Nov. 2013

[50] M. Khalid and A. V. Savkin, "A model predictive control approach to the problem of wind power smoothing with controlled battery storage," *Renew. Energy J.*, vol. 35, pp. 1520–1526, 2010.

[51] T. Brekken, A. Yokochi, A. von Jouanne, Z. Yen, H. Hapke, and D. Halamay, "Optimal energy storage sizing and control for wind power applications," *IEEE Trans. Sustain. Energy*, vol. 2, no. 1, pp. 69–77, Jan. 2011.

[52] C. Chen, S. Duan, T. Cai, B. Liu, and G. Hu, "Optimal allocation and economic analysis of energy storage system in microgrids," *IEEE Trans. Power Electron.*, vol. 26, no. 10, pp. 2762–2773, Oct. 2011.

[53] Q. Li, L. Yang and S. Lin, "Coordination strategy for decentralized reactive power optimization based on a probing mechanism," *IEEE Trans. Power Syst.*, vol. 30, no. 2, pp. 555-562, Mar. 2015.

[54] M. Tawarmalani and N. V. Sahinidis, "A polyhedral branch-and-cut approach to global optimization," *Math. Program.*, vol. 103, no. 2, pp. 225–249, 2005.

[55] R. A. Jabr, "Radial distribution load flow using conic programming," *IEEE Trans. Power Syst.*, vol. 21, no. 3, pp. 1458–1459, Aug. 2006.

[56] J. Lavaei, D. Tse, and B. Zhang, "Geometry of power flows and optimization in distribution networks," in Proc. IEEE PES General Meeting, San Diego, CA, USA, 2012.

[57] D. K. Molzahn, J. T. Holzer, B. C. Lesieutre, and C. L. DeMarco, "Implementation of a large-Scale optimal power flow solver based on semidefinite programming," *IEEE Trans. Power Syst.*, vol. 28, no. 4, pp. 3987–3998, 2013.

[58] H. Mittelmann, "An independent benchmarking of SDP and SOCP solvers," *Math. Program.*, vol. 95, pp. 407-429, 2003.

[59] N. Z. Shor, "Dual quadratic estimates in polynomial and Boolean programming." *Ann. Oper. Res.*, vol. 25, 163–168, 1990.

[60] M. Kojima and L. Tuncel, "Cones of matrices and successive convex relaxations of nonconvex sets." *SIAM J. Optim.*, vol. 10, pp. 750–778, 2000.

[61] H. Sherali and W. Adams, "A reformulation-linearization technique for solving discrete and continuous nonconvex problems," Springer Publishing, New York, U.S., 1999.

[62] G. McCormick, "Computability of global solutions to factorable nonconvex programs: Part I convex underestimating problems," *Math. Program.*, vol. 10, pp. 146–175, 1976.

[63] K. Anstreicher, "Semidefinite programming versus the reformulation-linearization technique for nonconvex quadratically constrained quadratic programming," *J. Glob. Optim.*, vol. 43, pp. 471-484, 2009.

[64] H. Wolkowicz, R. Saigal, L. Vandenberghe, *Handbook of semidefinite programming: theory, algorithms, and application*, Dordrecht: Kluwer, 2000.

[65] S. Boyd and L. Vandenberghe, "Convex Optimization," [Online] Cambridge Univ. Press, Cambridge, U.K., available at http://www.stanford.edu/~boyd/cvxbook.html, 2003.

[66] X. Zheng, X. Sun and D. Li, "Convex relaxations for nonconvex quadratically constrained quadratic programming: matrix cone decomposition and polyhedral approximation," *Math. Program., Ser. B*, vol. 129, pp. 301-329, 2011.

[67] R. Stubbs and S. Mehrotra, "A branch and cut method for 0-1 mixed convex programming," *Math. Program.*, vol. 86, no. 3, pp. 515–532, Dec. 1999.

[68] H. Sherali and W. Adams, "A hierarchy of relaxations between the continuous and convex hull representations for zero-one programming problems," *SIAM J. Disc. Math.*, vol. 3, no. 3, pp. 411-430, Aug. 1990.

[69] L. T. H. An and P. D. Tao, "Solving a class of linearly constrained indefinite quadratic problems by D.C. algorithms," *J. Glob. Optim.,* vol. 11, pp. 253–285, 1997.

[70] R. Horn and C. Johnson, "Matrix analysis," Cambridge Univ. Press, Cambridge, U.K., 1985.

[71] J. Lofberg, "YALMIP: a toolbox for modeling and optimization in Matlab," *IEEE Int. Symp. on Computer Aided Control Syst. Design*, Taipei, Taiwan, pp. 284-289, Sept. 2004.

[72] K. Toh, M. Todd and R. Tutuncu, "SDPT3--a Matlab software package for semidefinite programming," *Optim. Method Softw.*, vol. 11, pp. 545-581, 1999.

[73] R. H. Byrd, J. Nocedal, and R. A. Waltz, "Knitro: an integrated package for nonlinear optimization," in *Large-Scale Nonlinear Optimization*. New York: Springer-Verlag, 2006, pp. 35–59.

[74] R. Fourer, D. M. Gay, and B. W. Kernighan, "A modeling language for mathematical programming," *Manag. Sci.*, vol. 36, no. 5, pp. 519–554, 1990.

[75] IEEE PES Distribution System Analysis Subcommittee, "IEEE distribution test feeders," online at available at http://ewh.ieee.org/soc/pes/dsacom/testfeeders/.

[76] E. Andersen, C. Roos and T. Terlaky, "On implementing a primal-dual interior-point method for conic quadratic optimization," *Math. Program., Ser. B*, vol. 95, pp. 249-277, 2003.

[77] E. M. YoonAnn, “Branch and bound algorithm for binary quadratic programming with application in wireless network communications,” Master’s dissertation, Dept. Math., Iowa State Univ., Ames, IA, 2006.

[78] G. Nembauser and L. Wolsey, *Integer and combinatorial optimization*, New York: Wiley, 1999.

[79] D. Axehill, “Applications of integer quadratic programming in control and communication,” Licentiate’s Thesis, Linköpings Univ., 2005, URL: http://www.divaportal.org/liu/theses/abstract.xsql?dbid=5263.

[80] Y. Evtushenko, M. Posypkin and I. Sigal, “Aframework for parallel large-scale global optimization,” *Comput. Sci. Res. Develop.*, vol. 23, pp. 211–215, 2009.

APPENDIX A

PROOF OF PROPOSITION 4.1

Proof 1: DESOA with objective function 3.1 (DESOA_1).

Suppose that $\bar{\boldsymbol{S}}$ ((A.1)) is the optimal solution of (DESOA_1) which makes the greater-than sign hold in (4.2) in branch *kg* at moment *l*. To prove Proposition 4.1 by contradiction, another solution $\hat{\boldsymbol{S}}$ ((A.2)) is considered,

$$\bar{\boldsymbol{S}} = \left(\bar{\boldsymbol{p}}^{DES}, \bar{\boldsymbol{q}}^{DES}, \bar{p}^{Grid}, \bar{q}^{Grid}, \bar{\boldsymbol{P}}, \bar{\boldsymbol{Q}}, \bar{\boldsymbol{v}}, \bar{\ell}, \bar{\boldsymbol{u}} \right) \tag{A.1}$$

$$\hat{\boldsymbol{S}} = \left(\hat{\boldsymbol{p}}^{DES}, \hat{\boldsymbol{q}}^{DES}, \hat{p}^{Grid}, \hat{q}^{Grid}, \hat{\boldsymbol{P}}, \hat{\boldsymbol{Q}}, \hat{\boldsymbol{v}}, \hat{\ell}, \hat{\boldsymbol{u}} \right). \tag{A.2}$$

The details of $\hat{\boldsymbol{S}}$ are given as follows

$$\hat{\boldsymbol{v}} = \bar{\boldsymbol{v}} \tag{A.3}$$

$$\left(\hat{p}_{i,t}^{DES}, \hat{q}_{i,t}^{DES}, \hat{p}_{(i=1),t}^{Grid}, \hat{q}_{(i=1),t}^{Grid}, \hat{P}_{(i,j),t}, \hat{Q}_{(i,j),t}, \hat{\ell}_{(i,j),t} \right) = \left(\bar{p}_{i,t}^{DES}, \bar{q}_{i,t}^{DES}, \bar{p}_{(i=1),t}^{Grid}, \bar{q}_{(i=1),t}^{Grid}, \bar{P}_{(i,j),t}, \bar{Q}_{(i,j),t}, \bar{\ell}_{(i,j),t} \right)$$

$$i \in \left(N - (h,k,g) \right), (i,j) \in \left(E - (k,g)/(h,k) \right) \tag{A.4}$$

$$\begin{bmatrix} \hat{p}_{h,l}^{DES} \\ \hat{q}_{h,l}^{DES} \\ \hat{p}_{k,l}^{DES} \\ \hat{q}_{k,l}^{DES} \\ \hat{p}_{g,l}^{DES} \\ \hat{q}_{g,l}^{DES} \\ \hat{P}_{(h,k),l} \\ \hat{Q}_{(h,k),l} \\ \hat{P}_{(k,g),l} \\ \hat{Q}_{(k,g),l} \\ \hat{\ell}_{(h,k),l} \\ \hat{\ell}_{(k,g),l} \end{bmatrix} = \begin{bmatrix} \bar{p}_{h,l}^{DES} - \varepsilon_{h1} \\ \bar{q}_{h,l}^{DES} - \varepsilon_{h2} \\ \bar{p}_{k,l}^{DES} - \varepsilon_{k1} \\ \bar{q}_{k,l}^{DES} - \varepsilon_{k2} \\ \bar{p}_{g,l}^{DES} - \varepsilon_{g1} \\ \bar{q}_{g,l}^{DES} - \varepsilon_{g2} \\ \bar{P}_{(h,k),l} - \varepsilon_{(h,k)1} \\ \bar{Q}_{(h,k),l} - \varepsilon_{(h,k)2} \\ \bar{P}_{(k,g),l} - \varepsilon_{(k,g)1} \\ \bar{Q}_{(k,g),l} - \varepsilon_{(k,g)2} \\ \bar{\ell}_{(h,k),l} - \varepsilon_{(h,k)3} \\ \bar{\ell}_{(k,g),l} - \varepsilon_{(k,g)3} \end{bmatrix}. \tag{A.5}$$

If $\hat{\boldsymbol{S}}$ satisfies condition (A.6), by substituting it into (3.4) – (3.7), it can be easily proved that constraints (3.4) – (3.6) hold at each bus, and (3.7) holds in branch *kg* and (4.1) holds in branch *hk*.

$$\begin{cases}
\overline{v}_{k,l}\varepsilon_{(k,g)1}+\varepsilon^2_{(k,g)2}+\varepsilon^2_{(k,g)3}-2\overline{P}_{(k,g),l}\varepsilon_{(k,g)2}-2\overline{Q}_{(k,g),l}\varepsilon_{(k,g)3} \\
=\overline{v}_{k,l}\ell_{(k,g),l}-\overline{P}^2_{(k,g),l}-\overline{Q}^2_{(k,g),l} \\
r_{(k,g)}\varepsilon_{(k,g)1}-\varepsilon_{(k,g)2}-\varepsilon_{g1}=0 \\
x_{(k,g)}\varepsilon_{(h,k)1}-\varepsilon_{(k,g)3}-\varepsilon_{g2}=0 \\
2r_{(k,g)}\varepsilon_{(k,g)2}+2x_{(k,g)}\varepsilon_{(k,g)3}-\left(r^2_{(k,g)}+x^2_{(k,g)}\right)\varepsilon_{(k,g)1}=0 \\
r_{(h,k)}\varepsilon_{(h,k)1}-\varepsilon_{(h,k)2}-\varepsilon_{k1}=0 \\
x_{(h,k)}\varepsilon_{(h,k)1}-\varepsilon_{(h,k)3}-\varepsilon_{k2}=0 \\
2r_{(h,k)}\varepsilon_{(h,k)2}+2x_{(h,k)}\varepsilon_{(h,k)3}-\left(r^2_{(h,k)}+x^2_{(h,k)}\right)\varepsilon_{(h,k)1}=0 \\
2\overline{P}_{(h,k),l}\varepsilon_{(h,k)2}+2\overline{Q}_{(h,k),l}\varepsilon_{(h,k)3}-\varepsilon^2_{(h,k)2}-\varepsilon^2_{(h,k)3}-\overline{v}_{h,k}\varepsilon_{(h,k)1} \\
=\hat{v}_{h,l}\ell_{(h,k),l}-\hat{P}^2_{(h,k),l}-\hat{Q}^2_{(h,k),l}\geq 0 \\
\varepsilon_{h1}=\varepsilon_{(h,k)2} \\
\varepsilon_{h2}=\varepsilon_{(h,k)3} \\
\varepsilon_{h1},\varepsilon_{(h,k)1},\varepsilon_{(k,g)1}\geq 0
\end{cases} \tag{A.6}$$

Although the equality sign of (4.1) in branch *hk* no longer holds under condition (A.6), $\hat{\boldsymbol{S}}$ shows that the relation $v_i\ell_{ij}>P^2_{ij}+Q^2_{ij}$ can be transferred from a specific branch to its up-stream branch without deteriorating the objective value if the condition in Proposition 4.1 holds. Repeating the transformation as shown in Figure A.1, one can obtain

$$v_1\ell_{12}>P^2_{12}+Q^2_{12} \tag{A.7}$$

where $i = 1$ is the substation bus number, and the equals sign of (4.1) holds for all the other branches.

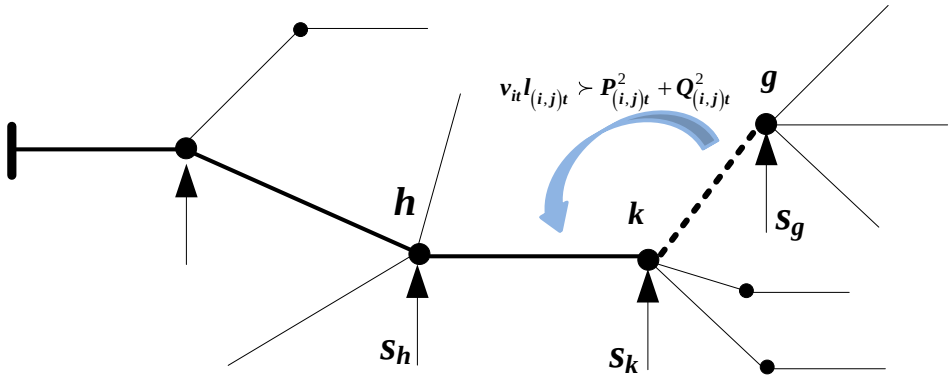

Figure A.1 Illustration of transformation of SOC constraint.

When the relation $v_i \ell_{ij} > P_{ij}^2 + Q_{ij}^2$ is transformed from branch *kg* to branch *hk*, a reduction of ε_{h1} is imposed on $p_{h,l}^{DES}$. Similarly, there is also a reduction imposed on $p_{(i=1),t}^{Grid}$ when $v_i \ell_{ij} > P_{ij}^2 + Q_{ij}^2$ is transformed to branch 12, which means

$$\hat{f}_1 = \sum_t^T \sum_i^N c_t \hat{p}_t^{Grid} < \overline{f}_1 . \tag{A.8}$$

Relation (A.8) means $\hat{\boldsymbol{S}}$ is the optimal solution of the SOCP relaxation of (DESOA_1) instead of $\overline{\boldsymbol{S}}$. In condition (A.6), there are 9 equalities and 4 inequalities while the number of variables is 13. According to some basic theorems in algebra, it is possible to obtain a feasible solution $\hat{\boldsymbol{S}}$ that satisfies (A.6). The details of $\hat{S}$ are not provided here. If some reader is interested in obtaining an $\hat{\boldsymbol{S}}$, one can replace other variables with ε_{g1}, ε_{g2}, ε_{k1} and ε_{k2} based on the equivalent relationship and choose suitable values for these four variables.

Proof 2: DESOA with objective function 3.2 (DESOA_2).

For (DESOA_2), if there exists an optimal solution $\overline{\boldsymbol{S}}$ ((A.1)) that makes the inequality sign hold in (4.1), a feasible solution $\hat{\boldsymbol{S}}$ ((A.2)) for which the details are given as

$$\hat{\boldsymbol{v}} = \overline{\boldsymbol{v}} \tag{A.9}$$

$$\begin{bmatrix} \hat{p}_{k,l}^{DES} \\ \hat{q}_{k,l}^{DES} \\ \hat{p}_{g,l}^{DES} \\ \hat{q}_{g,l}^{DES} \\ \hat{P}_{(k,g),l} \\ \hat{Q}_{(k,g),l} \\ \hat{\ell}_{(k,g),l} \end{bmatrix} = \begin{bmatrix} \overline{p}_{k,l}^{DES} - r_{(k,g)}\varepsilon_1/2 \\ \overline{q}_{k,l}^{DES} - x_{(k,g)}\varepsilon_1/2 \\ \overline{p}_{g,l}^{DES} - r_{(k,g)}\varepsilon_1/2 \\ \overline{q}_{g,l}^{DES} - x_{(k,g)}\varepsilon_1/2 \\ \overline{P}_{(k,g),l} - r_{(k,g)}\varepsilon_1/2 \\ \overline{Q}_{(k,g),l} - x_{(k,g)}\varepsilon_1/2 \\ \overline{\ell}_{(k,g),l} - \varepsilon_1 \end{bmatrix}. \tag{A.10}$$

$$\left(\hat{p}_{i,t}^{DES}, \hat{q}_{i,t}^{DES}, \hat{p}_{(i=1),t}^{Grid}, \hat{q}_{(i=1),t}^{Grid}, \hat{P}_{(i,j),t}, \hat{Q}_{(i,j),t}, \hat{\ell}_{(i,j),t}\right) = \left(\overline{p}_{i,t}^{DES}, \overline{q}_{i,t}^{DES}, \overline{p}_{(i=1),t}^{Grid}, \overline{q}_{(i=1),t}^{Grid}, \overline{P}_{(i,j),t}, \overline{Q}_{(i,j),t}, \overline{\ell}_{(i,j),t}\right)$$

$$i \in \left(N - (k,g)\right), (i,j) \in \left(E - (k,g)\right) \tag{A.11}$$

When $\hat{\boldsymbol{S}}$ is substituted into (3.4)-(3.7), it suffices to show that $\hat{\boldsymbol{S}}$ satisfies all equation. Substitute $\hat{\boldsymbol{S}}$ into the objective function (3.2), then

$$\begin{aligned} f_2\left(\hat{S}\right) &= \sum_t^T \sum_i^M r_i \hat{\ell}_{i,t} + \sum_t^T \sum_i^{N_T} k_i \hat{v}_{i,t} + \sum_t^T \sum_i^{N_S} k_i \hat{p}_{i,t}^{DESloss} \\ &= \sum_t^T \sum_i^M \left(r_i \overline{\ell}_{i,t} - r_{(k,g)}\varepsilon_1\right) + \sum_t^T \sum_i^{N_T} k_i \overline{v}_{i,t} + \sum_t^T \sum_i^{N_S} k_i \overline{p}_{i,t}^{DESloss} < f_2\left(\overline{S}\right) \end{aligned}. \tag{A.12}$$

Relation (A.12) means $\hat{\boldsymbol{S}}$ is the optimal solution of the SOCP relaxation of (DESOA_2) instead of $\overline{\boldsymbol{S}}$.

The proof of Proposition 4.1 is now completed.

APPENDIX B

PROOF OF PROPOSITION 4.2

If $\boldsymbol{d}$ belongs to a vector set Φ_k where there are no active SOCCNLCs ($j \in \emptyset$), there exists a point $\boldsymbol{x}^*$ on the SOCC surface at which the normal of the SOCC is parallel to $\boldsymbol{d}$. For a convex problem, it suffices to show that $\boldsymbol{x}^*$ is the optimal solution. If $\boldsymbol{x}^*$ is the optimal solution of the SOCP that is located on the SOCC surface, according to the first-order condition for optimality, $\boldsymbol{d}$ should be vertical to the tangent plane of the SOCC surface at $\boldsymbol{x}^*$, namely belong to Φ_k.

Let $\boldsymbol{x}^*$ be the optimal solution that is located on the boundaries which are the junctures of the SOCC and some of the SOCCNLCs (e.g. point 1 and 2 in Figure 4.2) and $\Delta\boldsymbol{x}$ be a small changes on $\boldsymbol{x}^*$ along the boundary of the feasible set. If $\boldsymbol{d}$ belongs to a vector set Φ_g where there exist active SOCCNLCs ($j \notin \emptyset$), without loss of generality, assume for simplicity that $l_1(\boldsymbol{x})$ is the only active SOCCNLC for $\boldsymbol{x}^*$, then $\boldsymbol{d}^{\mathrm{T}}(\boldsymbol{x}^* + \Delta\boldsymbol{x}) = \boldsymbol{d}^T\boldsymbol{x}^* - (\gamma_0\nabla s(\boldsymbol{x}^*) + \gamma_1\nabla l_1)^{\mathrm{T}}\Delta\boldsymbol{x}$. If $(\boldsymbol{x}^*+\Delta\boldsymbol{x})$ is located on the surface of SOCC, then $\nabla s(\boldsymbol{x})^{\mathrm{T}}\Delta\boldsymbol{x} \approx 0$ and $\nabla l_1{}^{\mathrm{T}}\Delta\boldsymbol{x} \leq 0$ since $s(\boldsymbol{x}^*) + \nabla s(\boldsymbol{x}^*)^{\mathrm{T}}\Delta\boldsymbol{x} \approx s(\boldsymbol{x}^* + \Delta\boldsymbol{x}) = 0$ and the included angle between ∇l_1 and $\Delta\boldsymbol{x}$ is an obtuse angle due to the convexity respectively. If $(\boldsymbol{x}^*+\Delta\boldsymbol{x})$ is located on SOCCNLC, then $\nabla l_1{}^{\mathrm{T}}\Delta\boldsymbol{x} = 0$ and $\nabla s(\boldsymbol{x}^*)^{\mathrm{T}}\Delta\boldsymbol{x} \leq 0$ since $l_1(\boldsymbol{x}^*+\Delta\boldsymbol{x}) = l_1(\boldsymbol{x}^*) + \nabla l_1{}^{\mathrm{T}}\Delta\boldsymbol{x} = 0$ and the included angle between $\nabla s(\boldsymbol{x}^*)$ and $\Delta\boldsymbol{x}$ is an obtuse angle due to the convexity respectively. Therefore, in both the cases, we have $\boldsymbol{d}^T(\boldsymbol{x}^* + \Delta\boldsymbol{x}) \geq \boldsymbol{d}^T\boldsymbol{x}^*$ ($\boldsymbol{x}^*$ is the optimum).

If $\boldsymbol{x}^*$ is the optimal solution of the SOCP and located on the boundary that connects s($\boldsymbol{x}$) and $l_1(\boldsymbol{x})$, it should satisfy $\boldsymbol{d}^T(\boldsymbol{x}^* + \Delta\boldsymbol{x}) = \boldsymbol{d}^T\boldsymbol{x}^* + \boldsymbol{d}^T\Delta\boldsymbol{x} \geq \boldsymbol{d}^T\boldsymbol{x}^*$ where $\boldsymbol{d}^T\Delta\boldsymbol{x} \geq 0$. Assume that $\boldsymbol{x}^*+\Delta\boldsymbol{x}_1$ and $\boldsymbol{x}^*+\Delta\boldsymbol{x}_2$ are on the SOCCNLC and SOCC respectively, then $\boldsymbol{d}$ should satisfy both $\boldsymbol{d}^T\Delta\boldsymbol{x}_1 \geq 0$ and $\boldsymbol{d}^T\Delta\boldsymbol{x}_2 \geq 0$. Since $\Delta\boldsymbol{x}_1$ and $\Delta\boldsymbol{x}_2$ are vertical to ∇l_1 and $\nabla s(\boldsymbol{x}^*)$ respectively, $\boldsymbol{d}$ satisfying $\boldsymbol{d}^T\Delta\boldsymbol{x}_1 \geq 0$ and $\boldsymbol{d}^T\Delta\boldsymbol{x}_2 \geq 0$ is equivalent to $\boldsymbol{d} = -\gamma_0\nabla s(\boldsymbol{x}) - \gamma_1\nabla l_1$ due to the geometrical characteristic of the convex feasible set.

APPENDIX C

PROOF OF PROPOSITION 4.3

Matrix $\boldsymbol{C}$ is a full-rank matrix means $|S_{LE}| = n$. Suppose that constraint (4.17) is imposed to generate the ESDP relaxation. $b_i\boldsymbol{x} = \boldsymbol{x}b_i = \boldsymbol{x}\boldsymbol{c}_i^{\mathrm{T}}\boldsymbol{x} = \boldsymbol{x}\boldsymbol{x}^{\mathrm{T}}\boldsymbol{c}_i$, as a result, $\boldsymbol{X}\boldsymbol{c}_i = \boldsymbol{x}\boldsymbol{x}^{\mathrm{T}}\boldsymbol{c}_i$ which is equivalent to $\boldsymbol{X}\boldsymbol{C} = \boldsymbol{x}\boldsymbol{x}^{\mathrm{T}}\boldsymbol{C}$. Post-multiply both sides of $\boldsymbol{X}\boldsymbol{C} = \boldsymbol{x}\boldsymbol{x}^{\mathrm{T}}\boldsymbol{C}$ by $\boldsymbol{C}^{-1}$, then $\boldsymbol{X} = \boldsymbol{x}\boldsymbol{x}^{\mathrm{T}}$. If (4.18) or (4.19) is adopted instead of (4.17), the resulting ESDP relaxation is also exact since (4.18) and (4.19) are tighter than (4.17).

APPENDIX D

PROOF OF THEOREM 5.1

(i) $\boldsymbol{B}^{\mathrm{T}}\boldsymbol{w} = d$ crosses all the $\tilde{\boldsymbol{w}}$ points.

Supposing that $\boldsymbol{u}$ is a 2-dimensional vector, then the $\tilde{\boldsymbol{w}}$ is given as

$$\begin{bmatrix} \tilde{\boldsymbol{w}}^1 \\ \tilde{\boldsymbol{w}}^2 \\ \tilde{\boldsymbol{w}}^3 \\ \tilde{\boldsymbol{w}}^4 \end{bmatrix} = \begin{bmatrix} \underline{u}_1 & \underline{u}_2 & \underline{u}_1^2 + \underline{u}_2^2 \\ \underline{u}_1 & \overline{u}_2 & \underline{u}_1^2 + \overline{u}_2^2 \\ \overline{u}_1 & \underline{u}_2 & \overline{u}_1^2 + \underline{u}_2^2 \\ \overline{u}_1 & \overline{u}_2 & \overline{u}_1^2 + \overline{u}_2^2 \end{bmatrix}. \tag{D.1}$$

It is easy to show that the rank of the above matrix is 3, assuming that $\underline{u}_1$, $\overline{u}_1$, $\underline{u}_2$ and $\overline{u}_2$ are different from each other. That means $\tilde{\boldsymbol{w}}^t$ (t = 1, …, 4) are linearly dependent. If the dimension of $\boldsymbol{u}$ is increased to 3, then $\tilde{\boldsymbol{w}}$ is changed into

$$\begin{bmatrix} \tilde{\boldsymbol{w}}^1 \\ \tilde{\boldsymbol{w}}^2 \\ \tilde{\boldsymbol{w}}^3 \\ \tilde{\boldsymbol{w}}^4 \\ \tilde{\boldsymbol{w}}^5 \\ \tilde{\boldsymbol{w}}^6 \\ \tilde{\boldsymbol{w}}^7 \\ \tilde{\boldsymbol{w}}^8 \end{bmatrix} = \begin{bmatrix} \underline{u}_3 & \underline{u}_1 & \underline{u}_2 & \underline{u}_3^2 + \underline{u}_1^2 + \underline{u}_2^2 \\ \underline{u}_3 & \underline{u}_1 & \overline{u}_2 & \underline{u}_3^2 + \underline{u}_1^2 + \overline{u}_2^2 \\ \underline{u}_3 & \overline{u}_1 & \underline{u}_2 & \underline{u}_3^2 + \overline{u}_1^2 + \underline{u}_2^2 \\ \underline{u}_3 & \overline{u}_1 & \overline{u}_2 & \underline{u}_3^2 + \overline{u}_1^2 + \overline{u}_2^2 \\ \overline{u}_3 & \underline{u}_1 & \underline{u}_2 & \overline{u}_3^2 + \underline{u}_1^2 + \underline{u}_2^2 \\ \overline{u}_3 & \underline{u}_1 & \overline{u}_2 & \overline{u}_3^2 + \underline{u}_1^2 + \overline{u}_2^2 \\ \overline{u}_3 & \overline{u}_1 & \underline{u}_2 & \overline{u}_3^2 + \overline{u}_1^2 + \underline{u}_2^2 \\ \overline{u}_3 & \overline{u}_1 & \overline{u}_2 & \overline{u}_3^2 + \overline{u}_1^2 + \overline{u}_2^2 \end{bmatrix}. \tag{D.2}$$

It also suffices to show that the rank of the above matrix is 4.

Supposing that the dimension of $\boldsymbol{u}$ is k, then the corresponding $\tilde{\boldsymbol{w}}$ is a $(2^k \times (k+1))$-dimensional matrix whose rank is $(k+1)$. If rank($\tilde{\boldsymbol{w}}$) $\geq (k+2)$, there always exists a set of $(k+2)$ row vectors of $\tilde{\boldsymbol{w}}$ that are linearly independent. However, in any arbitrarily selected $(k+2)$ row vectors of $\tilde{\boldsymbol{w}}$, one can always find a bound of one element of $\boldsymbol{u}$ that appears $(k+1)$ times according to the definition of $\tilde{\boldsymbol{w}}^t$. Cases (D.1) and (D.2) are two good examples. It suffices to show that the $(k+1)$ chosen vectors that contain this bound of the variable are linearly dependent, e.g. the first 4 rows in (D.2) all of which contain $\underline{u}_3$. Therefore, the rank

of $\tilde{\boldsymbol{w}}$ is not greater than (k+1), which means one can obtain a hyperplane $\boldsymbol{B}^{\mathrm{T}}\boldsymbol{w} = d$ that crosses all the points represented by $\tilde{\boldsymbol{w}}$.

(ii) $CONV((5.6)) \subseteq \left\{\boldsymbol{w} \middle| \boldsymbol{B}^{\mathrm{T}}\boldsymbol{w} \le d,\ \underline{\boldsymbol{u}} \le \boldsymbol{u} \le \bar{\boldsymbol{u}}\right\} = \Omega$

It follows from (i) that all the $\tilde{\boldsymbol{w}}$ points belong to the set Ω. The coefficient matrix of (5.6) is an (n+1)×(n+1) identity matrix which is positive definite. That means $f(\boldsymbol{u}) = 0$ is convex function so that

$$f\left(\alpha\tilde{\boldsymbol{u}}^i + (1-\alpha)\tilde{\boldsymbol{u}}^j\right) \le \alpha f\left(\tilde{\boldsymbol{u}}^i\right) + (1-\alpha) f\left(\tilde{\boldsymbol{u}}^j\right), \tag{D.3}$$

where $0 \le \alpha \le 1$. The right hand side of (D.3) is located on the hyperplane $\boldsymbol{B}^{\mathrm{T}}\boldsymbol{w} = d$ while the left hand side stays within Ω. It implies that the set described by (5.6) belongs to the convex set Ω so that (ii) holds.

(iii) $CONV((5.6)) \supseteq \left\{\boldsymbol{w} \middle| \boldsymbol{B}^{\mathrm{T}}\boldsymbol{w} \le d,\ \underline{\boldsymbol{u}} \le \boldsymbol{u} \le \bar{\boldsymbol{u}}\right\}$

Suppose that $\boldsymbol{\beta}^{\mathrm{T}}\boldsymbol{w} \ge g$ is a valid cut for *CONV*((5.6)). That means it will cut off at least one point of $\tilde{\boldsymbol{w}}$ since (D.3) holds. From the definition of Ω, it is direct to show that $\boldsymbol{\beta}^{\mathrm{T}}\boldsymbol{w} \ge g$ is also be valid for Ω. Hence, (iii) holds.

APPENDIX E

PROOF OF THEOREM 5.2

Note that, unless otherwise stated, all the discussions are within the set described by (5.18)-(5.20).

(i) $CONV(\Omega_0) \subseteq \Omega_1$.

It suffices to show that

$$\left\{ \boldsymbol{x}_{ik} \middle| v_i \ell_{ik} = P_{ik}^2 + Q_{ik}^2 \right\} \subseteq \left\{ \boldsymbol{x}_{ik} \middle\| \begin{matrix} P_{ik} \\ Q_{ik} \\ v_i - \ell_{ik} \end{matrix} \right\|_2 \le v_i + \ell_{ik} \Bigg\}.$$

Moreover,

$$\left\{ \boldsymbol{x}_{ik} \middle| \begin{matrix} v_i \ell_{ik} = P_{ik}^2 + Q_{ik}^2 \\ \boldsymbol{x}_{ik} \in (2) \end{matrix} \right\} \subseteq \left\{ \boldsymbol{x}_{ik} \middle| \begin{matrix} \underline{v}_i \overline{v}_i \ell_{ik} + \overline{S}_{ik}^2 v_i \le \overline{S}_{ik}^2 \left(\overline{v}_i + \underline{v}_i \right) \\ \overline{\ell}_{ik} = \overline{S}_{ik}^2 / \underline{v}_i \\ \boldsymbol{x}_{ik} \in (2) \end{matrix} \right\},$$

since

$$v_i \ell_{ik} \le \underline{v}_i \overline{v}_i \ell_{ik} + \overline{S}_{ik}^2 v_i \ \ (\boldsymbol{x}_{ik} \in (2) \text{ and } \overline{\ell}_{ik} = \overline{S}_{ik}^2 / \underline{v}_i \ ).$$

That means Ω_1 is convex relaxation of Ω_0. $CONV(\Omega_0)$ is defined as the intersection of all convex relaxations of Ω_0. As a result, (i) holds.

(ii) $CONV(\Omega_0) \supseteq \Omega_1$.

Supposed that $\boldsymbol{\alpha}^{\mathrm{T}} \boldsymbol{x}_{ik} \ge \beta$ is a valid inequality for $CONV(\Omega_0)$, it should be valid for all the points in Ω_0. Note that "an inequality is valid for a set" means the inequality is satisfied by all the points within this set. The convex set Ω_1 is enclosed by two sets of boundary. They are specified by the second and the third inequalities respectively. Within set (5.18)-(5.20), the first set of boundary of Ω_1 can be described as

$$\left\{ \boldsymbol{x}_{ik} \middle\| \begin{matrix} P_{ik} \\ Q_{ik} \\ v_i - \ell_{ik} \end{matrix} \right\|_2 = v_i + \ell_{ik} \Bigg\}, \tag{E.1}$$

which is exactly Ω_0. Hence, $\boldsymbol{\alpha}^{\mathrm{T}}\boldsymbol{x}_{ik} \geq \beta$ is valid for set (E.1).

In the $\boldsymbol{x}_{ik}$-space and within (5.18)-(5.20), assume four points, ($\tilde{P}_{ik,1}, \tilde{Q}_{ik,1}, \overline{v}_i + \underline{v}_i, 0$), ($\tilde{P}_{ik,2}, \tilde{Q}_{ik,2}, \underline{v}_i, \overline{\ell}_{ik}$), ($\tilde{P}_{ik,3}, \tilde{Q}_{ik,3}, \underline{v}_i, \overline{\ell}_{ik}$), and ($\tilde{P}_{ik,1}, \tilde{Q}_{ik,1}, \overline{v}_i, \underline{v}_i \overline{\ell}_{ik} / \overline{v}_i$), where

$$\begin{cases} \tilde{P}_{ik,1} = \tilde{Q}_{ik,1} = 0 \\ \tilde{P}_{ik,2}^2 + \tilde{Q}_{ik,2}^2 = \tilde{P}_{ik,3}^2 + \tilde{Q}_{ik,3}^2 = \tilde{P}_{ik,4}^2 + \tilde{Q}_{ik,4}^2 = \overline{S}_{ik}^2 \end{cases}.$$

All the above points are located on the hyper-surface (5.17). Therefore, $\boldsymbol{\alpha}^{\mathrm{T}}\boldsymbol{x}_{ik} \geq \beta$ is valid for them. The following equality represents an area on the hyperplane that crosses the above four points in the $\boldsymbol{x}_{ik}$-space.

$$\boldsymbol{x}_{ik} = \gamma_1 \begin{bmatrix} \tilde{P}_{ik,1} \\ \tilde{Q}_{ik,1} \\ \overline{v}_i + \underline{v}_i \\ 0 \end{bmatrix} + \gamma_2 \begin{bmatrix} \tilde{P}_{ik,2} \\ \tilde{Q}_{ik,2} \\ \underline{v}_i \\ \overline{\ell}_{ik} \end{bmatrix} + \gamma_3 \begin{bmatrix} \tilde{P}_{ik,3} \\ \tilde{Q}_{ik,3} \\ \underline{v}_i \\ \overline{\ell}_{ik} \end{bmatrix} + \gamma_4 \begin{bmatrix} \tilde{P}_{ik,4} \\ \tilde{Q}_{ik,4} \\ \overline{v}_i \\ \underline{v}_i \overline{\ell}_{ik} / \overline{v}_i \end{bmatrix}, \tag{E.2}$$

where $0 \leq \gamma i \leq 1$ (i = 1, …, 4) and $\sum_i^4 \gamma_i = 1$. Substituting (E.2) into $\boldsymbol{\alpha}^{\mathrm{T}}\boldsymbol{x}_{ik} \geq \beta$ results in

$$\boldsymbol{\alpha}^{\mathrm{T}}\boldsymbol{x}_{ik} = \gamma_1 \boldsymbol{\alpha}^{\mathrm{T}} \begin{bmatrix} \tilde{P}_{ik,1} \\ \tilde{Q}_{ik,1} \\ \overline{v}_i + \underline{v}_i \\ 0 \end{bmatrix} + \gamma_2 \boldsymbol{\alpha}^{\mathrm{T}} \begin{bmatrix} \tilde{P}_{ik,2} \\ \tilde{Q}_{ik,2} \\ \underline{v}_i \\ \overline{\ell}_{ik} \end{bmatrix} + \gamma_3 \boldsymbol{\alpha}^{\mathrm{T}} \begin{bmatrix} \tilde{P}_{ik,3} \\ \tilde{Q}_{ik,3} \\ \underline{v}_i \\ \overline{\ell}_{ik} \end{bmatrix} + \gamma_4 \boldsymbol{\alpha}^{\mathrm{T}} \begin{bmatrix} \tilde{P}_{ik,4} \\ \tilde{Q}_{ik,4} \\ \overline{v}_i \\ \underline{v}_i \overline{\ell}_{ik} / \overline{v}_i \end{bmatrix} \geq \left(\sum_i^4 \gamma_i \right) \beta = \beta$$

Hence, $\boldsymbol{\alpha}^{\mathrm{T}}\boldsymbol{x}_{ik} \geq \beta$ is valid for (E.2). Within (5.18)-(5.20), the line segment

$$\underline{v}_i \overline{v}_i \ell_{ik} + \overline{S}_{ik}^2 v_i = \overline{S}_{ik}^2 (\overline{v}_i + \underline{v}_i) \tag{E.3}$$

is exactly the projection of (E.2) onto the $(\ell_{ik}\, v_i)$-space. Consequently, $\boldsymbol{\alpha}^{\mathrm{T}}\boldsymbol{x}_{ik} \geq \beta$ is valid for set (E.3).

In other words, $\boldsymbol{\alpha}^{\mathrm{T}}\boldsymbol{x}_{ik} \geq \beta$ is valid for all the boundary points of Ω_1, which means $\boldsymbol{\alpha}^{\mathrm{T}}\boldsymbol{x}_{ik} \geq \beta$ is also valid for the set Ω_1. Hence, (ii) holds.

APPENDIX F

LIST OF PUBLICATIONS

[1] Q. Li, R. Ayyanar and V. Vittal, "Convex Optimization for DES Planning and Operation in Radial Distribution Systems with High Penetration of Photovoltaic Resources." *IEEE Trans. Sustain. Energ.*, vol. 7, no. 3, pp. 985-995, 2016.

[2] Q. Li and V. Vittal, "Non-iterative Enhanced SDP Relaxations for Optimal Scheduling of Distributed Energy Storage in Distribution Systems," *IEEE Trans. Power Syst.,* to appear.

[3] Q. Li and V. Vittal, "The Convex Hull of the AC Power Flow Equations in Rectangular Coordinates," *IEEE Power Eng. Soc. General Meeting,* 2016, accepted for publication.

[4] Q. Li and V. Vittal, "Convex Hull of the Quadratic Branch AC Power Flow Equations and Its Application," *IEEE Trans. Power Syst.,* a working paper.